MATHEMATICAL MODELING OF GATE CONTROL THEORY

A THESIS SUBMITTED TO
THE GRADUATE SCHOOL OF NATURAL AND APPLIED SCIENCES
OF
MIDDLE EAST TECHNICAL UNIVERSITY

BY

EGEMEN AGİ

IN PARTIAL FULFILLMENT OF THE REQUIREMENTS
FOR
THE DEGREE OF MASTER OF SCIENCE
IN
CHEMICAL ENGINEERING

DECEMBER 2009

Approval of the thesis:

MATHEMATICAL MODELING OF GATE CONTROL THEORY

submitted by **EGEMEN AGİ** in partial fulfillment of the requirements for the degree of **Master of Science in Chemical Engineering Department, Middle East Technical University** by,

Prof. Dr. Canan Özgen
Dean, Graduate School of **Natural and Applied Sciences** _____

Prof. Dr. Gürkan Karakaş
Head of Department, **Chemical Engineering** _____

Prof. Dr. Canan Özgen
Supervisor, **Department of Chemical Engineering, METU** _____

Prof. Dr. Nuhan Puralı
Co-supervisor, **Department of Biophysics, Medical School of Hacettepe University** _____

Examining Committee Members:

Prof. Dr. Işık Önal
Department of Chemical Engineering, METU _____

Prof. Dr. Canan Özgen
Department of Chemical Engineering, METU _____

Prof. Dr. Nuhan Puralı
Department of Biophysics, Medical School of Hacettepe University _____

Assoc. Prof. Dr. Haluk Külah
Department of Electrical and Electronics Engineering, METU _____

Assist. Prof. Dr. Serkan Kıncal
Department of Chemical Engineering, METU _____

Date: 28.12.2009

I hereby declare that all information in this document has been obtained and presented in accordance with academic rules and ethical conduct. I also declare that, as required by these rules and conduct, I have fully cited and referenced all material and results that are not original to this work.

Name, Last name : Egemen Agi

Signature :

ABSTRACT

MATHEMATICAL MODELING OF GATE CONTROL THEORY

Agi, Egemen

M.S., Department of Chemical Engineering

Supervisor : Prof. Dr. Canan Özgen

Co-Supervisor: Prof. Dr. Nuhan Puralı

December 2009, 115 pages

The purpose of this thesis work is to model the gate control theory, which explains the modulation of pain signals, with a motivation of finding new possible targets for pain treatment and to find novel control algorithms that can be used in engineering practice. The difference of the current study from the previous modeling trials is that morphologies of neurons that constitute gate control system are also included in the model by which structure-function relationship can be observed. Model of an excitable neuron is constructed and the response of the model for different perturbations are investigated. The simulation results of the excitable cell model is obtained and when compared with the experimental findings obtained by using crayfish, it is found that they are in good agreement. Model encodes stimulation intensity information as firing frequency and also it can add sub-threshold inputs and fire action potentials as real neurons. Moreover, model is able to predict depolarization block. Absolute refractory period of the single cell model is found as 3.7 ms. The developed model, produces no action potentials when the sodium channels are blocked by tetrodotoxin. Also, frequency and amplitudes of generated action potentials increase when the reversal potential of Na^+ is increased. In addition, propagation of signals along myelinated and

unmyelinated fibers is simulated and input current intensity-frequency relationships for both type of fibers are constructed. Myelinated fiber starts to conduct when current input is about 400 pA whereas this minimum threshold value for unmyelinated fiber is around 1100 pA. Propagation velocity in the 1 cm long unmyelinated fiber is found as 0.43 $\frac{m}{s}$ whereas velocity along myelinated fiber with the same length is found to be 64.35 $\frac{m}{s}$. Developed synapse model exhibits the summation and tetanization properties of real synapses while simulating the time dependency of neurotransmitter concentration in the synaptic cleft. Morphometric analysis of neurons that constitute gate control system are done in order to find electrophysiological properties according to dimensions of the neurons. All of the individual parts of the gate control system are connected and the whole system is simulated. For different connection configurations, results of the simulations predict the observed phenomena for the suppression of pain. If the myelinated fiber is dissected, the projection neuron generates action potentials that would convey to brain and elicit pain. However, if the unmyelinated fiber is dissected, projection neuron remains silent. In this study all of the simulations are preformed using Simulink.

Keywords: Hodgkin-Huxley model, ion channels, action potential propagation, synaptic transmission, conductance based models, substantia gelatinosa.

ÖZ

GEÇİT KONTROL KURAMININ MATEMATİKSEL MODELLENMESİ

Agi, Egemen

Yüksek Lisans, Kimya Mühendisliği Bölümü

Tez Yöneticisi : Prof. Dr. Canan Özgen

Ortak Tez Yöneticisi: Prof. Dr. Nuhan Puralı

Aralık 2009, 115 sayfa

Bu tez çalışmasının amacı, ağrı sinyallerinin modülasyonunu açıklayan geçit kontrol kuramının, ağrı tedavilerinde, tedavinin uygulanabileceği muhtemel hedeflerin saptanması ve mühendislik alanında kullanılabilecek yeni bir denetim algoritmasının bulunabilmesi amacıyla modellenmesidir. Bu çalışmanın önceki modelleme çalışmalarından farkı, geçit kontrol sistemini oluşturan nöronların morfolojilerinin de göz önüne alınması ve yapı-işlev ilişkisinin de modele dahil edilmesidir. Çalışmada, uyarılabilir bir sinir hücresinin modeli kurularak, bu modelin çeşitli değişkenler karşısında nasıl cevap verdiği incelenmiştir. Farklı fizyolojik koşullarda, model sonuçlarının kerevit balığı kullanılarak yapılan deneysel çalışma sonuçları ile uygun olduğu gözlenmiştir. Model, uyarı şiddeti bilgisini aksiyon potensiyeli frekansı olarak kodlamakta ve ayrıca eşik altı uyarıları gerçek nöronlar gibi toplayarak aksiyon potansiyeli üretmektedir. Model, depolarizasyon bloğunu da tahmin edebilmektedir. Geliştirilen hücre modelinin mutlak tepkisiz periyodu 3.7 ms olarak bulunmuştur. Sodyum kanallarından iyon geçişi tetrodotoxin ile engellendiğinde, geliştirilen model aksiyon potansiyeli üretememektedir. Ayrıca, sodyumun dönme potansiyeli arttırıldığında, oluşan aksiyon potansiyellerinin frekans ve genliklerinin arttığı gözlenmiştir. Biyoelektrik sinyallerin miyelinli ve

miyelinsiz sinir liflerindeki iletimi benzetilmiş ve her iki tip lif için uyarı akım şiddeti-frekans ilişkisi kurulmuştur. Bir cm uzunluğundaki miyelinsiz sinir lifinde iletim hızı 0.43 $\frac{m}{s}$ olarak bulunurken, aynı uzunluktaki miyelinli sinirde iletim hızı 64.35 $\frac{m}{s}$ olarak belirlenmiştir. Ayrıca geliştirilen sinaps modeli, sinaptik boşluktaki, zamana bağlı nörotransmiter konsantrasyonunu benzetirken, gerçek sinapslarda da görülen toplama ve tetanizasyon özelliklerini göstermiştir. Geçit kontrol sistemini oluşturan nöronların, boyutlarına bağlı elektrofizyolojik özelliklerini bulabilmek için, morfolojik analizleri yapılmıştır. Tüm sistem modeli, bütün üye parçaların birleştirilmesiyle çalıştırılmıştır. Farklı bağlanma düzenleri için, bentezim çalışmalarının sonuçları, ağrının baskılanmasıyla ilgili gözlemlenen olayları yakın bir biçimde benzetebilmiştir. Miyelinli sinir modelden çıkarıldığı zaman, beyne ileti taşıyan projeksiyon nöronu aksiyon potansiyelleri üretmiştir. Miyelinsiz sinir modelden çıkarıldığındaysa projeksiyon nöronu aktivite göstermemiştir. Bu çalışmadaki bütün benzetimler Simulink benzetim ortamında yapılmıştır.

Anahtar Kelimeler: Hodgkin-Huxley modeli, iyon kanalları, aksiyon potansiyeli iletimi, sinaptik iletim, iletkenlik temelli modeller, jelatin madde.

dedicated to the memory of my father

ACKNOWLEDGMENTS

I am very greatful to Prof. Dr. Canan Özgen for sharing her wisdom and knowledge not only in science but also in real life issues. I'd also like to thank for her infinite indulgence. I also would like to thank my co-supervisor Prof. Dr. Nuhan Puralı for his infinite support and making me feel the joy of making research.

I am very greatful for the endless support and love of my mother and my sister and also my father who is watching me every time.

My lab partner, Hatice Ceylan, who suffered as much as me during my research, deserves the best in life and I thank her very much.

I'd like to thank Metin Burak Altınoklu who helped me with the format of the thesis and save me a lot of trouble.

Last but not the least, I hail for Fulya Akpınar who makes my life glorius even with only her smile.

I would like to thank The Scientific and Technological Research Council of Turkey (TUBITAK) for their support through the 2210 National Scholarship Programme during my graduate studies.

TABLE OF CONTENTS

LIST OF TABLES

TABLES

LIST OF FIGURES

FIGURES

CHAPTER 1

INTRODUCTION

Control mechanisms in living organisms deserve attention since they are very stable and robust from an engineering perspective. pH control of the body fluids is a very good example for a biological control mechanism. Although various food that can change the pH is digested, pH value is always kept in between very narrow limits. Otherwise, the consequences can be detrimental. If the mechanism of control system can be understood, not only it can be imitated and applied in engineering sciences but also theories existing for engineering purposes can be utilized to fix any malfunction in the system like dialysis. However, to be able to extract a new theory from the living organisms or to apply engineering theory for treatments, the system at hand should be investigated thoroughly and this is a very hard task since biological systems posses multi-compartmental interactions which are usually not well understood [9].

Another example of a control structure in a living organism is the gate control mechanism, which modulates the pain signals with tactile signals so that the level of pain that is perceived is changed. For treatment of chronic pain, electrical stimulation of spinal cord, where the gate control structure takes place, is a common method [10]. However, to increase the efficiency of this method and to develop new treatment techniques gate control mechanism must be identified clearly. Apart from stimulation of spinal cord, for finding the possible targets for pain killers, the mechanism of suppression of pain must be studied thoroughly. Although neuronal structure of the gate control mechanism is very simple, which consists of two neurons and two fibers, since there is a vast heterogeneity in the electrophysiological and morphological characteristics of neurons, formation of an

exact circuit is extremely hard. In recent years, to find exact circuits that process pain signaling, connectivity patterns between neurons that are most probable to be included in gate control mechanism are investigated. In addition, morphological and electrophysiological properties of these neurons are being investigated so that their signaling properties are revealed [2].

Electrophysiological and morphological characteristics of the components of gate control structure are important because these properties directly affect the signal initiation and propagation. Pain sensation can be inhibited if initiation of signals that carry nociceptive (pain related) information is prevented. Neurons generate signals through the ion movements across their membranes. Ions move through ion channels that are embedded in cell membrane and these ion channels change their permeability to ions with membrane voltage. If the dynamics of these ion channels are understood, novel techniques can be improved to change their permeability. As a result, initiation of signals can be inhibited or promoted.

While propagating along nerve fibers, signals attenuates with time and space. Morphology is important because of the fact that the same signal can initiate a response when it reaches to the end of a fiber whereas it cannot in another one. Also, spatial summation of signals is a direct consequence of morphology of the neurons.

Previous models of gate control structure did not take into account the physiological and morphological properties of the components of the system. They were either phenomenological models in which signal initiation is modeled without regarding the biophysics behind the process [11] or black box models that use artificial neural networks and use only input and output data [12].

In the current work, gate control structure is investigated with an effort to model and find out the input-output relationship of the circuit with taking into account the electrophysiological, morphological and connectivity patterns of the neurons that are included. In this sense, signal initiation in an excitable neuron and the propagation of this signal along nerve fibers are modeled. In addition, signals travel from neuron to neuron through synapses so synaptic transmission is

modeled. Also the morphometric analysis of the component neurons is included in the model.

Main concern of this study is to model the system regarding the physiological and morphological properties of the components of the gate control structure and test it for different conditions to see if it predicts the observations for pain transmission.

CHAPTER 2

LITERATURE SURVEY

In this part, initially development of pain mechanism theories over a century is presented along with the gate control theory. After examining the modeling studies of gate control structure, clinical applications for pain treatments that were based on gate control theory is investigated. Afterwards literature on single cell excitability, signal propagation along fibers and morphology of components of gate control strcuture is given.

2.1 Previous Models

At the beginning of 20^{th} century, until the emergence of gate control theory there were two theories that tried to explain pain sensation. The first one was the specificity theory which proposed that receptors, which were specific to pain, were connected directly to a pain center in brain [13]. This meant that stimulation of these receptors would elicit pain and only pain. Although physiologically there were identified skin organs that acted as receptors that were excited by only nociceptive (pain related) stimuli, these stimuli did not necessarily evoke sensation of pain.

Another competing theory was pattern theory. In contrary to stimulus specific receptors and pathways, in this theory receptors were non-specific and different sensations were encoded according to spatio-temporal pattern in discharged impulses from the skin. In other words, distinctions in discharge properties of peripheral nerve fibers projecting from skin and nerve fibers of central nervous system that connected to peripherals were the reason of different kinds of sensations that were experienced [14]. This coded message was decoded in the central

nervous system. According to the theory pain was produced by the intense stimulation of non-specific receptors. As the quantity of nerve fiber discharge increased, quality of the sensation changed and pain was felt. So the theory said that there were no specific fibers that carry specific sensation. However, physiological evidence showed that there was "a high degree of receptor-fiber specialization" [15].

Modulation of pain by other sensory signals that are not related to nociceptive information was first proposed by Melzack and Wall [15]. In their work it was stated that after stimulation of skin, generated impulses were transmitted to three structures in spinal cord, substantia gelatinosa (SG) cells in dorsal horn of spinal cord, the dorsal column fibers that project to the brain and transmission cells (T cells) in the dorsal horn. Substantia gelatinosa cells regulate the activity of afferent fibers before they affect transmission cells. Dorsal column fibers activate brain processes that changes modulation properties of gate control system. Activity difference between nociceptive small diameter and non-nociceptive large diameter fibers determine the activity of transmission cells which in turn determines the level of perception of pain. Substantia gelatinosa cells are located in the lamina II of spinal cord and exact location of the transmission cells were not indicated explicitly in their paper. But with recent labeling studies it is understood that lamina I receives nociceptive signals from peripheral afferents and they relay this information to the brain, which makes them more likely to be transmission cells [16, 2].

After the proposal of the gate control theory, debate over the subject rised and Nathan made a critical review about the theory [14]. He indicated that the T-cell in the gate control theory is a hypothetical cell and gave possible neurons that could be T-cells. Furthermore, he stated that a theory of pain should explain different kinds of pain that arose from stimulation of different tissues. Finally he criticzed the theory for neglecting "the facts known about stimulus-specificity of nerve fibres". In a re-examination of the theory, Wall [17] indicated that neurons of lamina I and lamina V of dorsal horn were candidate neurons for being T-cells. Moreover, as a response to the critics of Nathan [14], he

explained two different uses of word specifity; one is diagnostic use and the other is predictive use. He stated that predictive use of specificity was misleading since it could not be predicted if the stimulation of one fiber would cause the expected sensation eventually. However, "past cause of an observed nerve impulse" could be determined and this was referred as the diagnostic use of specificity.

A neural network model of pain mechanism was presented by Minamitani and Hagita [18]. In their model, peripheral receptors, afferent Aβ, Aδ and C fibers, receptive cells of spinal cord, brain stem, thalamus, and the cerebral cortex were involved and the simualations were done only for one directional ascending and descending pathways for pain sensation. Model only coped with signals that were elicited by cutaneous stimulation. Firing properties of the component cells that were related to pain generation were investigated and "spatial information processing" mechanisms were not explained analytically. Although adaptation and conduction velocity in the fibers were considered, each neural unit in the model had constant conduction velocity and discharge threshold. With their model, different modalities of pain could be could be simulated such as fast stinging pain and slow burning pain. In addition graded touch sensation was simulated.

Duty of brain in the gate control theory was a significant contribution to understanding pain but duty of the brain and how it performed its task was poorly understood. In this respect Melzack proposed that brain possesed a neural network, which was called neuromatrix, and this neural network combined multiple inputs to form the signal pattern that generates pain [19]. Melzack stated that synaptic connections of the neuromatrix was initially determined genetically and later shaped by sensory inputs. Output of this genetically determined neuromatrix was called neurosignature, which was the characteristic nerve impulse pattern, and this characteristic neurosignature determined quality of pain experience. In his work, inputs that acted on neurosignature were stated as follows: 1) sensory inputs from cutaneous receptors, 2) inputs that helped "congnitive interpretation of the situation" like visual signals, 3) tonic inputs from other parts of the brain that were related to emotions, 4) inhibitory modulation that was built

in all brain function, 5) activity of stress regulation system which was activated by any threat to biological stability or homeostasis. With the brain's function, pain was not a direct consequence of only injury.

First mathematical model of the gate control theory of pain was made in 1989 [11]. In their paper Britton and Skevington indicates that a pain theory must be capable of addressing five observations:

1. Increased stimulation of small nerve fibers increases pain.
2. Stimulation of large nerve fibers may increase pain temporarily but it will reduce pain eventually.
3. Electrical stimulation of grey matter of the midbrain may reduce pain.
4. During situations like war, pain may not be felt even if you are wounded severely.
5. Expectation of pain may augment the perceived pain.

Their model is composed of one excitatory, one inhibitory SG cells, one T cell, cognitive control and descending control structures which represents the function of the brain. They pick up arbitrary functions for frequency of outputs of cognitive and descending control structures, which are strictly monotone increasing functions of impulse frequencies in afferent pathways, and for frequencies of outputs of three cells, which are strictly monotone increasing functions of slow potentials of the cells. With their model, Britton and Skevington not only achieved to explain the five observations but also they explained that the cause of rhythmic pain is the sudden changes in firing frequencies of the cells. However, in their paper mathematical equations were arbitrary and were not derived regarding the physical phenomena behind pain process [12]. Also physiological and morphological properties of cells and afferent fibers were not included.

Regarding the nonlinear interactions between components of gate control system, another model is developed by Haeri *et al.* by using artificial neural networks (ANN) [12]. They defined the inputs to be the frequency of impulses conveyed

by afferent fibers and output to be the potential of T cell, which represents pain level. Using the results of mathematical model in [11], they got a set of training data to be used to train their ANN. With their model they managed to explain pain situations in which small diameter fibers are not excited. But again, their model does not consider physiological and morphological properties of cells and afferent fibers.

In a more recent study in 2008 Xu and co-workers investigated pain, which is caused by thermal means, in a holistic method [20]. They started to model the transduction of thermal stimulus into bioelectrical pain signals by nociceptors, in other words pain receptors. For the bioelectrical signal generation, they used Hodgkin-Huxley formalism, which is the main formalism used in this current work. For model of the transmission of the signal they used only nerve length and conduction velocity data and did not take into account the morphology of the fibers and the limitations that morphology may cause. For the gate control system, they used the mathematical model of Britton and Skevington which had the limitations that are mentioned above.

Stojanovic *et.al.* [10] indicated that for the treatment of chronic low back pain, spinal cord stimulation is the most common technique that is used. Clinical studies revealed a success rate above 50% and considering its relatively low cost it is one the best techniques. They indicated that the base for this technique was attributed to gate control theory but also there were possible new mechanisms. Chaudhari *et.al.* [21] stated that treatment with neuromodulation aims to decrease the activity in the pathways that carry pain signals and indicated that implantation of spinal cord stimulators require high level of expertise since these devices are implemented by invasive methods.

2.2 Electrical Properties of Neurons

For a complete model that will include physiological and morphological properties of the cells and afferent fibers, certain structures that constitutes the gate control circuitry must be modeled. These are model of an excitable cell which

will generate an action potential (unit signal in nervous system), model of propagation of action potential along afferent fibers, model of synapses that connects cells, morphology of cells, namely SG and T cells.

Model of a neuron can have different complexity levels [22]and model should be chose according to the particular goal of the study. For a big network of neurons, simpler models are preferred to provide computational efficiency, where action potential initiation is described by simple mathematical expressions [23]. Since gate control system is a small circuit and computation powers of computers are vast, detailed compartmental modeling, where the anatomical features of cells are included into the model would be better to be used.

Model of an excitable cell was first modeled by Hodgkin and Huxley [24]using squid giant axon and they received Nobel Prize in 1963 for this work. They represented the electrical behaviour of membrane of an excitable cell by a simple electrical circuit that is composed of a capacitor, resistors and batteries. They proposed that ion channels that provide the transportation of Na^+ and K^+ ions across cell membrane open or close with respect to voltage across membrane, so there is a non-linear relationship between voltage across membrane and current through ion channels. This non-linearity creates the specific action potential shape. Electrical behaviour of human neurons is investigated by Schwarz *et.al.* They performed their experiments on "nerve material that was obtained from patients undergoing nerve graft operations" [8]. Different from squid, human nerve fibers are myelinated, in other words they are wrapped with myelin which is an insulating material that changes the electrophysiological characteristic of the fiber.

With the foundation of electrical excitability of cell membrane, the question how action potentials propagate along afferent fibers arose. Attenuation of voltage along dendrite of a neuron was shown by the cable theory of Rall [25,26]. This passive propagation describes how voltage changes with time and space along homogeneous non-excitable part of the afferents. In this model, cable is composed of parallel connected RC first order circuits. However, saltatory conduction was

observed over myelinated fibers [27]. Myelin is an electrically insulating material and covers the non-excitable parts of fibers. So an action potential that is initiated in the excitable part of the fiber propagates along myelinated part passively and attenuates, but if magnitude of the attenuated signal is big enough when it reaches the neighbouring excitable part, it can excite that excitable part. In this way signal makes a saltatory propagation. Since conduction velocity is proportional the square root of axon diameter [28], there are giant axons in invertebrates (creatures without spine) to achieve to give fast responses to stimuli. In vertebrates, myelinated axons are developed to increase the conduction velocity of action potentials without increasing the diameter of the axon [29] so that nerve bundles can be confined to a limited area. Since myelinated axons are not uniform, propagation of action potentials along these fibers cannot be described by only cable theory of Rall. To solve this non-homogeneity problem, compartmental modeling is used [30]. In this method, axon is divided into small compartments and every compartment is modeled according to their electrical properties.

2.3 Synaptic Transmission

After the propagation of the action potential over a neuron, it should be transmitted to the neighboring neurons. This is accomplished by synaptic transmission. In central nervous system transmission is done by chemical synapses [1]. When an action potential reaches the terminals of an axon, it triggers neurotransmitter release into the synaptic cleft. These neurotransmitters diffuse in the cleft and bind to receptors that are located on post-synaptic neuron. Upon binding of transmitters, receptors gate ion channels that allow the passage of specific ions. There are inhibitory and excitatory receptors; inhibitory receptors gate ion channels that would let transport of ions which will decrease the membrane potential of post-synaptic cell whereas excitatory receptors gate ion channels that would let transport of ions which will increase the membrane potential of post-synaptic cell and helps action potential to be initiated on the post-synaptic neuron.

When modeling this process, there are two main things to consider; time course of the neurotransmitter in the synaptic cleft and the dynamics of receptors. Concentration of neurotransmitter in the synaptic cleft changes with diffusion out of the cleft, uptake by post-synaptic neuron receptors [31] and opening and closing dynamics of post-synaptic ion channels are dependent on this concentration. Simplified models of these receptors that are compatible with Hodgkin-Huxley formalism are present in literature [32]. In this model concentration of neurotransmitter in synaptic cleft is approximated with a brief pulse. In another model transmitter concentration is defined with a function of pre-synaptic neuron membrane voltage [33].

2.4 Morphologies of Lamina I-II Neurons

Propagation along a neuron is influenced by the shape of the neuron. Since passive parts of the neuron are modeled as RC circuits, these compartments act as low-pass filter. As the diameter of the neuron changes, parameters of RC circuit change, which means filter characteristics also change.

Gate control system constitutes two neurons; one substantia gelatinosa and one transmission cell. Differentiating the layers of spinal cord was a debate for a long time and a review can be found in the work of Cervero and Iggo [34]. Substantia gelatinosa is the lamina II region of the spinal cord. Transmission cell takes place in lamina I. These two regions receive a heavy synaptic input from fibers that carry nociceptive signals [16] and that is why these two regions are thought to be take part in modulation of pain signals [35].

With recent labeling studies in these two regions it is seen that there are more neuron groups that differ in electrophysiological and morphological characteristics [3, 36]. Since substantia gelatinosa cells have inhibitory effect on transmission cells, they should posses neurotransmitters that would gate inhibitory receptors. Again in labeling studies, islet cells of lamina II are determined to have GABA transmitter, which is a transmitter that gates inhibitory receptors [36]. So islet cells are great candidates for the substantia gelatinosa cell that take place in

gate control system. A morphometric and physiologic analysis of islet cells is done by Melnick [4] and it is stated that "islet cells fire action potentials tonically in response to sustained depolarization". Transmission cell in the gate control system integrates the incoming signals from substantia gelatinosa cell and afferent fibers. Prescott and Koninck indicated that tonic cells of lamina I have integrative properties, so this makes them a candidate for being transmission cells [3].

CHAPTER 3

PAIN CONTROL MECHANISMS

In this chapter, working principle of gate control theory is presented. The candidate component neurons of the structure are identified and the ones that are most suitable are chosen to be used in the model regarding their electrophysiological properties.

3.1 Pain Perception

Pain is defined as "an unpleasant sensory and emotional experience associated with actual or potential tissue damage, or described in terms of such damage" by The International Association for the Study of Pain [20]. Pain is a sensory modality like vision, hearing, touch and it is the result of tissue damage. With its nature, pain perception is a protective mechanism; "it warns of injury that should be avoided or treated" [1]. If someone who cannot perceive pain puts his/her hand on a hot stove, s/he will not feel any pain expectedly and will not pull his/her hand back so this will cause severe tissue damage. It should be emphasized that pain is a perception and is different from nociception which is "the response to perceived or actual tissue damage" [1]. Sensation is the transduction of stimulus by body receptors into signals that can be conveyed in the body. Perception is the processing and abstraction of the sensory input. In this regard nociception does not cause pain necessarily. Since pain is a percept, level of perception of it changes from person to person with past experience, environmental conditions and emotional state. This subjectivity makes pain treatment rather difficult [1].

Nociceptors are receptors that are activated by unpleasant stimulus to peripheral tissues. There are three types of nociceptors; mechanical, thermal and

polymodal which are responsive to mechanical, thermal and high intensity chemical, thermal, mechanical stimuli, respectively. Most of them are free nerve endings [1]. One important characteristic of nociceptors is that in general they do not adapt. Adaptation is the decrease in the frequency of any sensory signal with time, although the stimulus that evokes the sensory signal is still active. One example is that although they are continually in contact with the body, clothes are not felt to be touching all the time. The non-adapting nature of nociceptors is important since it keeps the person alert for any tissue damage as long as the noxious stimuli persists [5].

Thermal and mechanical receptors have thinly myelinated fibers, Aδ fibers, that carry the nociceptive signal at a speed of 5-30 m/s. Whereas polymodal nociceptors have unmyelinated C fibers that carry signal at 1m/s. Both types of these fibers are known to be small diameter fibers; C fibers having diameters between 0.25-1.5 microns and Aδ fibers having diameters between 1-5 microns. The non-nociceptive signals like tactile sensory signals are generally carried by Aβ fibers which are heavily myelinated and large in diameter (5-15 microns) [11].

3.2 Gate Control Theory of Pain

For explaining the perception of pain, before gate control theory was proposed in 1965, there were two theories. One was the specificity theory and the other was pattern theory. Specificity theory states that like vision, hearing and smell modalities, pain also has "its own peripheral and central apparatus" [15], which means there are specialized receptors, nociceptors, that are excited by only noxious stimuli and this stimuli will be transmitted by Aδ and C fibers to specific pain center in the brain. This type of transmission implies that stimulation of nociceptors will definitely evoke pain and only pain. However, Aβ sensory fibers which do not transmit pain signals have effect on pain perception. When Aβ fibers of one region is selectively blocked, distinct unpleasant stimuli that would cause different pain like pin-prick, pinch and cold, could not be distinguished and all of them causes burning pain [1]. Also activating Aβ fibers at the site of injury

decreases pain and this is the reason why people rub their arm after they hit somewhere or shake their hands after burning them. So modality and level of pain that is perceived is not only a result of activity in pain specific peripheral and central structures but also sensory signals that are not related to pain are also effective in perception.

According to pattern theory, all sensations are produced by different spatio-temporal patterns of nerve impulses and there is no "modality specific" transmission pathways [15]. However, it is known there is specialization in sensory modalities, like information related to vision is transmitted through specific pathways to vision center of the brain. Also pattern theory cannot explain how the sensory codes that are embedded in impulse patterns are decoded by the central nervous system.

Psychological state has also effect on pain perception. During stressful situations like battles, severely wounded soldiers would feel little pain, although the same injury would normally cause great pain [15, 11]. If something is expected to cause pain, this expectation may augment the intensity of perceived pain [11]. Also past experience may modulate the level of perception of pain. Dogs which are served food after being shocked, burned and cut, "soon respond to these stimuli as signals for food and salivate, without showing any signs of pain"; however they react and howl as normal dogs when the site of stimuli is changed [15].

With the need of a new theory that would explain how the activities in nociceptive and non-nociceptive fibers affect the level and quality of pain, and how psychological state can modulate perception of pain, Melzack and Wall proposed gate control theory in 1965 [15]. Their theory included an explicit mechanism showing how the balance of activity in nociceptive and non-nociceptive afferents modulate pain. In addition they included descending control mechanism from brain, that would be responsible for the effects of psychological state on pain. Also stimulation of grey matter of midbrain is reported to cause pain relief [11], so descending control also accounts for this observation. However, in this study descending control will be excluded since there is no data on how brain interacts

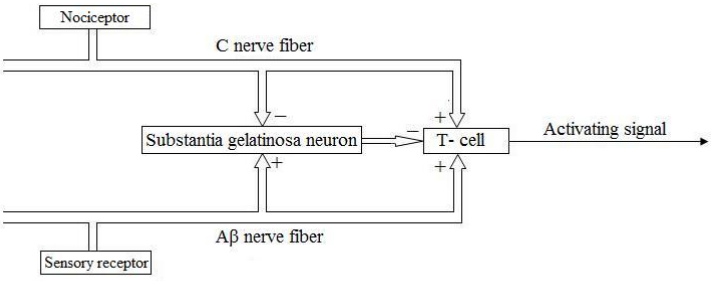

Figure 3.1 Schematic of gate control mechanism.

with other parts of the gate control system and the control action that it takes.

Gate control theory is best explained by a simple diagram as Figure 3.1.

Small diameter C and Aδ fibers excite transmission cells whereas inhibit substantia gelatinosa cells which inhibit transmission cells; in other words they increase the excitability of transmission cells indirectly also. On the other hand, Aβ fibers stimulate both substantia gelatinosa and transmission cells, which means that while Aβ fibers excite transmission cells directly, they inhibit them indirectly [15, 1]. Output of the transmission cell determines the level of perception. Consequently, intensity of pain is modulated by this small neuronal circuitry and it is composed of four parts: 1) unmyelinated, small diameter C fiber that carries nociceptive signals 2) myelinated, large diameter, A fiber that conveys non-nociceptive signals 3) transmission cell 4) substantia gelatinosa cell which inhibits transmission cell [1].

The gate control system is located in the spinal cord which is the initial site of modulation of pain. It is also important to mention that this mechanism is topographically specific. This means every part of the body is connected to the specific parts of spinal cord where nociceptive and non-nociceptive afferent fibers terminate. So when pain is felt in upper part of the left arm, exact place where pain is felt, upper part of the left arm, should be rubbed; rubbing right foot would not ease pain [1]. Substantia gelatinosa neurons and T-cells are situated at the dorsal horn of the spinal cord. Dorsal horn is the part of the gray matter (which

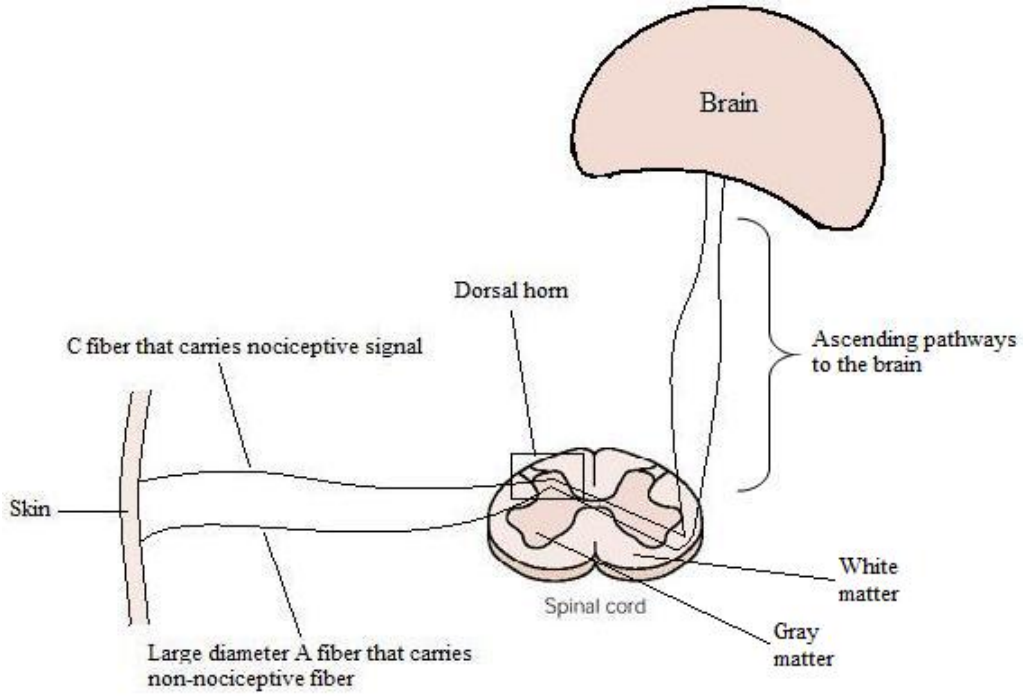

Figure 3.2 Peripheral and central pathway for nociceptive and non-nociceptive sensory signals (adapted from [1]).

is the butterfly shaped inner part of the cord) that is positioned near the back of a human anatomically. Opposite of dorsal is ventral and it corresponds to part of body near the belly. After integrating all coming signals, T-cell projects through ascending pathways to activating system in the brain and brain interprets the meaning of the incoming signal. The pathway that is dealed here is shown in Figure 3.2.

Dorsal horn is composed of multiple laminars and substantia gelatinosa (gelatinous substance) corresponds to lamina II. The neurons of this lamina are thought to be the interneurons in the gate control system because it receives a heavy synaptic input from unmyelinated C fibers and thinly myelinated Aδ fibers, which convey nociceptive information [16, 35]. Also in their recent work, Daniele and MacDermott found GABAergic, in other words inhibitory neurons that receive Aβ projection and inhibit the same Aβ drive onto projection neurons in a feedforward manner in superficial dorsal horn (lamina I and II) [37], which is consistent

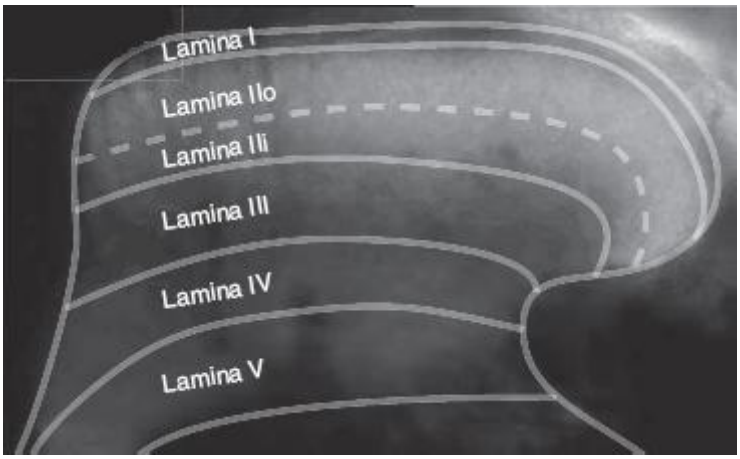

Figure 3.3 Laminar structure of dorsal horn [2].

with the gate control theory. In their work Melzack and Wall did not mention what the T-cells are and the place of T-cells in the dorsal horn due to lack of data. However, in a re-examination of the theory, Wall gave two candidate lamina where T-cells may be present. One is the lamina I (marginal zone) and the other is lamina V [17]. In lamina I, there were cells which were only responsive to noxious stimuli and to no others. Also some of these cells projected to higher centers in the central nervous system. It was also shown that electrical stimulation of large diameter cutaneous (related to skin) fibers inhibited the firing of these cells [17]. Wall stated that lamina V cells had a wide receptive field; not only nociceptive afferents but also non-nociceptive afferents converged on this lamina and activity of non-nociceptive fibers inhibited them. These cells were also responsive to injury [17]. This was consistent with the receptive field of T-cells. In the most recent papers lamina I neurons are associated with nociception and are stated to be projection neurons that send nociceptive signals to brain through ascending pathways [3, 38, 16]. In this regard lamina I neurons will be treated to be the T-cells in the gate control mechanism in this current study.

There is not one kind of neuron neither in substantia gelatinosa nor in marginal zone. Neurons of these layers differ morphologically and also with their response to same stimuli. There are attempts to classify the neurons of these layers according to their morphological and electrophysiological properties and try to find

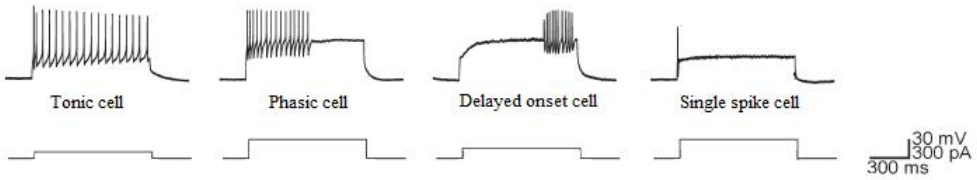

Figure 3.4 Firing properties of different lamina I neurons [3].

correlations between these properties [38, 36, 3]. In the work of Prescott De Koninck with adult rat, based on the responses to current injection to soma, four cell types are identified [3]; tonic cells fire action potentials continuously as long as the stimuli persists, phasic cells fire high frequency burst of action potentials with variable durations depending on the amplitude of the stimuli, however they stop firing before the end of stimulation, delayed onset cells start to fire with a delay to the first action potential and single spike cells fire only one action potential or a very short burst (≤ 4 spikes) and become silent during the rest of the stimulation. Firing properties of these cells are shown in Figure 3.4. Upper plots indicates the membrane potentials of the cells that are produced upon stimulation with current injections that are shown in lower plots. Membrane potentials are in the order of mV and currents are in the order of pA.

In the same study, upon investigation of the responses of these cells to train of pulses, it is stated that tonic and delayed onset cells tend to integrate inputs whereas phasic and single spike cells operate as coincide detectors, so phasic and single spike cells can follow high frequency inputs. In addition, tonic cells are reported to be able to transduce stimulus intensity into firing frequency [3] which is the general method of transduction in nervous system. Since T-cells in gate control system sums inputs from three different sources, they act as integrators. So tonic cell will be chosen to be T-cell in this current work. When the firing property and morphology of the cells are explored, it is found that tonic cells corresponds to fusiform cells. Cells of lamina I are differentiated according to their soma shape and number of primary dendrites which are fusiform, pyramidal and multipolar [3, 39]. Fusiform cells are identified with their elongated soma

and primary dendrites arising from each end of the soma [39] which means they have two primary dendrites [3], pyramidal cells have triangular soma and three primary dendrites arising from the corners of the soma, multipolar cells have no specific soma shape but they posses four or more primary dendrites. These cell morphologies are not specific to rat, they are also found in cat and monkey, so this indicates that these cell types are a mammalian feature [39]. In the work of Han *et.al.*, responses of cat lamina I neurons were recorded and it was found that all of the fusiform cells that were labeled were nociceptive specific, in other words they were responsive only to noxious stimuli like pinch and heat [40]. This is another reason why fusiform cells may be chosen as T-cells in gate control system. Fusiform lamina I cell in Figure 3.5 is a 3-D reconstruction that is obtained from the confocal images of the labeled neuron that were obtained by Zeiss Axioplan2 microscope equipped with a 40X water immersion objective [3] and it will be used as the T-cell in the current work. Axon is determined to be the thin branch coming out of the soma and labeled with the arrow in Figure 3.5. This is consistent with the criteria that Grudt and Perl used to identify axons of the cells in superficial dorsal horn (lamina I and II); they are "generally thinner and relatively constant size from the soma outward" and they do not contain spines [38]; mushroom shaped small parts that are connected to dendrites or axons with thin necks. Vertical axis of Figure 3.5 corresponds to the rostro-caudal axis which is the line connecting tail and head in animals like rats, horses; in humans it is the line connecting foot and head. Neither the neuron in Figure 3.5 nor other fusiform cells are classified as projection neurons in the work of Prescott and De Koninck [3]. However, there are studies that explored ascending pathways from lamina I to brain and found samples of all three classes of neurons projecting to these ascending pathways [41, 39]. So the neuron in Figure 3.5 will be assumed to be projecting to ascending pathways as the T-cell in gate control system does.

Substantia gelatinosa is generally indicated to be composed of four different classes of neurons that differ morphologically; islet cells, central cells, radial cells

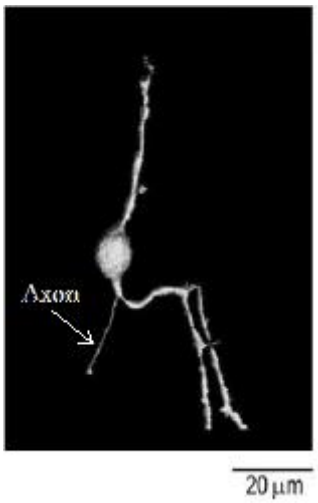

Figure 3.5 Fusiform, tonic lamina I cell [3].

and vertical cells [38, 35]. More specifically they are classified according to their branching pattern of dendrites and principal orientation of the dendritic tree. Schematics of these neuron types are shown in Figure 3.6. Islet cells have relatively longer dendrites than the other types of neurons and these dendrites mainly extend along the rostro-caudal axis. Central cells are similar to islet cells but they have shorter dendritic tree along rostro-caudal axis. Radial cells have dendrites that extends in every direction. Dendritic tree of vertical cells extends ventrally to laminae II-IV [38, 35]. Substantia gelatinosa neuron in the gate control system is an inhibitory interneuron that inhibits the T-cell. The neuron that will be chosen as the substantia gelatinosa neuron in the gate control system should posses inhibitory neurotransmitter so upon secretion it will inhibit T-cell. With labeling studies, islet cells were showed to be immunoreactive for γ-aminobutyric acid (GABA) which is the main neurotransmitter in superficial dorsal horn [42]. In the work of Maxwell *et.al.*, morphology of inhibitory and excitatory interneurons in the superficial laminae of the rat dorsal horn were investigated and all of the islet cells were found to be inhibitory whereas other cell types shows multiple actions; either excitatory or inhibitory. They also stated that islet cells had axons that project outside the territory of dendritic tree which made them great candidates for being inhibitory interneurons since they may collect information

Figure 3.6 Neuron types in substantia gelatinosa.

from one sensory region and inhibit other neurons outside this region [36]. Under sustained depolarization islet cells fire action potentials tonically which means they fire repetitively with regular intervals [43, 16, 4] and this electrophysiological property is stated to be consistent with an inhibitory function [36]. With the evidence at hand they are the major class of inhibitory interneurons in lamina II [44]. For the inhibitory interneuron in the gate control mechanism an islet cell will be used.

Axons of islet cells are confined in their dendritic trees and the dendritic tree of islet cells are so dense that their axons and primary dendrites are hard to be identified. But a clear image of a labeled islet cell from work of Melnick will be used in this work [4] which is shown in Figure 3.7. This image was taken and processed with a Zeiss LSM510 confocal microscope [4]. Probable axon of the islet cell in Figure 3.7 is determined according to the definition given by Grudt and Perl; axon is identified by its generally thinner and relatively constant size, emerging from soma outwards and does not contain spines [38]. It should be noted that there is not a work that shows the inhibitory connectivity between a lamina II islet cell and lamina I fusiform cell. To find such a connectivity, simultaneous recordings should be done from the fusiform and islet cells so that it can be shown, an activity in islet cell mediates a response in fusiform cell, which is the postsynaptic neuron in the gate control system. In literature such simultaneous recordings were done to reveal connectivity patterns between superficial dorsal horn neurons [43, 16] so that possible modulatory circuits can be found. Such connectivity studies should be done to explore precise targets for therapies in pain conditions. However, simultaneous paired recordings have technical challenges.

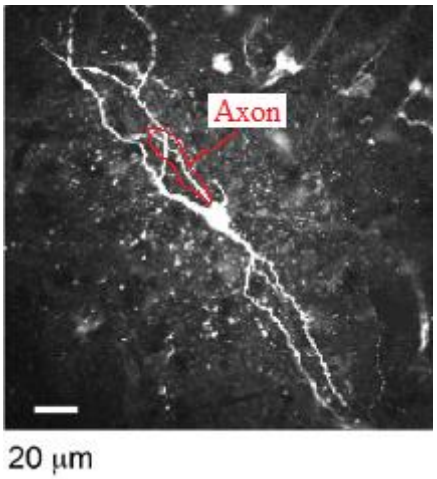

Figure 3.7 Islet cell in substantia gelatinosa [4].

First of all, probability of encountering connected neurons is very low, almost 10% of the tested pairs are found to be connected. Other shortcoming of the technique is that data sets are relatively small [2]. It should also be noted that there may be other gate control structures that are different from the one proposed by Melzack and Wall [15]. Lu and Perl proposed a probable gate system where both presynaptic and postsynaptic neurons were located in lamina II and inhibitory interneuron received only innocuous input from unmyelinated C fiber unlike the interneuron in original gate control system which received input from a myelinated Aβ fiber and nociceptive C fiber [43].

Connectivities between the neurons and the fibers that convey noxious and non-nociceptive signals to them will be treated to be monosynaptic, which means every component of the gate control system will be in contact with each other at only one point. So, while morphometric analysis is being done, not all the dendrites will be investigated since number of dendrites may be higher than the number of inputs to the neuron. Dendrites that receive no input will not affect the behaviour of the neuron and will not be included. There are works in literature pointing monosynaptic connections in superficial dorsal horn. In the work of Grudt and Perl, stimulation of dorsal root (a term that is used for collection nerve fibers that carry sensory information to central nervous system) evoked

responses in superficial dorsal horn which were judged to be monosynaptic [38]. In the inhibitory network that Lu and Perl proposed, islet cell and central cell of substantia gelatinosa, which are connected monosynaptically, received monosynaptic excitatory inputs from C fibers [43]. It should be noted that, monosynaptic connectivity is one of the major assumptions in the current modeling study.

CHAPTER 4

ELECTRICAL PROPERTIES OF CELL MEMBRANE

In this chapter, action potential generation is explained. First, the forces that act on ions and make them move through the cell membrane are presented. After that, electrical circuit model of cell membrane is explained which is followed by formulation of the propagation of action potentials along myelinated and unmyelinated fibers.

4.1 Mechanism of Ion Movement Through Cell Membrane

Cell membrane is a lipid bilayer, in which proteins that span the whole membrane exist [5]. A simple figure of this structure is shown in Figure 4.1.

This membrane separates internal and external conducting solutions and constitutes a barrier for lipid-nonsoluble substances, namely water and free ions in the body fluid. Electrical activity in the nerves is accomplished by the movement of intracellular and extracellular free mobile ions through the cell membrane. Since ions cannot dissolve and diffuse through membrane, they are transported through watery channels, ion channels, which are proteins that span the cell membrane. There are two forces that make ions move through ion channels, across the membrane:

1. Chemical driving force

2. Electrical driving force

Chemical driving force is the result of concentration gradient of ions that exists across cell membrane. One dimensional movement of ions under this force is

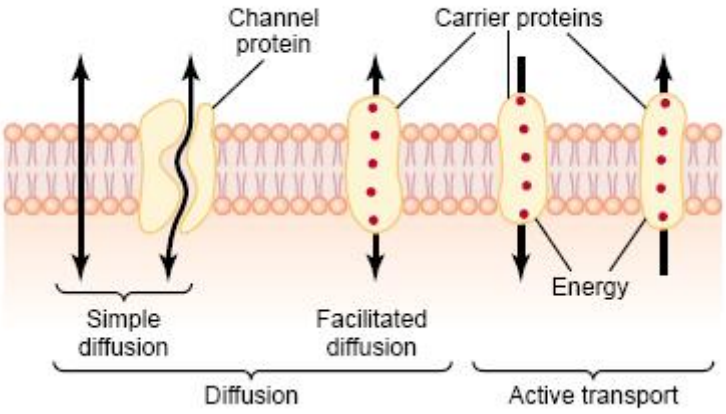

Figure 4.1 Cell membrane structure. [5]

explained by Fick's Law of Diffusion which has the following form:

$$J_{A_{diffusion}} = -D_{AB}\frac{dC_A}{dx} \tag{4.1}$$

where $J_{A_{diffusion}}$ is the molar flux of ion A, that is generated by concentration gradient, in $mol/cm^2 \cdot s$, D_{AB} is the molecular diffusivity of ion A in B in cm^2/s and C_A is the local concentration of ion A in mol/cm^3 [45,6]. B in Equation 4.1 is the body fluid in ion channels.

As mentioned before, cell membrane separates intracellular and extracellular conducting solutions, which consist of ions at different concentrations. As a result of accumulation of these ions on both sides of membrane, a potential difference is created. This potential difference creates an electric field which is the source of electrical driving force. Flux that is generated by drift of ions in electric field is calculated as:

$$J_{A_{electrical\,drift}} = -z_A\mu_A C_A\frac{dV}{dx} \tag{4.2}$$

where $J_{A_{electrical\ drift}}$ is the molar flux of ion A, that is generated by the potential gradient, in $mol/cm^2 \cdot s$, z_A is the valence of A (dimensionless), μ_A is the mobility of A in membrane in $cm^2/V \cdot s$, C_A is the local concentration of ion A in mol/cm^3, V is the local electrical potential in membrane in V [6]. Multiplying the right side of Equation 4.2 by ionic valance, z_A, and Faraday's constant, F in $\frac{C}{mol}$, gives

the current density I_A in terms of A/cm^2. Under the assumption that electric field,$-\frac{dV}{dx}$, and mobility across the membrane are constant, which means they are independent of x, derivative term can be replaced by $\frac{E}{l}$ where E is the potential difference across the membrane and l is thickness of membrane. Equation 4.2 takes the following form:

$$I_{A_{Drift}} = z_A^2 F \mu_A C_A \frac{E}{l} \tag{4.3}$$

In fact Equation 4.3 is an explicit form of Ohm's law where conductivity of an electrolyte solution has the form $\frac{z_A^2 F \mu_A C_A}{l}$. Total flux resulting from diffusion and electrical drift has the following form:

$$J_{total} = -D_{AB}\frac{dC_A}{dx} - z_A \mu_A C_A \frac{dV}{dx} \tag{4.4}$$

Multiplying both sides of Equation 4.4 by ionic valance, z_A, and Faraday's constant, F in $\frac{C}{mol}$, gives the total current density $I_{A_{total}}$ in terms of A/cm^2:

$$I_{A_{total}} = z_A F(-D_{AB}\frac{dC_A}{dx} - z_A \mu_A C_A \frac{dV}{dx}) \tag{4.5}$$

Molecular diffusivity in Fick's law and the mobility in electrical drift equation "express a similar quantity: the ease of motion through the fluid" [6] and these parameters has a connecting formula known as Einstein Relationship:

$$D_{AB} = \mu_A \frac{kT}{q} = \frac{RT}{F}\mu_A \tag{4.6}$$

where R is the gas constant in $\frac{J}{K \cdot mol}$. Using Einstein relationship in Equation 4.5, Nernst-Planck electrodiffusion equation is obtained:

$$I_{A_{total}} = (-z_A \mu_A RT \frac{dC_A}{dx} - z_A^2 F \mu_A C_A \frac{dV}{dx}) \tag{4.7}$$

Equation 4.7 is the basic relation that explains the movement of ions in electric field through a membrane where concentration gradient exists. As the ions "diffuse through the membrane, the electrical potential difference that is set up across the membrane retards the diffusion of more ions" [46]. In other words, electrical and chemical forces oppose each other and an equilibrium is reached and total current density becomes 0. At this point, Equation 4.7 takes the following form:

$$0 = (-z_A \mu_A RT \frac{dC_A}{dx} - z_A^2 F \mu_A C_A \frac{dV}{dx}) \tag{4.8}$$

Rearranging gives

$$\frac{dV}{dx} = \frac{-RT}{z_A F} \frac{1}{C_A} \frac{dC_A}{dx} \tag{4.9}$$

Integrating with proper limits gives

$$\int_{V_1}^{V_2} dV = \frac{-RT}{z_A F} \int_{C_1}^{C_2} \frac{dC_A}{C_A} \tag{4.10}$$

$$V_2 - V_1 = \frac{-RT}{z_A F} \ln \frac{C_2}{C_1} \tag{4.11}$$

where V_1 and C_1 are extracellular potential and extracellular concentration, respectively; V_2 and C_2 are intracellular potential and intracellular concentration, respectively. By convention, extracellular side is taken as reference so membrane potential is defined as

$$V_{membrane} = V_{intracellular} - V_{extracellular} = V_2 - V_1 \tag{4.12}$$

So the final form of the equation is

$$V_{membrane} = \frac{RT}{z_A F} \ln \frac{C_1}{C_2} \tag{4.13}$$

Potential difference that is generated by concentration difference of one kind of ion across cell membrane is given by Equation 4.13. We may write

$$E_A = \frac{RT}{z_A F} \ln \frac{C_{outside}}{C_{inside}} \tag{4.14}$$

where E_A is known to be *equilibrium potential* of ion A. When membrane potential is equal to equilibrium potential of ion A, net flux of A ions is zero. Equation 4.14 is the *Nernst equation*. In fact in the original form of Nernst equation, instead of concentrations, chemical activity coefficients of ion A in extracellular and intracellular solutions are used. But, if the activity coefficients are nearly the same in two solutions, intracellular and extracellular concentrations can be used [46].

Movement of ions through the cell membrane and the currents that they create was first investigated by David E. Goldman, Alan Lloyd Hodgkin and Bernard Katz and *GHK current* and *GHK voltage* equations were formulated [6].

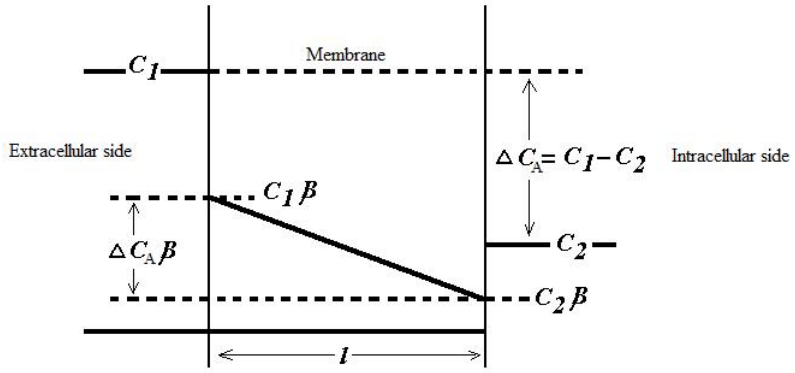

Figure 4.2 Model of transport through cell membrane [6].

GHK current equation is a solution of Nernst-Planck electrodiffusion equation with two additional assumptions: electric field across the cell membrane is constant and movements of different ions are independent from each other, in other words species do not interrupt the movement of different species. Membrane is selectively permeable to substances and has different membrane permeabilities to different substances. For a substance to pass though the membrane, it should be first dissolved in the lipid membrane. So the flux of the substance is determined by the concentration difference inside the membrane. To find the concentration difference inside the membrane, the extracellular and intracellular concentrations of ion A are multiplied by β, water-membrane partition coefficient for ion A which is a dimensionless number. A simple model of transport through cell membrane is shown in Figure 4.2.

Permeability of an ion A is defined by the empirical flux equation

$$M_A = -P_A \Delta C_A \tag{4.15}$$

where M_A is the molar flux density of A in $\frac{mol}{cm^2 \cdot s}$, P_A is the membrane permeability to A in $\frac{cm}{s}$ and ΔC_A is the concentration difference of A between extracellular and intracellular bulk solutions. Under the condition that partitioning of A between membrane and extracellular and intracellular solutions is very rapid, this process may be assumed to be in equilibrium and concentration of A inside the membrane, at membrane-solution interface can be found by multiplying the bulk solution

concentration by membrane-water partition coefficient, β. With the assumption that concentration gradient is constant, from Fick's first law flux can be written as

$$M_A = -\frac{\Delta C_A D_{AB} \beta}{l} \tag{4.16}$$

Equating Equation 4.15 and Equation 4.16 P_A can be found as

$$P_A = \frac{D_{AB}\beta}{l} \tag{4.17}$$

Using Equation 4.6 in Equation 4.17, relationship between permeability and mobility can be expressed as

$$P_A = \frac{\beta \mu_A RT}{lF} \tag{4.18}$$

With the use of permeability and the aforementioned two assumptions, GHK current equation takes the following form

$$I_A = P_A z_A^2 \frac{VF^2}{RT} \frac{[C_A]_{in} - [C_A]_{out} \exp(-z_A \frac{FV}{RT})}{1 - \exp(-z_A \frac{FV}{RT})} \tag{4.19}$$

As it can be seen, ionic current is a non-linear function of membrane voltage. Since transport of different ions is independent from each other, Equation 4.19 can be split into unidirectional efflux and influx of the ions as

$$I_{A_{efflux}} = P_A z_A F\theta \frac{[C_A]_{in}}{1 - \exp(-\theta)} \tag{4.20}$$

$$I_{A_{influx}} = -P_A z_A F\theta \frac{[C_A]_{out} \exp(-\theta)}{1 - \exp(-\theta)} = P_A z_A F\theta \frac{[C_A]_{out}}{1 - \exp(\theta)} \tag{4.21}$$

where θ is equal to $z_A \frac{FV}{RT}$. These two equations are nonlinear functions of membrane voltage, but for large voltages they become asymptotic to straight lines which have the following forms

$$I_{A_{efflux}} = P_A z_A F\theta \, [C_A]_{in} \text{ for } E \gg 0 \tag{4.22}$$

$$I_{A_{influx}} = P_A z_A F\theta \, [C_A]_{out} \text{ for } E \ll 0 \tag{4.23}$$

Current-voltage relation, which is expressed in GHK current equation, changes between these two lines. From the current-voltage relation it can be deduced that membrane conductance changes with membrane voltage. Nonlinear dependence

of current on membrane voltage and the asymptotic behaviour of GHK current equation can be seen more clearly in Figure 4.3. By convention outward current is taken as positive and inward current is taken as negative. When the intracellular concentration is much higher than extracellular concentration, as the voltage increases total current curve approaches the outward current (efflux) asymptote and as the voltage decreases it approaches inward current (influx) asymptote as in Figure 4.3(a). When the extracellular concentration is much higher than intracellular concentration, for smaller voltages total current curve approaches inward current asymptote and for higher voltages it approaches outward current asymptote as in Figure 4.3(b). If Figure 4.3(b)and Figure 4.3(a) are investigated more closely, it can be seen that total current changes direction at some specific point. The voltage at which total current changes direction is the *reversal potential* and it is the membrane potential when the net ionic flux, in other words total current through membrane is zero. If only Na^+, K^+ and Cl^- ions are assumed to pass through the cell membrane, total current at any moment will be equal to the following:

$$I_{total} = I_{Na} + I_K + I_{Cl} \tag{4.24}$$

$$I_{total} = \frac{VF^2}{RT\left[1 - \exp(\frac{-VF}{RT})\right]}Y \tag{4.25}$$

$$X = P_{Na}\left[Na\right]_{in} + P_K\left[K\right]_{in} + P_{Cl}\left[Cl\right]_{out} \tag{4.26}$$

$$Y = \left\{X - (P_{Na}\left[Na\right]_{out} + P_K\left[K\right]_{out} + P_{Cl}\left[Cl\right]_{in})\exp(\frac{-VF}{RT})\right\} \tag{4.27}$$

At the resting condition, there is no ionic flux through the membrane so total current is zero. I_{total} becomes zero when the term Y equals zero in Equation 4.25. After equating that term to zero the following equation is obtained

$$\frac{P_{Na}\left[Na\right]_{out} + P_K\left[K\right]_{out} + P_{Cl}\left[Cl\right]_{in}}{P_{Na}\left[Na\right]_{in} + P_K\left[K\right]_{in} + P_{Cl}\left[Cl\right]_{out}} = \exp(\frac{VF}{RT}) \tag{4.28}$$

If the membrane voltage is left alone, *GHK voltage equation* is obtained as

$$V = \frac{RT}{F}\ln\frac{P_{Na}\left[Na\right]_{out} + P_K\left[K\right]_{out} + P_{Cl}\left[Cl\right]_{in}}{P_{Na}\left[Na\right]_{in} + P_K\left[K\right]_{in} + P_{Cl}\left[Cl\right]_{out}} \tag{4.29}$$

Equation 4.29 gives the resting membrane potential when the membrane is permeable to more than one species and it gives the point where total current changes direction. If the membrane is permeable to only one specie, Equation 4.29 becomes Nernst potential of that specie. GHK voltage equation is used to calculate the resting membrane potential from the experimentally determined values which are the permeabilities and extracellular and intracellular concentrations.

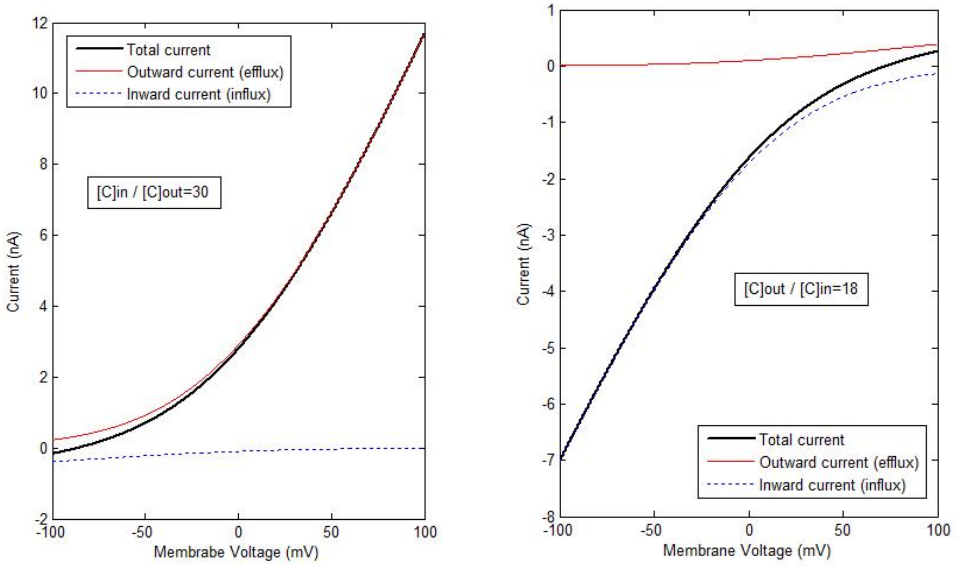

(a) High intracellular concentration. (b) High extracellular concentration.

Figure 4.3 Current-voltage relation according to GHK current equation.

Although GHK current equation can explain how current-voltage relation of the membrane is altered by concentration difference and how it is dependent on permeability, this relation is not as steep as observed [6]. During the formation of an unit signal (action potential) permeabilities of ions change with voltage so the ion channel concept is introduced. Every specie is selectively permeable through certain ion channels which open and close with voltage and this changes the permeabilities of the ions. However, instead of permeability of ions, conductances of ionic channels are included in the models.

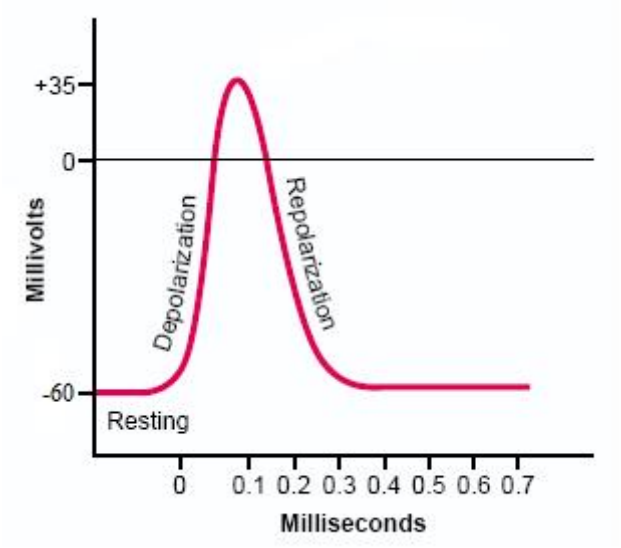

Figure 4.4 A representative action potential. (Modified from [5]).

4.2 Hodgkin-Huxley Formalism

The concentration difference of ions and movement of these ions across cell membrane let electrical signal formation. All the information in living organisms is carried in the form of this electrical signal. Unit electrical signal in a living body is called *action potential* (AP) and the cells that generate AP upon stimulation are called *excitable cells*. The striking characteristic of AP is that while it is transmitted by nerve cells even over long distances it is not attenuated because of its regenerative nature. Also an AP is formed in a "all or none" fashion which means AP is formed only when membrane potential exceeds a threshold value. A very simple sketch of an action potential is shown in Figure 4.4. The first question is how a nerve cell generates an electrical signal, and the second question is how this signal propagates without attenuation over a wide range of distances.

Alan Hodgkin and Andrew Huxley answered the first question by defining the cell membrane with an equivalent electrical circuit [24]. Their work is a milestone in biophysics and they got Nobel Prize in 1963 with this work. But the importance of their work is not because of the Nobel Prize they got, it is because Hodgkin-Huxley formalism is still valid and utilized with minor alterations today.

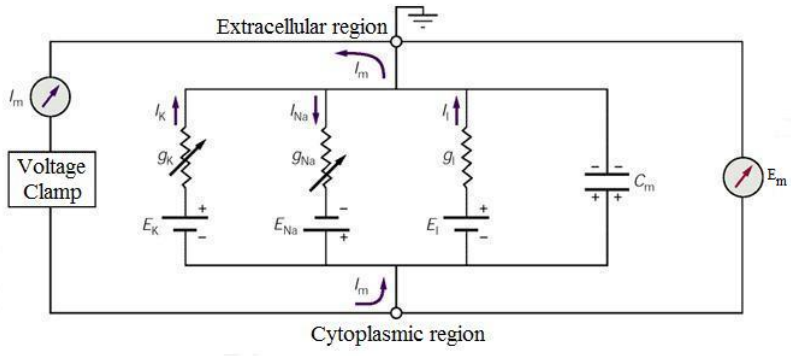

Figure 4.5 Equivalent circuit of membrane proposed by Hodgkin and Huxley. [1]

The first thing to be done was to explain movement of which ions contribute to the formation of an AP. An action potential was recorded by two separate groups; Kenneth Cole and Howard Curtis in the USA, Alan Hodgkin and Andrew Huxley in Britain [6]. What they observed was during the action potential ion conductances, in other means permeability to ions change dramatically. To specify conductances of which ions change most, Alan Hodgkin and Bernard Katz changed extracellular concentration of Na^+ ion and observed that amplitude of action potential decreases. This shows that rising phase of AP is mediated by influx Na^+. Their work also suggested that falling phase of AP was due to increase in permeability to K^+ ions which is led by efflux of these ions. Hodgkin and Huxley represented the membrane with the circuit in Figure 4.5.

Cell membrane acts as a capacitor since lipid bilayer separates conducting intracellular and extracellular solutions as an insulating layer. So they stated that "current can be carried through the membrane either by charging the membrane capacity or by movement of ions through the resistances in parallel with the capacity." [24]. Previously they had found that Na^+ and K^+ ions are the major components in the formation of an action potential. So in their model they included I_{Na} and I_K as ionic currents. In addition they included a "leakage current" component, I_l that is generated by movement of other ions. The permeability change of the membrane to Na^+ and K^+ ions are described as variable conductances whereas leakage current flows over a constant conductance. They

have shown that Na^+ conductance (g_{Na}) and K^+ conductance (g_K) are functions of time and voltage whereas E_{Na} (equilibrium potential of Na^+ ions), E_K (equilibrium potential of K^+ ions), E_l (equilibrium potential for ions that create leakage currents), C_m (membrane capacitance) and g_l (leakage conductance) are taken as constant. For the physical mechanism of how permeabilities change with time and membrane voltage, Hodgkin and Huxley proposed that specific gating particles for Na^+ and K^+ ions form a bridge and let the passage of these ions [24]. Following this idea, today it is known that there are ion channels which are membrane spanning proteins that let the passage of ions selectively through a pore that is formed after the protein has a conformational change due to varying electric field [1]. Sodium ion channels let only sodium ion flux, potassium channels let only potassium ion flux. Permeabilities of these ion channels change with voltage as proposed and they are called *voltage-gated ion channels*. Leakage current is formed by ion movement through resting channels which are independent of voltage and always open. All of these channels work independently from each other, so conductances that they constitute are work in parallel and also shown in the electrical circuit as parallel. Equilibrium potentials of ions are added as voltage sources in the equivalent circuit and the net potential over the conductances are $V_{membrane} - E_{Na,K,l}$. The reason for this is since electrochemical driving force changes direction when membrane voltage crosses equilibrium potential, current that is resulted from the movement of ions also change directions. It should be noted that, polarities of E_{Na} and E_K are opposite to each other since their concentration gradients are different: Na^+ is more concentrated in extracellular side than intracellular side whereas K^+ is more concentrated in intracellular side than extracellular side. Also it should be mentioned that by convention the reference point is taken as extracellular side and currents that are from inside to outside are to be positive.

The next step in the model is to find how g_{Na} and g_K depends on voltage and time. At this point it is important to mention one method that Hodgkin and Huxley utilized while determining voltage dependence of conductances. The method

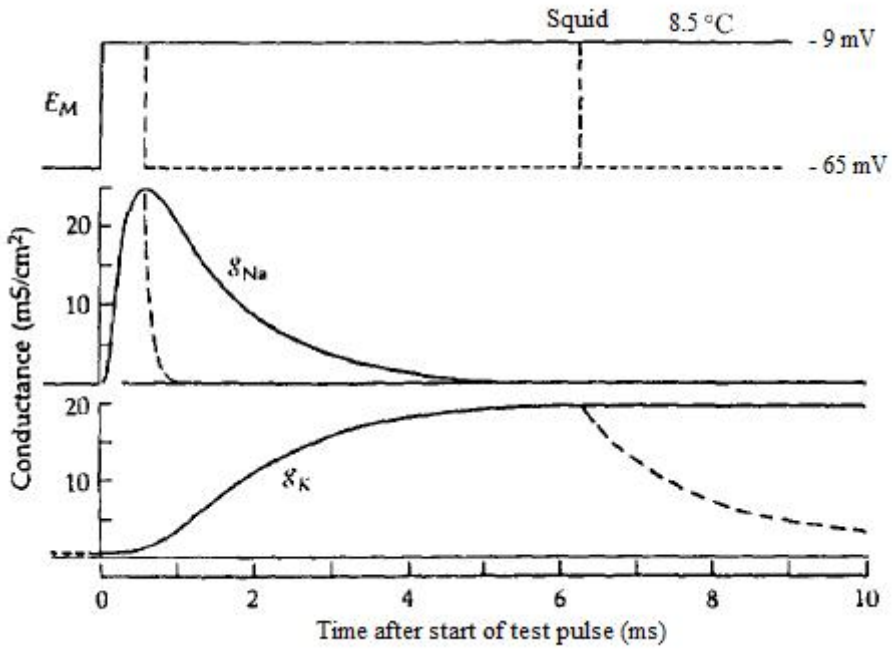

Figure 4.6 Changes in g_K and g_{Na} when membrane potential is stepped from -65 mV to -9 mV. [6]

is called *voltage clamp.* Basic duty of voltage clamp is to hold the membrane potential at a fixed command voltage. This is done by injecting a current that is "equal and opposite to the current flowing through the voltage-gated membrane channels" [1]. By this way at a specific command voltage, the current flowing through membrane can be determined and hence conductance at that that voltage value is determined. To find g_{Na} and g_K one kind of channel can be blocked selectively. Tetrodotoxin is a substance which has an affinity to bind to the opening pore of sodium channels and block these channels and prevent sodium current. After injecting tetrodotoxin, with voltage clamp g_K can be found. Subtracting this conductance value from the total conductance at that voltage level would give us g_{Na}. Hodgkin and Huxley used squid giant axon in their experiments.

In Figure 4.6 membrane voltage, E_M is stepped from -65 mV to -9 mV and corresponding changes in g_K and g_{Na} are shown with bold traces. It is seen that if the voltage is kept at -9 mV, g_K reaches a maximum value following an S-

shaped curve whereas g_{Na} drops back to its initial value after reaching a peak. If the voltage is droped back to its resting value, -65 mV, g_{Na} also drops to its resting value immediately (dashed line in g_{Na} plot). In the same manner, with voltage step down, g_K also drops to its resting value but more slowly than g_{Na} and not following an S-shaped curve; it drops exponentially. So the opening and closing dynamics of g_K and g_{Na} are different. Hodgkin and Huxley found empirical equations that would fit the experimentally found data points. So for the conductance of K^+ ions they proposed the following mechanism:

$$g_K = \overline{g_K} n^4 \tag{4.30}$$

where $\overline{g_K}$ is the maximum conductance and n is the probability of potassium gating particle to be in the open position. Here HH model assumes that for the passage of K^+ ions 4 activating particles must be in open position. So this n^4term explains the variable conductance. The transition of activating particles between open state and closed state is represented by a first order reaction:

$$1 - n \underset{\beta_n}{\overset{\alpha_n}{\rightleftharpoons}} n \tag{4.31}$$

where $1 - n$ is the probability of gating particle to be in closed state, α_n is the voltage dependent forward rate constant that defines the rate of particles going from closed state to open state, β_n is the voltage dependent backward rate constant that defines rate of particles going from open state to closed state. n is a dimensionless variable and the rate constants have the dimension of $[time]^{-1}$.

The time dependence of n is given by

$$\frac{dn}{dt} = \alpha_n(1 - n) - \beta_n n \tag{4.32}$$

If the membrane voltage is kept constant for a long time, n will reach steady state value, n_∞, and $\frac{dn}{dt}$ term will vanish:

$$n_\infty = \frac{\alpha_n}{\alpha_n + \beta_n} \tag{4.33}$$

When membrane voltage is changed, it would take some time for n and consequently for g_K to reach its final value from its initial value. If Equation 4.33 is

reorganized and inserted in Equation 4.32 the following is obtained:

$$\frac{dn}{dt} = \alpha_n - (\alpha_n + \beta_n)n = n_\infty(\alpha_n + \beta_n) - (\alpha_n + \beta_n)n = (\alpha_n + \beta_n)(n_\infty - n) \quad (4.34)$$

After reorganizing and integrating

$$\ln(n_\infty - n) = -(\alpha_n + \beta_n)t + C \quad (4.35)$$

is got where C is constant resulting from the integration. Leaving n alone

$$n = n_\infty - A\exp^{-(\alpha_n+\beta_n)t} \quad (4.36)$$

is reached. Using the initial condition $n_0 = n(t = 0)$, A is found to be $(n_\infty - n_0)$. So the final equation will take the following form

$$n = n_\infty(1 - \exp^{-(\alpha_n+\beta_n)t}) + n_0\exp^{-(\alpha_n+\beta_n)t} \quad (4.37)$$

Equation 4.37 states that when voltage is altered, probability of activating particle for K^+ ion to be in open state goes from n_0 to $n_\infty$with a time constant of $\tau_n = \frac{1}{\alpha_n+\beta_n}$. If n_∞ is divided by τ_n, α_n would be obtained;

$$\frac{n_\infty}{\tau_n} = \frac{\frac{\alpha_n}{\alpha_n+\beta_n}}{\frac{1}{\alpha_n+\beta_n}} = \alpha_n \quad (4.38)$$

Since n_∞ and τ_n can be obtained experimentally at every voltage level, by Equation 4.38 α_n at every voltage level can be found. In the same manner from Equation 4.33 β_n can be driven as

$$\beta_n = \frac{\alpha_n(1 - n_\infty)}{n_\infty} = \frac{\frac{n_\infty}{\tau_n}(1 - n_\infty)}{n_\infty} = \frac{1 - n_\infty}{\tau_n} \quad (4.39)$$

So knowing n_∞ and τ_n for certain voltage levels, voltage dependence of β_n can be found. Knowing function forms of α_n and β_n, n can be found at different voltage levels and hence K^+ ion current can be found by the following relation,

$$I_K = \overline{g_K}n^4(E_M - E_K) \quad (4.40)$$

Sodium ion channel has a different mechanism than potassium ion channel. In Figure 4.6, when membrane voltage is sustained at a fixed value potassium conductance reaches a maximum steady state value. However, sodium conductance

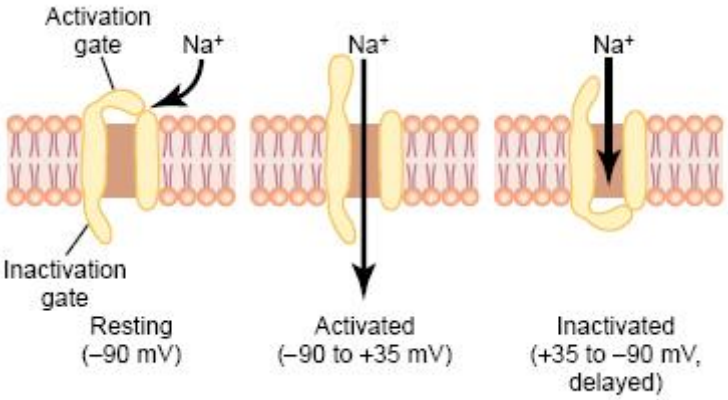

Figure 4.7 Representative schematic of sodium channels. [5]

returns back to its resting value. In this regard, Hodgkin and Huxley proposed that, Na^+ channel is composed of 4 particles, 3 of them activating and 1 is inactivating. For the channel to conduct, all four particles should be in open position. m represents the probability of Na^+ channel activating particle to be in open position and h represents the probability of Na^+ channel inactivating particle to be in open position. Sodium channels can be visualized as in Figure 4.7.

At resting membrane potential, m is low, which means activating particles are in closed state, whereas h is high, which means inactivating particle is in open state. As depolarization starts, m starts to rise rapidly and h starts to fall slowly. So the dynamics of activating particles are faster than dynamics of inactivating particle which causes the sodium channel to be permeable for sodium ions. Here it should be noted that, as membrane potential increases, sodium channels will open and with the inflow of sodium ions membrane potential will increase further, which will cause more sodium channels to open. If there were no inactivating particles involved in sodium channel like potassium channel, because of the positive feedback the membrane potential would increase until many sodium ions flow into the cell and electrochemical force over sodium ions become zero. However, as the potential increases inactivating particle gets closer to closed state and at one point it closes the channel so sodium inflow is interrupted. Inactivating particle is the reason why sodium conductance falls to its resting value after reaching

a peak value. Empirical formula that is proposed by Hodgkin and Huxley is

$$g_{Na} = \overline{g_{Na}} m^3 h \tag{4.41}$$

where $\overline{g_{Na}}$ is the maximum conductance. As for the potassium channel activating particle n, transitions of m and h are modeled as first order reaction;

$$1 - m \underset{\beta_m}{\overset{\alpha_m}{\rightleftharpoons}} m \tag{4.42}$$

$$1 - h \underset{\beta_h}{\overset{\alpha_h}{\rightleftharpoons}} h \tag{4.43}$$

where α_m and α_h are forward rate constants as going from closed state to open state, β_m and β_h are backward rate constants as going from open state to closed state. Time dependence of m and h are given as

$$\frac{dm}{dt} = \alpha_m(1 - m) - \beta_m m \tag{4.44}$$

$$\frac{dh}{dt} = \alpha_h(1 - h) - \beta_h h \tag{4.45}$$

and with the very same derivation that is done for potassium activating particles steady state values and time constants of m and h are found as

$$m_\infty = \frac{\alpha_m}{\alpha_m + \beta_m} \tag{4.46}$$

$$h_\infty = \frac{\alpha_h}{\alpha_h + \beta_h} \tag{4.47}$$

$$\tau_m = \frac{1}{\alpha_m + \beta_m} \tag{4.48}$$

$$\tau_h = \frac{1}{\alpha_h + \beta_h} \tag{4.49}$$

Then, α_m is equal to $\frac{m_\infty}{\tau_m}$ and α_h is equal to $\frac{h_\infty}{\tau_h}$. Also β_m equals to $\frac{1-m_\infty}{\tau_m}$ and β_h equals to $\frac{1-h_\infty}{\tau_h}$. Final form of Na^+ current has the following form

$$I_{Na} = \overline{g_{Na}} m^3 h (E_M - E_{Na}) \tag{4.50}$$

Noting that current over leakage channels is $g_l(E_M - E_l)$ the total ionic current over cell membrane is

$$I_{\text{total ionic}} = I_{Na} + I_K + I_l = \overline{g_{Na}} m^3 h (E_M - E_{Na}) + \overline{g_K} n^4 (E_M - E_K) + g_l(E_M - E_l) \tag{4.51}$$

With the summation of total ionic current and the capacitive current total membrane current can be found.

$$I_{total} = C_m \frac{dE_M}{dt} + \overline{g_{Na}} m^3 h (E_M - E_{Na}) + \overline{g_K} n^4 (E_M - E_K) + g_l (E_M - E_l) \quad (4.52)$$

If a stimulus is applied to the excitable cell, stimulus current I_{stim} should be added to the right hand side of Equation 4.52 and if the amplitude of the stimulus is large enough excitable cell would fire an action potential. Solving Equation 4.52 for membrane voltage E_M numerically would give the shape of the action potential.

Formation of action potential waveform is because of the difference of dynamics of ion channels. Principally with increasing voltage, activating gates of Na^+ and K^+ channels open and inversely, inactivating gates of Na^+ channels closes. If the membrane voltage of an excitable cell starts to rise with stimulation, Na^+ activating particles start to get into open position and Na^+ ion channels open. Because the opening dynamics of activating particles of Na^+ channel is faster that closing dynamics of inactivating particles of Na^+ channel and initially inactivating particles are in open position, Na^+ channel stays open for a while. During this time Na^+ ions flow into the cell and increase the membrane voltage further. As voltage increases, more Na^+ channels open. By this way a steep depolarization, namely the rising phase of the action potential, occurs. At the same time activating particles of K^+ channels start to get into open position but more slowly than activating particles of Na^+ channels. So an efflux of K^+ starts.

When inactivating particles of Na^+ channels get into closed position, Na^+ channels cannot let passage of Na^+. So further depolarization is not possible by Na^+ ions. As the channels for K^+ are open, K^+ outflows and decreases the membrane potential. Although membrane potential reaches its resting value, K^+ channels cannot close immediately and efflux of K^+ hyperpolarizes the membrane. As all voltage-gated channels are closed, flow through leakage channels bring the membrane potential back to its resting value. So the component that keeps the membrane voltage at a negative value (this resting membrane voltage values

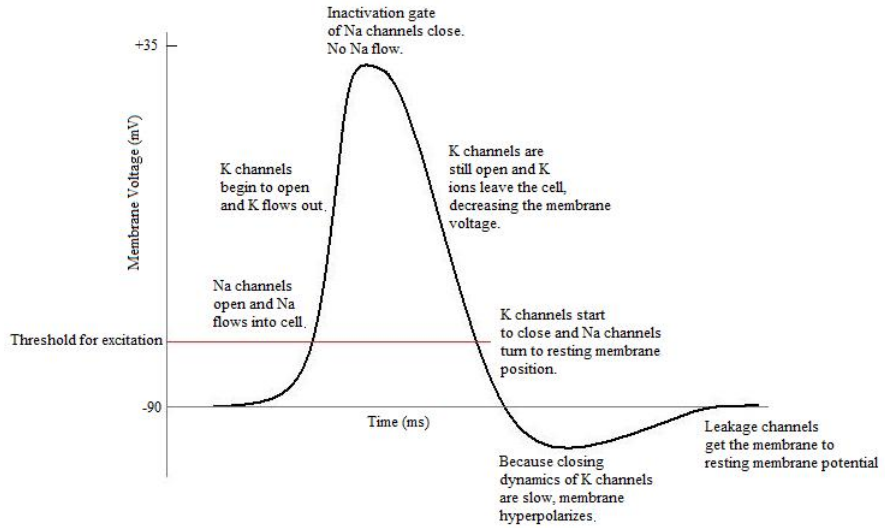

Figure 4.8 The conditions of ion channels at different phases of an action potential.

changes from species to species, it is not the same in all living organisms.) is the leakage current through leakage channels that are open all the time.

4.3 Propagation of Action Potential Along Neuron

Information flow in the nervous system occurs with the propagation of initiated action potentials. When an excitable cell produces an AP, it travels through axon and dendrites of the cell which have passive parts, the parts that cannot generate AP. Propagation of electrical signals through these passive parts are determined by the three passive electrical properties of the neuron; membrane resistance, membrane capacitance and intracellular axial resistance along axons and dendrites [1].

A passive spherical neuron membrane is modeled by a parallel resistor and capacitor. Leakage channels that are independent of membrane voltage and open all the time is modeled as the resistor, R_m, and the lipid bilayer membrane is modeled as a capacitor, C_m. A passive neuron does not involve voltage-gated ion channels so the value of the resistor is constant. When a stimulating current I_s is applied to the membrane, it will dissociate into two components; current

flowing over the resistor I_r and current flowing over the capacitor I_c, so that $I_s = I_r + I_c$. Since the components are in parallel, voltage across resistor, E_r, and voltage across capacitor, E_c, will be equal to each other and to membrane potential E. By using Ohm's law E_r can be found as

$$E_r = I_r \cdot R_m \tag{4.53}$$

Current over the capacitor is found as such

$$I_c = C_m \frac{dE_C}{dt} \tag{4.54}$$

Replacing E_r in Equation 4.53 with E and I_r with $I_s - I_c$ the following equation is obtained

$$E = (I_s - I_c) \cdot R_m \tag{4.55}$$

Putting Equation 4.54 in Equation 4.55, Equation 4.56 is obtained

$$E = (I_s - C_m \frac{dE_C}{dt}) \cdot R_m \tag{4.56}$$

Noting that $E_c = E$, Equation 4.56 takes the following form

$$E = (I_s - C_m \frac{dE}{dt}) \cdot R_m \tag{4.57}$$

Rearranging Equation 4.57 gives the following differential equation

$$R_m C_m \frac{dE}{dt} + E = I_s R_m \tag{4.58}$$

Under the assumption of zero initial conditions solution of Equation 4.58 is

$$E = I_s R_m (1 - \exp^{\frac{-t}{R_m C_m}}) \tag{4.59}$$

$R_m C_m$ multiplication is the time constant of the membrane and represented by τ_m. It shows how fast the membrane capacitance charges under current stimulation and how fast it discharges when there is no stimulation. Under sustained stimulation, as time goes to infinity membrane potential in Equation 4.59 reaches a constant value as $E = E_\infty = I_s R_m$. Responses of a model circuit with $R_m = 1\Omega$, $C_m = 1F$ to current pulses with durations $12s$ and amplitudes $1mA$ and $2mA$

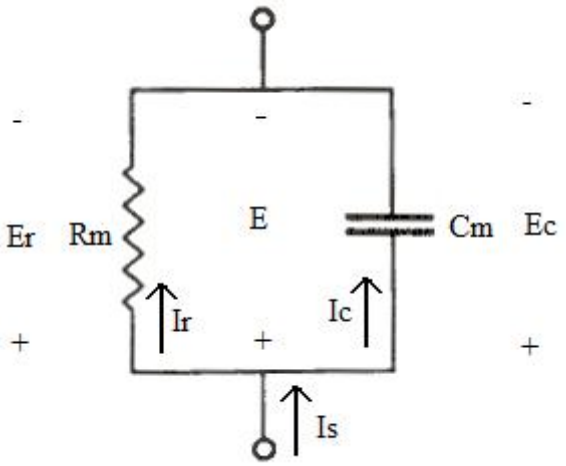

Figure 4.9 A simple RC circuit.

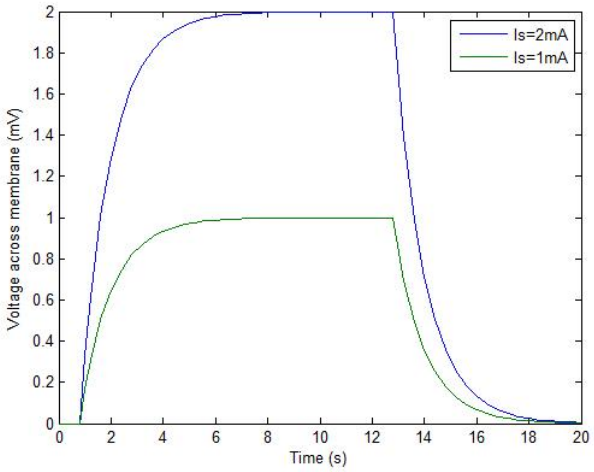

Figure 4.10 Responses of a model RC circuit to input current pulses.

are shown in Figure 4.10; membrane potential starts to rise with the start of the current pulse at $Time = 1s$ and reaches a steady value of $1mV$ for $1mA$ input and $2mV$ for $2mA$ input. As the input vanishes at $Time = 13s$, membrane voltage immediately starts to fall to its initial value.

If the capacitance of the model is changed under the same stimulation then timing of the signal will change. Responses of two models with different capacitances to the same current input of $1mA$ are shown in Figure 4.11. Model circuit with higher capacitance has a higher time constant which means that dynamics of it is slower than the one with lower capacitance; membrane voltage with the lower

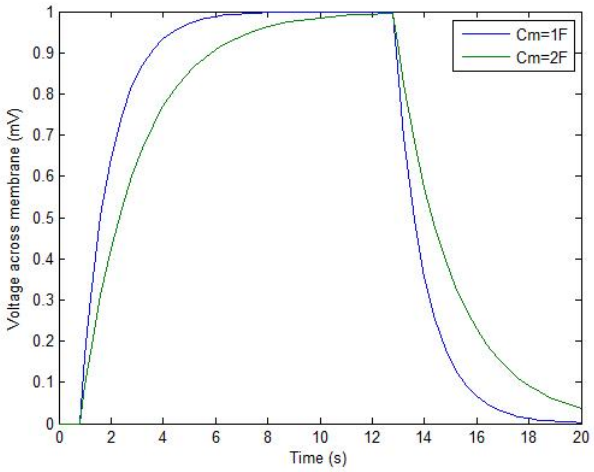

Figure 4.11 Responses of two models with different capacitances to same current stimulus.

capacitance reaches its final value quicker than the one with higher capacitance. For cell membrane, capacitance is proportional to the area of the membrane, so it is harder to charge bigger cells.

Neurons have complex morphologies and only soma of the neuron can be approximated to be spherical. It is more realistic to approximate the shapes of axon and dendrites to a cylinder. For this geometry, spread of the electrotonic voltage (membrane voltage that is not regenerative like action potential) along homogeneous axon and dendrites was first modeled by Rall [25, 26] with the following assumptions:

- Membrane of the axon is homogeneous which means capacitance and resistance of the membrane is constant along the axon.
- Membrane properties like membrane capacitance and membrane conductance are voltage independent and constant which means membrane is passive.
- Axon is a cylinder.
- Resistance of the extracellular fluid is negligible.

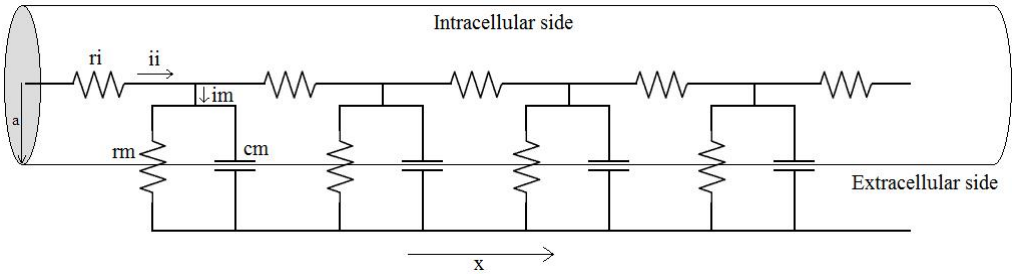

Figure 4.12 Model of an axon.

With these assumptions an axon is approximated as in Figure 4.12 and time and space dependence of membrane voltage can be driven. In Figure 4.12 r_m represents the membrane resistance, c_m represents the membrane capacitance, r_i is the intracellular axial resistance, i_m is the current through membrane, i_i is the axial current along the axon and a is the radius of the axon.

When going from one node to the adjacent node in x direction, membrane voltage drops with the amount of voltage that is across the resistance r_i:

$$\frac{dV_m}{dx} = -r_i \cdot i_i \tag{4.60}$$

In addition, axial current i_i drops with an amount of i_m:

$$\frac{di_i}{dx} = -i_m \tag{4.61}$$

Taking the derivative of Equation 4.60 and putting Equation 4.61 in it the following equation is obtained:

$$\frac{d^2V_m}{dx^2} = i_m \cdot r_i \tag{4.62}$$

$$\frac{1}{r_i}\frac{d^2V_m}{dx^2} = i_m \tag{4.63}$$

Membrane current is composed of two components; one is the current over membrane resistance, i_r, and the other is current over the membrane capacitance, i_c.

$$i_m = i_r + i_c = \frac{V_m}{r_m} + c_m\frac{dV_m}{dt} \tag{4.64}$$

After equating Equation 4.63 and Equation 4.64 and rearranging, *cable equation of Rall* is obtained:

$$\frac{1}{r_i}\frac{\partial^2V_m}{\partial x^2} - \frac{V_m}{r_m} = c_m\frac{\partial V_m}{\partial t} \tag{4.65}$$

Equation 4.65 shows the time and space dependence of membrane voltage of a homogeneous cylindrical axon.

To compare passive membrane properties of neurons of differing sizes, three different values are defined; *specific intracellular resistance,* R_i in units of $\Omega.cm$, *specific membrane resistance,* R_m in units of $\Omega.cm^2$, *specific membrane capacitance,* C_m in units of F/cm^2. R_m and C_m are defined with respect to $1cm^2$ membrane area; as area gets bigger the number of resting ion channels will increase which in turn decreases the membrane resistance but bigger area means bigger capacitance.So to find the resistance and capacitance of a cylindrical membrane with length l and radius a, R_m should be divided by $2\pi al$ and C_m should be multiplied with $2\pi al$, respectively. R_i represents the resistivity of the biological cable; resistance of a cable decreases with increasing area and increases with increasing length and the proportionality constant is called resistivity, ρ. So resistance of a cable with length l and cross-sectional area A is given by $R = \rho\frac{l}{A}$ in Ω. To find passive properties of a cylindrical axon membrane of unit length, the following equations are used:

$$r_m = \frac{R_m}{2\pi a} \tag{4.66}$$

where r_m is in $\Omega.cm$,

$$c_m = C_m 2\pi a \tag{4.67}$$

where c_m is in F/cm,

$$r_i = \frac{R_i}{\pi a^2} \tag{4.68}$$

where r_i is in Ω/cm.

One very important constant is the *length constant* and it is defined as

$$\lambda = \sqrt{\frac{r_m}{r_i}} = \sqrt{\frac{a.R_m}{2R_i}} \tag{4.69}$$

and it has the units of cm. By using length constant and time constant, dimensionless variables can be derived and Equation 4.65 can be made dimensionless. Dimensionless length is $X = x/\lambda$ and dimensionless time is $T = t/\tau_m$. Multiplying both sides of Equation 4.65 by r_m and replacing the dimensionless variables

X and T the following equation is obtained:

$$\frac{\partial^2 V_m}{\partial X^2} - V_m = \frac{\partial V_m}{\partial T} \tag{4.70}$$

At steady state Equation 4.70 takes the following form

$$\frac{\partial^2 V_m}{\partial X^2} - V_m = 0 \tag{4.71}$$

which has the general solution as

$$V_m = V_0 e^{-X} = V_0 e^{-\frac{x}{\lambda}} \tag{4.72}$$

As moving along the axon in x direction, voltage will decrease according to Equation 4.72 and at every length constant the amplitude of the signal drops to the $1/e$ of the original voltage. So along an axon with big length constant, the signal will travel long distances with less attenuation in comparison to propagation along an axon with smaller length constant. As the length constant is proportional to the square root of axon radius, signals will travel longer distances with less attenuation along axons which have big radius. By definition propagation speed of the electrotonic voltage is given as

$$\Theta = \frac{2\lambda}{\tau_m} = \sqrt{\frac{2a}{R_m R_i C_m^2}} \tag{4.73}$$

It can be seen that propagation speed is proportional to square root of radius which means that to increase propagation speed, axon diameter should increase. Since any living organism seeks food and escapes from possible dangers to survive, they should move fast. Fast movement requires fast signaling so that muscles rapidly contract and escape movements can be done. In order to increase propagation speed, axon diameter gets bigger and that is why giant axons can be found in invertebrates (creatures without spine, like squid). However, in vertebrates operation of nervous system requires too many fast conducting fibers for processes like maintenance of posture, reflexes, motor actions and if axon diameters increase to provide the necessary propagation speed, bundles of fibers will be gigantic and occupy a lot of space. In the process of evolution, this problem

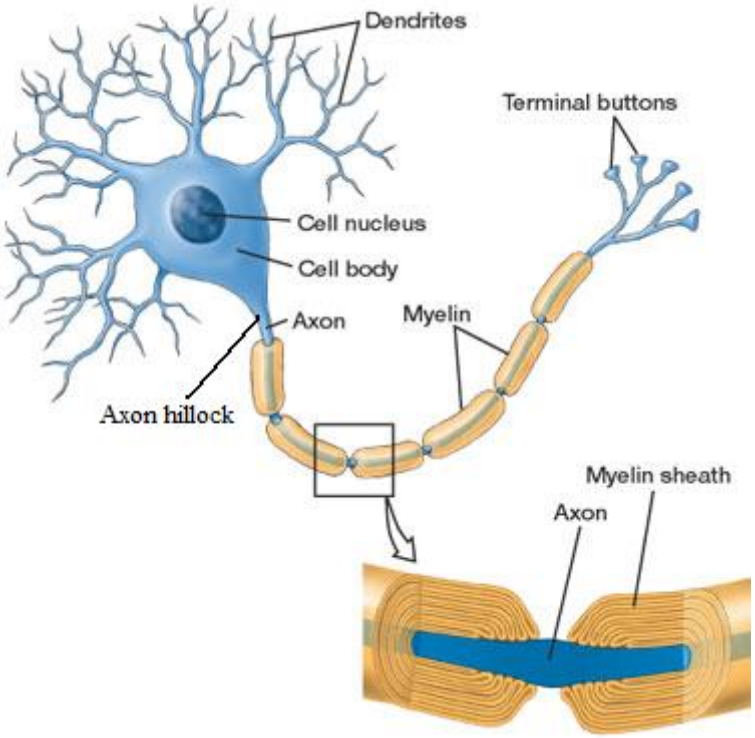

Figure 4.13 Schematic of a neuron (cwx.prenhall.com).

is solved by myelin coated fibers [29]. Myelin is an insulating material that is wrapped around the axon and it is reported that myelin sheath increases the specific membrane resistance with 60 fold whereas decreases the specific membrane capacitance with 20 fold. Schematic of a neuron with myelinated axon is given in Figure 4.13. Certain points of the axon do not posses myelin sheath and these parts are called *node* and the parts that are wrapped by myelin are called *paranode*. Action potential is initiated at the axon hillock where a high concentration of voltage gated sodium ion channels is present [47]. As the signal attenuates while traveling along paranodes, not to lose information, action potential is regenerated at the adjacent node again. This way of propagation is called *saltatory conduction* since only at nodes action potentials are seen [27]. Nodes of an axon are excitable parts and paranodes are the passive parts.

As the specific membrane resistance increases, length constant also gets bigger, so that signal can propagate long distances with little attenuation with respect to unmyelinated fibers. This implies that myelinated fibers are energetically ad-

vantageous over unmyelinated fibers. Because an initiated action potential can propagate through myelinated fiber longer distances, so the transmission of the signal can be achieved by less nodes. However, in unmyelinated fibers, to restore the action potential, nodes should be placed closer to each other in comparison to myelinated fibers so number of nodes increases and the energy that is spent to restore and keep the ion concentrations at resting conditions increases. In addition in myelinated fibers propagation velocity gets bigger as it is inversely proportional to $\sqrt{R_m}$ and C_m.

Cable equation is derived under the assumption of homogeneous fiber. However, as it can be seen from the schematic of the neuron in Figure 4.13 and more specifically from the actual figures of neurons that will be used in this study in Figure 3.5 and Figure 3.7 neuron not uniform, it has a highly non-uniform shape. Soma has a spherical shape whereas dendrites and axon are cylindrical in shape. Furthermore, axon is divided into many parts as nodes and paranodes where nodes are excitable, in other words they posses voltage-gated ion channels, however, paranodes are passive elements with only passive components. To overcome this difficulty compartmental modeling is utilized. In this type of modeling neuron is decomposed into parts which are homogeneous separately. Three adjacent compartments are shown in Figure 4.14 and they are modeled as RC circuits. It should be noted that if one of the compartments is excitable, then that part is modeled as in Figure 4.5, voltage gated ion channels are also added to the model.

Membrane current, i_m, over J^{th} part is found by applying Kirchhoff's current law at J^{th} node:

$$i_m = i_{J-1,J} - i_{J,J+1} \tag{4.74}$$

where $i_{J-1,J}$ is the current flowing from $J-1^{th}$ node to J^{th} node and $i_{J,J+1}$ is the current flowing from J^{th} node to $J+1^{th}$ node. Axoplasmic resistance, r_j in Figure 4.14, of one compartment is calculated according to its dimensions by the use of the specific intracellular resistance. While calculating the axoplasmic resistance between compartments, axoplasmic resistances of adjacent compartments

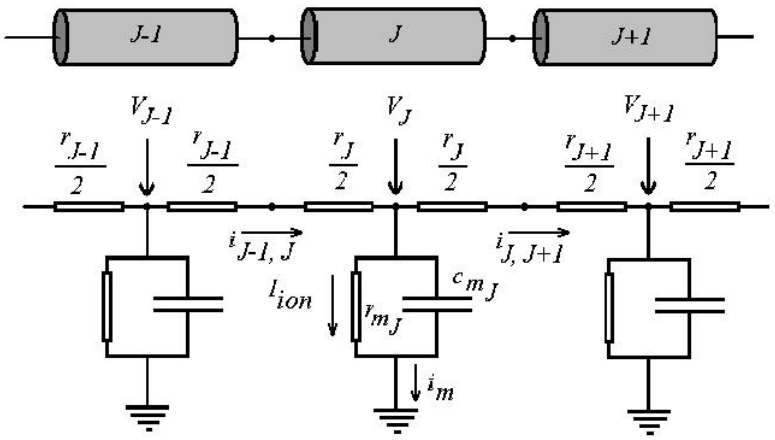

Figure 4.14 Adjacent compartments in a compartmental model.

are summed and divided by two. So Equation 4.74 can be rewritten as

$$i_m = \frac{V_{J-1} - V_J}{\frac{r_{J-1}+r_J}{2}} - \frac{V_J - V_{J+1}}{\frac{r_J+r_{j+1}}{2}} \tag{4.75}$$

Membrane current can be decomposed into two components as ionic current and capacitive current:

$$i_m = I_{ion} + c_{m_j}\frac{dV_j}{dt} \tag{4.76}$$

If there is an external current input, I_{ext}, addition of this current on the right side of Equation 4.76 and combining with Equation 4.75 will give the following equation:

$$I_{ion} + c_{m_j}\frac{dV_j}{dt} + I_{ext} = \frac{V_{J-1} - V_J}{\frac{r_{J-1}+r_J}{2}} - \frac{V_J - V_{J+1}}{\frac{r_J+r_{j+1}}{2}} \tag{4.77}$$

Numerical solution of Equation 4.77 for voltage at every compartment at any instant, will give the propagation of signal along the axon that is comprised of the compartments.

CHAPTER 5

SYNAPTIC TRANSMISSION

In the complex network of neurons in the nervous system, synapses are the nodes that connect neurons to each other and direct the flow of information. Transmission of signals along synapses is achieved by secretion of neurotransmitters. Types of the receptors that neurotransmitters bind determine the types of the synapses as being excitatory or inhibitory. In this chapter, firstly general characteristics of synapses and mechanism of synaptic transmission are examined and after that types of neurotransmitters and properties of inhibitory and excitatory synapses are explained.

5.1 General Characteristics of Synapses

Signal transmission between the neurons of central nervous system is achieved by chemical synapses. Here synapse refers to the contact zone between neurons that are communicating. In fact, neurons on both sides of the synapse do not form a continuum, they are separated by a region called synaptic cleft. Neuron which conveys signal to the synapse is called pre-synaptic neuron and the neuron that rests at other side of the synapse is called post-synaptic neuron. Schematic of a synapse is shown in Figure 5.1.

The word "chemical" in the phrase "chemical synapse" indicates that electrical signal gets through the synapse by the help of chemicals which are called neurotransmitters. For a substance to be called as neurotransmitter four criteria must be fulfilled [1]:

1. It must be synthesized in the neuron.

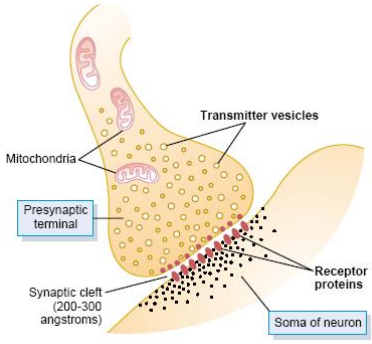

Figure 5.1 Schematic of a synapse [5].

2. It must be contained by presynaptic neuron and after its release it must have a specific action on the postsynaptic neuron.

3. Upon injecting into the body, it must have the same effect that is induced when it is released from the presynaptic neuron.

4. It should be removed from the synaptic cleft by a specific mechanism.

Regarding the spinal cord, mainly two amino acid transmitters are used for excitation and inhibition, glutamate and γ-aminobutyric acid (GABA) respectively [35, 2]. Structures of both molecules are shown in Figure 5.2. Here it should be noted that the response of the postsynaptic cell, whether it is excitatory or inhibitory, is not determined by the neurotransmitter that is released by the presynaptic cell; the effect is determined by the receptors of the postsynaptic neuron that transmitters bind. In a simple analogy, transmitters are the keys and receptors are the doors and ions that will pass is determined by the door itself.

(a) Glutamate (b) GABA

Figure 5.2 Structures of amino acid transmitters [1].

Receptors are divided into two main groups, ionotropic and metabotropic receptors. In ionotropic receptors the receptor and the ion channel that it gates are parts of the same protein [48]. As the neurotransmitter binds to the receptor, protein undergoes a conformational change which leads to opening of a passage through the protein that lets transport of specific ions. Whereas metabotropic receptors gates ion channels indirectly. Upon binding of a neurotransmitter, related cytoplasmic proteins produce diffusible second messengers which triggers biochemical cascades in the cytoplasm. After these processes ion channels can be opened or closed, but more importantly metabolic machinery and structure of the neuron can be altered.

According to "speed of onset and duration of the postsynaptic effect", actions of transmitters on receptors are classified as being slow or fast [1]. Gating of ion channels through ionotropic receptors is on the order of milliseconds and referred as being fast. On the other hand, gating of ion channels through metabotropic receptors is slower; onset of the postsynaptic effect takes tens of milliseconds to seconds and duration of the effect takes second to minutes, which is because of the cascade of biochemical reactions that is involved [1]. Moreover, physiological functions of these two types of receptors differ; ionotropic receptors excite or inhibit a neuron. They do not alter the electrophysiological properties of

cells, only act as on-off switches. On the other hand, although slow dynamics of metabotropic receptors prevents them to generate an action potential, they can change the electrophysiological characteristics of cell, namely resting membrane potential, threshold potential, length and time constants and input resistance [1]. This means that metabotropic receptors modulates synaptic actions by having long term influence on membrane characteristics.

Sensory signals, namely vision, audio, touch, pain etc., are transmitted rapidly in the central nervous system and that is way in this study, receptors in the synapses of the gate control system are to be ionotropic receptors. Long term modulation of these synapses by action of metabotropic receptors will not be considered.

5.2 Mechanism of Synaptic Transmission

Transmission of an action potential across a synapse involves a cascade of biochemical reactions. For the transmission to occur, neurotransmitters must be released into synaptic cleft. Neurotransmitters are packed in synaptic vesicles and these vesicles are accumulated in active zones, which are transmitter release sites. This series of reactions is triggered by the action potential that arrives to terminal of presynaptic neuron. Upon arrival of this action potential, voltage-gated calcium ion (Ca^{2+}) channels open and since extracellular Ca^{2+} concentration is much higher than intracellular Ca^{2+} [5], an influx of Ca^{2+} ions occurs. This is depicted in Figure 5.3. With the influx of Ca^{2+} ions, Ca^{2+} concentration near active zones increases and this high concentration of Ca^{2+} causes synaptic vesicles to fuse with presynaptic cell membrane and release the neurotransmitter molecules into synaptic cleft. Release of transmitters into synaptic cleft is called exocytosis.

After releasing their neurotransmitter content, synaptic vesicles are taken into the cell and processed to form new vesicles. Transmitters diffuse in the synaptic cleft and bind to their respective receptors and make them open or close. But in the case of ionotropic receptors, transmitters only cause them to open. As the

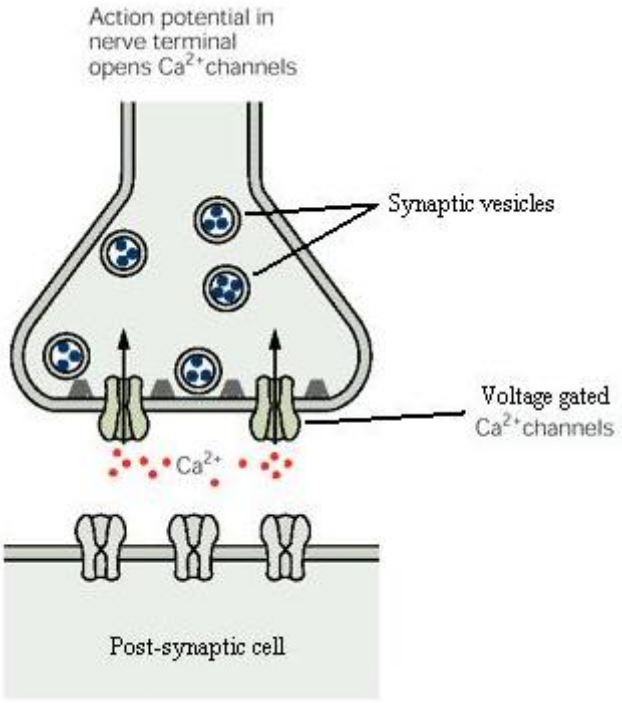

Figure 5.3 After opening of calcium channels, inflow of calcium ions increase intracellular calcium concentration [1].

receptor-channels open, conductance of the membrane of postsynaptic cell increases and Na^+ ions flow into the cell, causing membrane potential to increase. This increase of voltage is called excitatory postsynaptic potential (EPSP) and the Na^+ current that is mediated by Na^+ influx is called excitatory postsynaptic current (EPSC). When the neurotransmitter is inhibitory, upon binding to inhibitory receptors, Cl^- ions will flow into the cell and decrease the postsynaptic membrane potential. This decrease in membrane potential is called inhibitory postsynaptic potential (IPSP) and the Cl^- current is called inhibitory postsynaptic current (IPSC).

It should be noted that, EPSP that is mediated by the action of only one terminal is not sufficient to make postsynaptic cell to fire an action potential. Simultaneous EPSPs should be summed to cause the postsynaptic cell to fire an action potential. Alternatively, as excitatory inputs elevate postsynaptic membrane potential, competing inhibitory inputs may decrease the potential, pre-

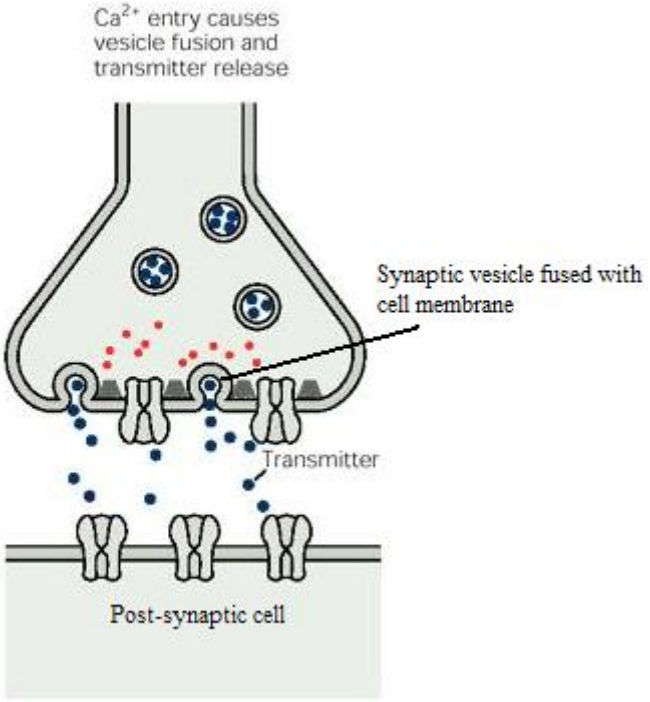

Figure 5.4 After synaptic vesicles fused with cell membrane, transmitter molecules are released into synaptic cleft [1].

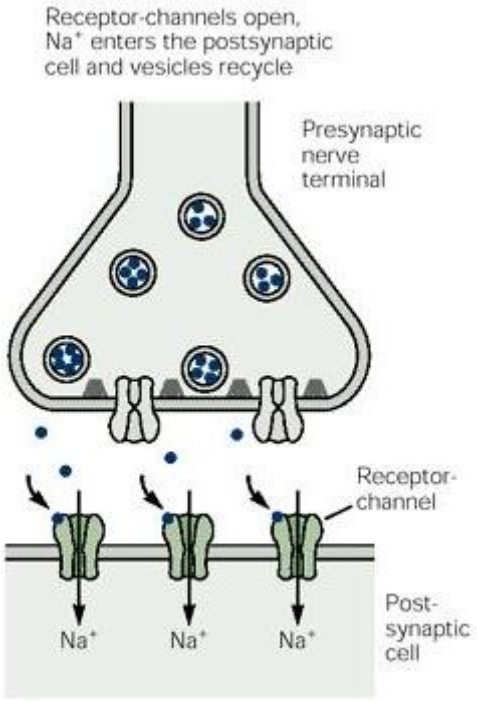

Figure 5.5 Upon binding of transmitters, receptor-channels open and Na^+ influx increases postsynaptic membrane potential [1].

venting postsynaptic cell from firing an action potential. Synaptic integration of different inputs is the basis for the fundamental operation of brain: decision making [1]. Inputs are integrated in two different aspects; temporally and spatially. Temporal summation is the addition of consecutive synaptic potentials at the same site. If the time constant of the cell is long enough, before potential that is mediated by the first input attenuates, potential that is created by the second input adds up to the previous potential and postsynaptic potential gets closer to threshold voltage for action potential initiation. If the time constant of the cell is not long enough, the two consecutive potentials cannot add up since until second input is received, potential that is created by first input diminishes. Spatial summation is related to the integration of potentials that are generated at different sites. If the length constant of a neuron is long enough, signal can propagate with minimum attenuation so potentials that are formed at different sites can be summed before any one of them dies out. In this regard, besides electrophysiological properties of neurons, the location of the synapses and their relative strengths are important factors that determine synaptic integration.

5.3 Glutamate and GABA Receptors

As mentioned before in the central nervous system main excitatory and inhibitory neurotransmitters are glutamate and GABA, respectively. Although these transmitters can gate both ionotropic and metabotropic receptors, for gate control system only ionotropic receptors will be considered due to their fast dynamics. The substantia gelatinosa (lamina II) and lamina I of spinal cord are major targets that receive heavy primary afferent input that is related with nociception and also skin sensory neurons [16, 49] so these two layers take part in the modulation of pain signals. The kinds of receptors and transmitters that neurons of these two layers possess determines the synaptic action in the gate control system.

5.3.1 Glutamate Receptors

There are both ionotropic and metabotropic glutamate receptors in the central nervous system, however only ionotropic ones will be mentioned. Ionotropic glutamate receptors can be divided into three classes: 1) AMPA 2) Kainate 3) NMDA. These receptors are named according to the synthetic agonists (substance that makes receptor work, produce an action) that activate them; α-amino-3-hydroxy-5-methyl-4-isoxazolepropionic acid, kainate and N-methyl-D-aspartate, respectively [1]. Since AMPA and kainate receptors are very similar to each other they are also called as non-NMDA receptors. Non-NMDA receptors are permeable to Na^+ and K^+ ions but not to Ca^{2+} ions whereas NMDA receptors are permeable to whole of these ions. Channels that these receptors gate have different conductance values. Channels, which non-NMDA receptors gate, have low conductance ranging in between 0.2-25 pS in comparison to channels, which NMDA receptors gate, that have conductance level ranging from 17 to 75 pS [50]. One important difference of channels that NMDA receptors gate is that their opening depends not only on the presence of transmitter, in this case glutamate, but also on membrane voltage. However, mechanism of this voltage dependence is different from the mechanism of voltage-gated ion channels that generate action potentials. In NMDA receptor-channels, "extracellular Mg^{2+} binds to a site in the pore of the open channel and acts like a plug, blocking the current flow" [1]. When the membrane depolarizes, in other words when the intracellular side becomes more positive, Mg^{2+} is repelled by electrostatic force. Because of this voltage dependence, NMDA receptor-channels do not conduct immediately at the presence of glutamate so do not contribute very much to EPSP at resting membrane potential. NMDA receptor-channels have effect on the late phase of EPSP due to its slow opening and closing dynamics [1]. As EPSCs formed by non-NMDA receptor-channels are briefer (decay time constants 1-8 ms) with respect to EPSCs formed by NMDA receptor-channels (decay time constants 10-200 ms), fast transmission of excitatory signals is achieved by utilization of non-NMDA receptors [51]. Regarding the dynamics of channels and their contribution to formation

of EPSPs, non-NMDA receptor-channels are better candidates to be used in a model of synapse.

Immunolabeling studies show that ionotropic glutamate receptors mainly concentrate in lamina II of dorsal horn, and also they are found in lamina I. Since these two layers receive heavy primary afferent input that carry nociceptive and sensory signals, glutamate receptors in dorsal horn are related with transmission mechanism of nociception [52]. As stated before, the islet cell of substantia gelatinosa will be used as the interneuron in the gate control system since they are mostly GABAergic cells. Myelinated fibers in the gate control system that carry non-nociceptive sensory information make excitatory synapse on these cells. With Co^{2+} labeling study, these cells are found to contain mainly kainate and NMDA receptors [52]. However, in the study of Lu and Perl, where they investigated an inhibitory circuit in substantia gelatinosa, inhibitory interneuron, which is to be an islet cell, have an excitatory connection with a C-fiber that is mediated by AMPA receptor [43]. This shows islet cells may have AMPA receptors as well. As mentioned before AMPA and kainate receptors are grouped together as non-NMDA receptors because of their similarities, namely the ions that they are selective for, blockage by same antagonist (substance that prevents the action of the receptor) which is CNQX (6-cyano-7-nitroquinoxaline-2,3-dione), their conductance values etc. Their dynamics are also closely matched to each other so in modeling studies their dynamics are taken to be identical [33]. So knowing that islet cells have predominantly kainate receptors and also may have AMPA receptors, non-NMDA receptor dynamics will be used for glutamate driven excitatory synaptic transmission.

5.3.2 GABA Receptors

In the central nervous system the main inhibitory neurotransmitter is γ-aminobutyric acid (GABA) and it is secreted by GABAergic cells [53]. There two major subtypes of receptors that bind GABA: $GABA_A$ and $GABA_B$ where the first one is an ionotropic receptor and the other is a metabotropic receptor. $GABA_A$ recep-

tors will be investigated due to the fact that fast inhibitory signalling is mediated by them.

$GABA_A$ receptor-channels are selectively permeable to Cl^- ions and extracellular concentration of Cl^- is almost 25 fold of intracellular Cl^- concentration [5]. Reversal potential for Cl^- with this concentration difference is estimated to be $-70\ mv$. For membrane voltages that are more positive than the reversal potential of Cl^-, the electrochemical driving force ($V_m - E_{Cl}$; where V_m is membrane potential and E_{Cl} is the Cl^- reversal potential) acting on Cl^- ions is positive. So this will lead an outward current because by convention current from inside to outside is chosen to be positive. Since the charge carrier is an anion, positive current means anion movement in the opposite direction of the current itself. This means Cl^- ions flow from outside to inside and decrease the potential of cell membrane and prevents it from depolarization. The current mediated by Cl^- ions is called inhibitory postsynaptic current (IPSC) and the voltage drop caused by this current is called inhibitory postsynaptic potential (IPSP) [1]. Although $GABA_A$ receptor-channels have multiple conductance levels, the predominant and main level is 27-30 pS conductance level [53].

Most of the islet cells in lamina II of dorsal horn are GABAergic cells and this suggests that they are inhibitory interneurons [42,36]. In the work of Lu and Perl, an inhibitory pathway between lamina II neurons was investigated and in the pathway they found islet cell inhibits central cell of the same lamina so this is an example for the inhibitory function of the islet cells [43]. Another important thing is transmission cell and inhibitory interneuron should have $GABA_A$ receptors since they receive inhibitory connections in the gate control system. Although there is not information whether specific cell types of lamina I and II contain $GABA_A$ receptors, in general terms two layers have $GABA_A$ receptors. In human and monkey spinal cord, $GABA_A$ receptors are found in high densities in lamina II and in moderate densities in lamina I [52]. In this work the chosen inhibitory islet cell from lamina II and transmission cell from lamina I will be treated to contain $GABA_A$ receptors.

CHAPTER 6

MODELING STUDIES

In this part, model equations that are used for the simulation of gate control system are presented. Firstly model for an excitable nerve cell is given and unmyelinated and myelinated fibers are constructed by the use of this basic nerve cell model. Morphometric analysis of the component neurons, which are inhibitory interneuron and projection neuron, is done and compartmental models of these neurons are built according to the morphometric analysis. After giving the model parameters for individual components, model for transmission of electrical signal by chemical means through synapse is given. Synapse model includes the time dependency of neurotransmitter concentration in the synaptic cleft and the dynamics of neurotransmitter-gated post-synaptic receptors.

6.1 Model of Single Excitable Nerve Cell Membrane

Dynamics of ion channels, which are leaky channels and voltage-gated Na^+ and K^+ channels, are based on the work of Schwarz *et.al.* [8]. The data for the dynamics was acquired from single human myelinated nerve fibers and mathematical model was derived based on Frankenhauser-Huxley (FH) equations [54]. Major difference between HH and FH equations is that Na^+ current is modeled with GHK current equation in FH model instead of the ohmic relation as in HH model. But as it can be seen from Equation 4.19 as membrane voltage becomes 0, current relation becomes uncertain due to $\frac{0}{0}$ division. In the work of Frankenhauser and Huxley voltage axis was shifted by the amount of resting membrane potential so membrane potential never crossed zero. Instead of using GHK current equation, in the current work ohmic relations are used for all of the ionic

currents. In the work of Schwarz *et.al.* [8] current equation for Na^+ was given as

$$I_{Na} = m^3 h \left[P_{Na} \frac{E_m F^2}{RT} \frac{[Na]_0 - [Na]_i \exp(E_m F/RT)}{1 - \exp(E_m F/RT)} \right] \tag{6.1}$$

By fitting a linear equation to the part of Equation 6.1 that is in brackets for the values of E_m ranging between $-0.1V$ and $0.1V$, the following ohmic relation is obtained

$$I_{Na} = m^3 h \overline{g_{Na}} (E_m - E_{Na}) \tag{6.2}$$

which has the same form as in the HH model. Before the fit, value of P_{Na} is increased from $3.52 \times 10^{-12} \frac{cm^3}{s}$ to $15 \times 10^{-12} \frac{cm^3}{s}$ because after increasing to this level, final model starts to produce repetitive firing on sustained depolarization. From the linear fit $E_{Na}$is found as $45.4mV$. This value is consistent with the value that was used by Wesselink *et.al.* [55] who used the model parameters that was given by Schwarz *et.al.* [8]. Maximum Na^+ conductance, $\overline{g_{Na}}$, is found to be $5120nS$. Schwarz *et.al.* [8] did not give the dimensions of the nodal part in their work so area of nodal part is taken as 50 μm^2 in accordance with the work of Wesselink *et.al.* [55]. Scholz *et.al.* [56] reported maximum conductance of a single Na^+ channel in human axons as $13pS$. In the work of Ritchie and Rogart [57], density of sodium channels in mammalian nodes was found to be 12000 channels per μm^2 from the measurements in rabbit sciatic nerve. By using these values, for a 50 μm^2nodal area, $\overline{g_{Na}}$ is found as 7800 nS, so the value that is used in the current work is comparable with the physiological values. Maximum K^+ conductance $\overline{g_K}$ for 50 μm^2 membrane is taken as 30 nS [8, 55] and the K^+ current is calculated as

$$I_K = n^4 \overline{g_K} (E_m - E_K) \tag{6.3}$$

where E_K is -84 mV. Leakage conductance, $\overline{g_{leakage}}$, for 50 μm^2 membrane is taken as 30 nS and $E_{leakage}$ is -84 mV [8]. Current resulting from ion flow through leakage channels is given as

$$I_{leakage} = \overline{g_{leakage}} (E_m - E_{leakage}) \tag{6.4}$$

Capacitance of 50 μm^2 membrane is 1.4 pF.

Another alteration that is made in the model equations is that, the rate constants of Na^+ activation and inactivation gates are doubled. This is done to decrease the width of the AP signal and to obtain a conduction velocity that is well in the range for myelinated and unmyelinated fibers. Dynamics of K^+ activation gates remain the same since in the work of Schwarz *et.al.* [8], it was noted that AP shape was determined mainly by Na^+ conductance and K^+ conductance determined the repetitive firing behaviour. Model equations for dynamics of ions channels of excitable nerve cell are as follows:

$$\alpha_n = \frac{0.00798 \times (E_m + 93.2)}{1 - \exp((-93.2 - E_m)/1.10)} \tag{6.5}$$

$$\beta_n = \frac{0.0142 \times (-76 - E_m)}{1 - \exp((E_m + 76)/10.5)} \tag{6.6}$$

$$\alpha_m = \frac{3.72 \times (E_m + 18.4)}{1 - \exp((-18.4 - E_m)/10.3)} \tag{6.7}$$

$$\beta_m = \frac{0.172 \times (-22.7 - E_m)}{1 - \exp((E_m + 22.7)/9.16)} \tag{6.8}$$

$$\alpha_h = \frac{0.0672 \times (-111 - E_m)}{1 - \exp((E_m + 111)/11)} \tag{6.9}$$

$$\beta_h = \frac{4.6}{1 + \exp((-28.8 - E_m)/13.4)} \tag{6.10}$$

all of which are in $\frac{1}{ms}$.

6.2 Model for Unmyelinated and Myelinated Fibers

Unmyelinated fiber is homogeneous and AP propagates passively. Its model is composed of cylindrical identical compartments which are all excitable. Every compartment has a length of $100\mu m$ and diameter of the fiber is $1.5\mu m$. Phases of modeling of unmyelinated fiber is shown in Figure 6.1.

Myelinated fiber is not homogeneous and its compartmental model has non-identical parts. Phases of the modeling is shown in Figure 6.2. Fiber is decomposed into cylindrical nodal and paranodal parts. Axon diameter is chosen to be $10\mu m$ and the fiber diameter, which is the sum of axon diameter and myelin

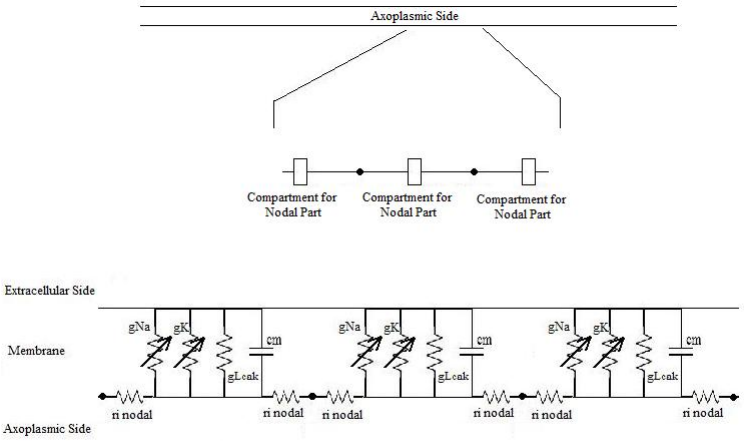

Figure 6.1 Compartmental modeling of unmyelinated fiber.

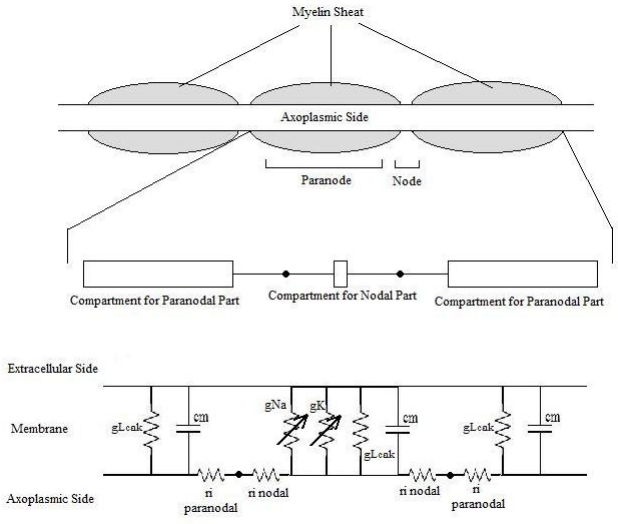

Figure 6.2 Compartmental modeling of myelinated fiber.

sheath thickness, is determined to be $15\mu m$. These values are in the range of diameters of large diameter fibers [11]. Area of nodal part is $50\mu m^2$ and this results in a length of $1.59\mu m$ for nodal part. Length of paranodal part is determined as $5000\mu m$ which is the longest length for paranodal part that saltatory conduction can be obtained along the fiber. Also, the length constant λ for the paranodal part is found as $4123\mu m$ so the selected paranodal part length is about 1.21 λ. Thus, the signal along paranodal part would decay to $e^{-1.21}$, i.e. 0.3 of its starting amplitude from the cable equation, which is enough to elicit an AP in the adjacent node. Paranodal part is composed of 5 identical parts that are$1000\mu m$ in length. However, shorter paranodal lengths can be used. In the study, $\frac{1}{4}$ and $\frac{1}{2}$ of $5000\mu m$ is used for the best selection of length for the paranodal part. This length must be such that propagation velocity evaluated must be within physiological ranges. If the same propagation velocity is found for all lengths selected, the maximum value can be used in the simulations. Paranodal part is not composed of one compartment because in that case the intraaxonal resistance between the nodal and paranodal part is so big that signal cannot propagate. However, if the paranodal part is divided into parts as in this study, signals can travel along the fiber. Only nodal parts are excitable and posses voltage-gated Na^+ and K^+ channels. Under the myelin sheath, Na^+ and K^+ ionic currents are ignored so the paranodal part is modeled as passive RC circuit [58]. Specific membrane resistance of paranodal part is chosen to be 2500 times the specific membrane resistance of nodal part and specific membrane capacitance of paranodal part is determined by dividing the specific membrane capacitance of nodal part by 350. These parameters are tuned by hand until paranodal part lets saltatory propagation along the fiber. Frijns *et.al.* [59] noted that specific intracellular resistance was not measured reliably and used a value of $0.7\Omega.m$. To achieve a propagation velocity that is comparable with physiological measurements and other fiber models, specific intracellular resistance is chosen to be $1.25\Omega.m$ which is the same for both paranodal and nodal parts. Electrical parameters for myelinated and unmyelinated fibers are given in Table 6.1.

Table 6.1: Membrane Parameters

	C_m $(\frac{F}{m^2})$	R_m $(\Omega \cdot m^2)$	R_i $(\Omega \cdot m)$
Nodal part of myelinated fiber	0.028	0.0017	1.25
Paranodal part of myelinated fiber	0.00008	4.25	1.25
Unmyelinated fiber	0.028	0.0017	1.25

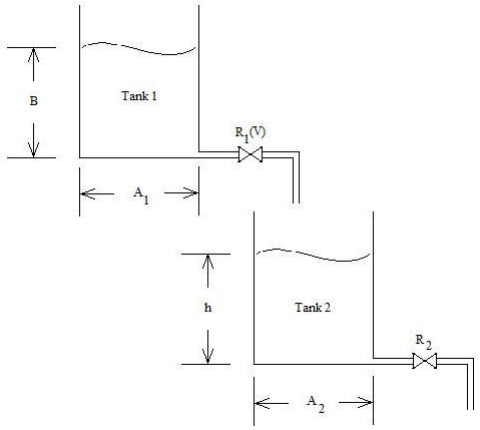

Figure 6.3 Two tank system for the model of synapse.

6.3 Model of Synaptic Transmission

In the modeling studies two issues must be considered: one is the time course of concentration of neurotransmitter in the synaptic cleft and the other is the dynamics of the receptors that will be gated by the neurotransmitters in the cleft. Upon arrival of action potential to the terminals of pre-synaptic neuron, many processes occur: inflow of Ca^{2+} ions, fusion of vesicles with membrane, exocytosis of neurotransmitters into the cleft. However, all of these processes are so rapid that they are not the main determinants of the time course of neurotransmitter in the synaptic cleft [33].

Exocytosis of neurotransmitters and the concentration change in the synaptic cleft are modeled as a two tank system as in Figure 6.3.

Tank 1 represents the vesicle pool in the presynaptic neuron and Tank 2 represents synaptic cleft. Height of liquid in Tank 1, B, is constant with the assumption that vesicles that hold neurotransmitter molecules do not run out.

$R_1(V)$ is the resistance to flow at the outlet of the Tank 1 which is dependent on presynaptic voltage. As the presynaptic membrane voltage is at resting membrane potential, $R_1(V)$ is so high that no flow of transmitters occur. When an AP arrives at the terminal of pre-synaptic neuron, membrane voltage will increase and $R_1(V)$ will decrease so that neurotransmitters will flow into synaptic cleft. R_2 at the outlet of Tank 2 represents all of the processes in which neurotransmitters diffuse out of the synaptic cleft and it is constant. A_2 is the area of Tank 2 and it is constant. It determines the time constant of neurotransmitters in the synaptic cleft with R_2. Height of the liquid in Tank 2, h, is the analog for neurotransmitter concentration in the synaptic cleft. Material balance for the liquid in Tank 2 gives the following relation

$$\frac{B}{R_1(V)} - \frac{h}{R_2} = \frac{dV}{dt} = A\frac{dh}{dt} \tag{6.11}$$

where $\frac{B}{R_1(V)}$ is the inlet flow, $\frac{h}{R_2}$ is the outlet flow and $\frac{dV}{dt} = A\frac{dh}{dt}$ is the accumulation term where V is the volume of the liquid in Tank 2. There is no generation term since in the synaptic cleft no neurotransmitter is formed. Transfer function of this process is found as

$$G_p = \frac{R}{ARs + 1} \tag{6.12}$$

where AR is the time constant of the process and represents the time constant of concentration of neurotransmitters in synaptic cleft. R is the steady state gain and it is determinant of maximum concentration of neurotransmitters in the cleft. These parameters are chosen in a manner that maximum concentration and time constant values for transmitters in the cleft are in experimentally determined ranges [60]. Time constants for both excitatory and inhibitory transmitters are chosen as 2.5 ms and steady state gain is taken as 5.

Post-synaptic transmitter receptors open upon binding of neurotransmitters. Model of these receptors have two states, bound and unbound which are open and close states, respectively. Dynamics of these receptors can be shown by first order reaction kinetics as

$$1 - r \underset{\beta_r}{\overset{\alpha_r}{\rightleftharpoons}} r \tag{6.13}$$

where r is the fraction of bound (open) receptors, α_r is the forward rate constant for transmitter binding and it is dependent on neurotransmitter concentration, $[T]$, β_r is the backward rate constant for binding and it is constant. Fraction of bound receptors change with respect to time with the following equation

$$\frac{dr}{dt} = \alpha_r[T](1-r) - \beta_r r \tag{6.14}$$

α_r is $2ms^{-1}mM^{-1}$ and $\beta_r$is $1ms^{-1}$ for excitatory synapses and α_r is $0.5ms^{-1}mM^{-1}$ and $\beta_r$is $0.1ms^{-1}$ for inhibitory synapses [61].

Current through these receptors is calculated with the following equation

$$I_{receptor} = \overline{g_{syn}} r(E_{post} - E_{syn\,rev}) \tag{6.15}$$

where $\overline{g_{syn}}$ is the maximum synaptic conductance, E_{post} is the membrane voltage of post-synaptic neuron and $E_{syn\,rev}$ is the reversal potential of the synapse. For excitatory synapses $E_{syn\,rev}$ is 0mV [61] and for inhibitory synapses $E_{syn\,rev}$ is -90mV which is the reversal potential of Cl^-.

6.4 Morphometric Analysis of Component Neurons

Dimensions of the neurons that constitute gate control system must be known since electrophysiological properties such as membrane resistance and membrane capacitance depend on these dimensions. Neurons are partitioned into segments that are homogeneous within themselves for compartmental modeling. Morphometric analysis is done in MATLAB. Upon loading the pictures of the fusiform and islet cells that are given in Figure 3.5 and Figure 3.7 into the workspace, with the use of function *"imdistline"* length of two specified points are found.

As mentioned before every connection in gate control system is monosynaptic. Substantia gelatinosa neuron receives two inputs, one from C fiber and the other from Aβ fiber. Assuming these two inputs acts on different dendrites, two dendrites of the neuron is investigated for morphometric analysis and those dendrites are shown in Figure 6.4. Islet cell is divided into six segments, each of which has a constant diameter. Dimensions of these segments of islet cell are given in Table

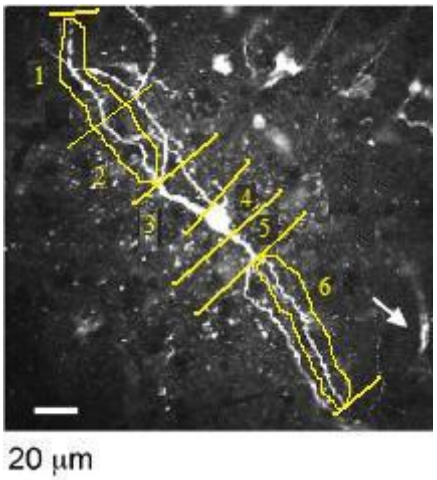

Figure 6.4 Partitioning of islet cell into segments.

Table 6.2: Dimensions of segments of islet cell.

	Diameter (μm)	Length (μm)	Area (μm^2)
Part 1	3.00	60	565.5
Part 2	3.00	40	377
Part 3	4.03	27.39	346.77
Part 4 (Soma)	10.63	-	355.00
Part 5	3.60	18.44	208.55
Part 6	2.8	89.03	783.15
Axon	1.86	48.03	280.66

6.2. Part 4 is assumed to be spherical and all other segments are considered as cylindrical. Thus, part 4 has only diameter without a length. Axon of the cell may be longer than the value given in Table 6.2 because it is very thin. Therefore it may only be labeled poorly or the labeled part may not be inspected by bare eye. However, the value given in Table 6.2 will be used in the model development. Axon of the islet cell is made spontaneously active which means that it produces APs without need of any excitation. This is done because of the fact that islet cell should inhibit fusiform cell continuously so that fusiform cell would not generate APs when there is no incoming nociceptive signals.

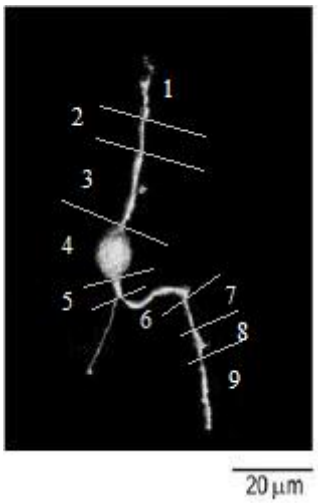

Figure 6.5 Partitioning of lamina I fusiform cell into segments.

Lamina I fusiform cell receives three inputs, one from substantia gelatinosa, one from C fiber and one from Aβ fiber. C fiber and Aβ fiber will be assumed to be making contacts on separate dendrites. Substantia gelatinosa cell will make contact on soma since most of the inhibitory synapses end on cell body. So one of the dendrites in Figure 3.5 is neglected and this is done arbitrarily: there is not a specific reason for choosing the dendrite that is to be neglected. Segments of the lamina I fusiform cell are shown in Figure 6.5. Part 4 corresponds to the soma of the cell and it is assumed to be spherical whereas the rest are considered to be cylindrical.

Dimensions of the segments of lamina I cell are given in Table 6.3 where length of the axon of lamina I cell is taken as 100 μm and not longer because the output of the system is the action potentials that are initiated at the initial region of the axon and propagation of these signals are not the concern of the current work. In both neurons soma is divided into two identical parts since it is very hard to charge soma due to its dimensions and part of the soma that is connected to axon is made excitable for the ease of propagation of AP signals.

Table 6.3: Dimensions of segments of fusiform cell.

	Diameter (μm)	Length (μm)	Area (μm^2)
Part 1	1.9	10.42	54.34
Part 2	1.6	8.41	34.35
Part 3	2.9	20.85	189.96
Part 4 (Soma)	9.11	-	260.73
Part 5	2.40	4.16	31.37
Part 6	2.61	19.51	159.97
Part 7	0.94	9.94	29.35
Part 8	2.34	5.86	43.08
Part 9	1.82	17.30	98.92
Axon	1.118	100	3.51

CHAPTER 7

EXPERIMENTAL STUDIES

In this chapter, experimental procedure for recording action potentials (AP) from the giant axon of crayfish (*Astacus leptodactylus*), which is an invertebrate (species with no spine), is given. Train of APs are recorded from the crayfish for the purpose of comparison with the developed model. This animal is collected from the lakes of Central Turkey and kept in an aquarium at 18-20^oC. The experiments are held in Biophysics Department of Hacettepe University. "In the use of the experimental animals national guidelines have been followed and approval from the Hacettepe University Ethics Committee has been obtained" [62].

7.1 Experimental Set-Up

In the experiments a vertical puller (PC10 Narishige, Japan) is used for the manufacture of glass microelectrodes and it is shown in Figure 7.1. A microscope (TE Eclipse 200, Nikon, Japan) is used for visualizing the giant axon of the crayfish. In addition, manipulaters are used to change the position of microelectrodes and stick them into the neuron. The microscope and one of the manipulaters are shown in Figure 7.2.

One electrode current clamp set-up is shown in Figure 7.3. This set-up is composed of one glass chamber with a diameter of 5 cm and height of 7 mm, and the manufactured glass microelectrode. This system is designed to control potential across R_f so that injected current, I, can be controlled.

Figure 7.1 Vertical puller that is used for the manufacture of microelectrodes.

(a) Nikon microscope

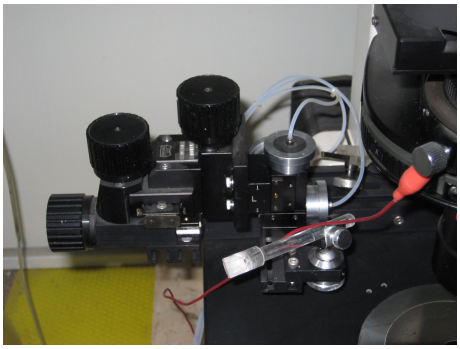

(b) Microelectrode manipulator

Figure 7.2 Set-up that is used to stick microelectrodes into the neuron accurately.

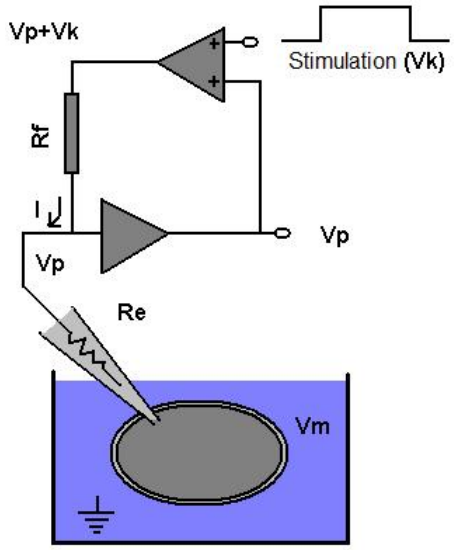

Figure 7.3 One electrode current clamp setup [7].

The experiment duration is determined by the amount of fluid and its concentration in the pipette. Toward the end of the experiment ion concentration changes in the pipette and also ion concentrations in the neuron are distorted which results wrong recordings. The time to measure APs without major distortions is approximately 20 minutes.

In this set-up, the voltage across the pipette, V_p, is followed by a voltage follower and added to the command voltage V_k. This is done in order to control the current across the resistance R_f. If this correction is not done, then the voltage across R_f will be different from the command voltage and the current injected to the membrane cannot be known. Thus, the current injecion is achieved by applying a command voltage over a known resistance which is in this case is 100 $M\Omega$. Pipette voltage V_p is not the membrane voltage, V_m. Instead it is equal to the summation of the membrane voltage and the voltage across the resistance of the electrode R_e. Membrane voltage can be extracted if the voltage across the electrode resistance is subtracted from the pipette voltage. For this purpose, command voltage is fed through an adjustable resistance to a difference amplifier and this correction voltage is subtracted from the pipette voltage to find the membrane voltage. This correction setup is shown in Figure 7.4.

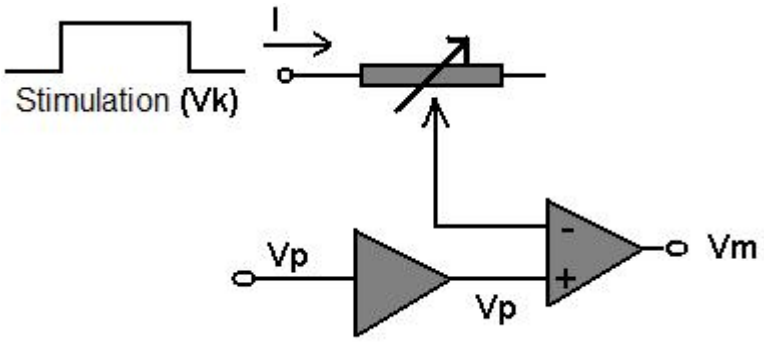

Figure 7.4 Voltage correction setup to extract membrane voltage from pipette voltage [7].

7.2 Experimental Procedure

In the experiments AP from the giant axon of a crayfish is measured. This selection of the animal is based on the size of its axon which is giant and which can be used experimentally. Also since it is an invertebrate, its handling is easy.

Giant receptor neuron of the crayfish is dissected from the first to forth abdominal segments and dissected receptor neuron is mounted in a recording chamber and immersed in control solution. Control solution is composed of 200 mM NaCl, 5.4 mM KCl, 13.5 mM CaCl2, 2.6 mM MgCl2 and it is buffered to pH of 7.4 using 10 mM HEPES (4-(2-hydroxyethyl)-1-piperazineethanesulfonic acid) [63].

Glass capillary (GC150F, Clarke Electromedical Instruments, Reading, UK) is heated in the vertical puller for the manufacture of glass microelectrodes for intracellular recordings and stimulation. Glass capillary is held by the holders and the temperature of the filament is set to the desired level. Weights of the puller can be changed as light and heavy. As the filamnt is heated, the glass softens, weights in the puller pulls down the glass and two microelectrodes are formed. By adjusting the level of temperature of the filament and the weights of the puller, the diameter and length of the tip of the microelectrode can be altered. Recording chamber is placed onto the microscope. The electrodes are filled with 3 M KCL solution. The reference electrode is an Ag/AgCl wire immersed into the bathing solution. With the use of the microscope and the manipulaters (MHW-

3, Narishige, Japan) that position the microelectrodes, the microelectrodes are sticked into the neuron. A multi-functional clamp amplifier (Axoclamp 900A, Axon Instruments USA) is used for electrophysiological recordings. For current-clamp studies, the input current to the neuron is kept constant and the membrane voltage is recorded. Current stimulus is generated in a computer and converted to analogue form and delivered to the amplifier. The recorded analogue membrane voltage signals are digitized (Digidata 1440, Axon Instruments, USA) and stored in a computer. While viewing the specimen under microscope, the space for multi microelectrodes is limited. Because of this physical limitation, stimulation and recording is done by the same electrode so one electrode current clamp is used.

CHAPTER 8

RESULTS AND DISCUSSIONS

In this chapter first the simulation results for the components of the gate control system are presented and followed by the response of gate control network for different configurations. The results of the behaviour of single excitable cell model under different physiological conditions is followed by the model results of action potential propagation along myelinated and unmyelinated fibers. Afterwards, simulation results of synaptic transmission is presented. Finally, response of the neuronal circuit for different configurations is investigated.

8.1 Behaviour of Single Excitable Cell Model

For the simulation of the response of a single excitable cell, a nodal part with $50\mu m^2$ membrane area is used. Current pulse stimulus that is shown in Figure 8.1 is applied for the stimulation of the cell. Current that is applied is negative since current flows into the cell and by convention inward currents are negative. Pulse

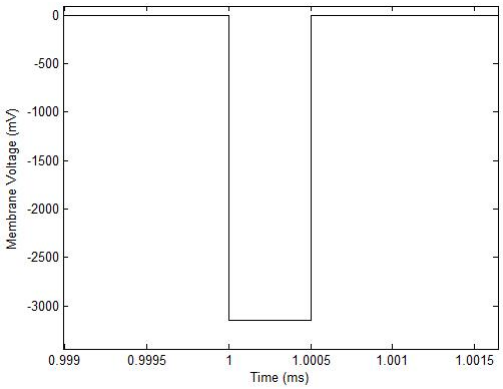

Figure 8.1 Current stimulus that initiated the action potential in Figure 8.2 (a).

width of the current pulse is 0.0005 ms and its amplitude is 3150 pA which is the threshold value for the specific pulse duration. The generated AP has a proper shape with its depolarization and repolarization phases and it is shown in Figure 8.2(a). Amplitude of the action potential is 126 mV and it is 10 mV bigger than the experimentally recorded action potential that is recorded from human nerve fibers in the work of Schwarz *et.al.* [8] which has an amplitude of 116 mV and it is shown in Figure 8.2(b). This difference is mainly due to different Na^+ reversal potential that is used in this study. As depicted in Figure 8.2(a), membrane voltage increases very rapidly after passing a threshold value, which is around -74 mV and it is 9 mV higher than the resting membrane potential which is 83 mV.

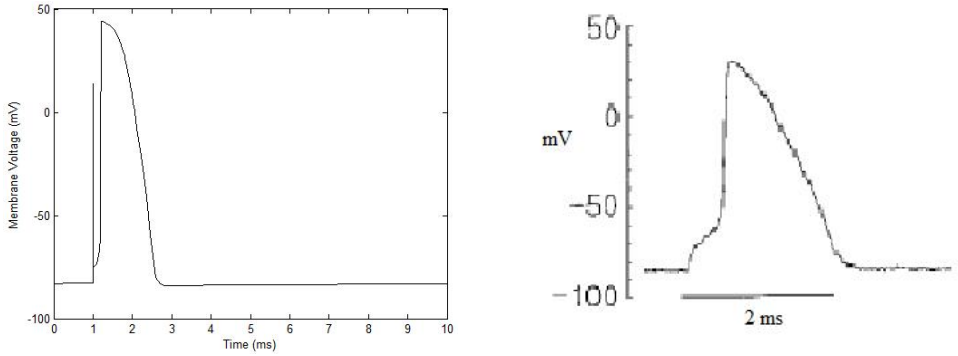

(a) Simualted AP. (b) Experimental AP.

Figure 8.2 Simulated AP in the current work and experimental AP from the work of Schwarz *et.al.* [8] .

This rapid increase is caused by the progressive opening of voltage sensitive sodium channels. At the peak of the action potential, inactivation gates of sodium channels close and potassium channels open which start to polarize the cell back to its resting membrane potential. After passing the resting membrane potential, since potassium channels cannot close immediately, outflow of potassium ions further polarizes the membrane, below the resting membrane potential level. During

this hyperpolarization, Na^+ inactivation gates return to their initial open state. After potassium channels close, resting ion channels bring the membrane potential to its resting membrane potential. For comparison, single AP and train of APs that are generated by giant neuron of crayfish are recorded experimentally. The current stimulus is 6.5 nA and the resting membrane potential of the crayfish is around -67 mV. The resulting AP has an amplitude of 105 mV. Recorded single AP and AP train are given in Figure 8.3.

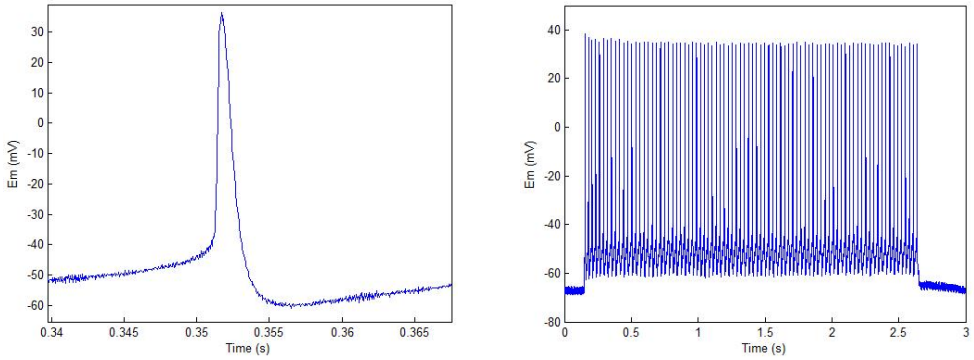

(a) Single AP. (b) Train of APs.

Figure 8.3 Recorded APs from crayfish.

After initiation of an AP, for a certain time, neurons cannot generate a second AP in response to a second stimulus "even if its strength is unlimited" [59]. This period of time is called *absolute refractory period* and Na^+ channel inactivation is the main reason of this phenomenon. At the repolarization phase of the AP, Na^+ inactivation gates start to close and they do not get into open state until membrane voltage decreases to resting membrane potential. If any stimulus is applied at this period, since Na^+ channels do not let passage of Na^+ ions, membrane voltage will not increase and AP will not be generated. To find the absolute refractory period of the developed model in this study, two current pulses with pulse width of 0.0005 ms are applied at different times. Amplitudes of the current pulses are chosen to be 150% of the threshold value of 3150 pA in accordance with

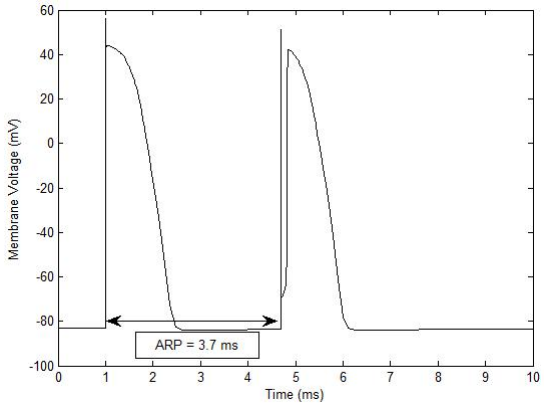

Figure 8.4 Absolute refractory period for the model cell.

the work of Frijns *et.al.* [59]. Time difference between pulses is decreased until the second pulse cannot initiate an AP. With this procedure, absolute refractory period of the model is found as 3.7 ms. This value imposes an upper limit for the maximum frequency of AP train which is 270 Hz. In Figure 8.4 absolute refractory period of the model cell is shown.

If the pulse width of the current stimulus is increased, model generates action potentials as long as the stimulus sustains. When the input current pulse width is increased to 29 ms and the amplitude is taken as 110 pA, the model generates the train of action potentials as given in Figure 8.5. Sensation of touch is felt as long as the skin is touched, so the receptor neurons should generate action potentials as long as the stimulation sustains. Amplitude of input current is decreased due to the fact that, as the stimulation duration increases threshold decreases so if the threshold value for 0.0005 ms input is applied for 29 ms, input and generated action potentials cannot be separated as in .

Intensity of stimulus is encoded as the frequency of generated action potentials. So if the amplitude of the current stimulus is increased, the frequency of generated action potentials increase. However, there is no study to quantify the current-frequency relation for all models [20]. Every model has its own current-frequency relation. For the unmyelinated and myelinated fibers current-frequency relations will be given in the next section but this relation is not given for single

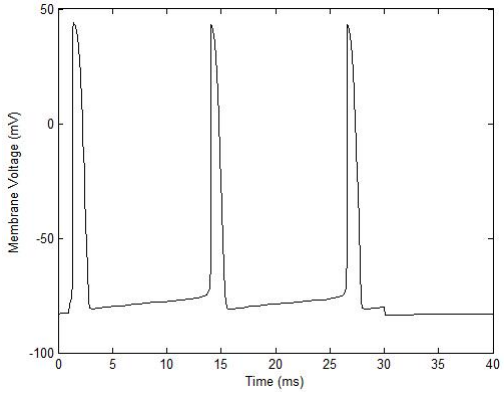

Figure 8.5 Action potentials generated under sustained stimulation with 110 pA for 29 ms.

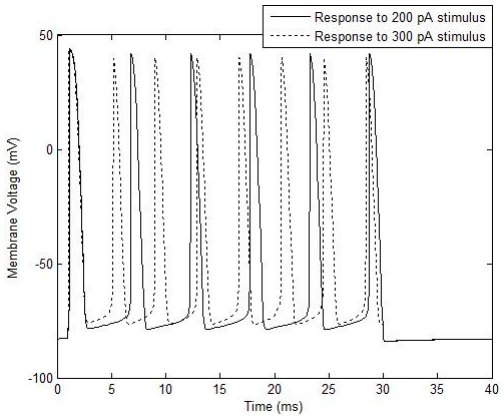

Figure 8.6 Frequency differences of train of action potentials in response to different current intensities.

excitable cell. However, to observe the frequency change upon increasing stimulation intensity, two current inputs are applied with amplitudes 200 pA and 300 pA for 29 ms and results are given in Figure 8.6. In the same time interval, model generates eight action potentials to higher intensity stimulus whereas it generates six action potentials to lower intensity stimulus. When the frequencies of the train of action potentials are calculated as the inverse of the time interval between the first two spikes, it is found that under higher intensity stimulus, frequency becomes 246 Hz whereas under lower intensity stimulus frequency is found to be 177.3 Hz. The spikes after the first one have smaller amplitude according to the amplitude of first spike and this difference becomes clear as

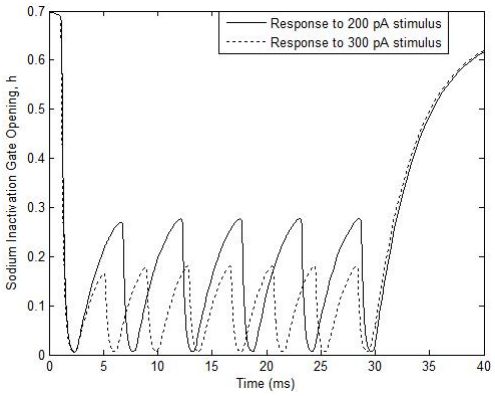

Figure 8.7 States of sodium inactivation gates during different current intensities.

the stimulus intensity is increased. This is observed in experimental studies of Schwarz *et.al.* [8] and also in modeling studies of Frijns *et.al.* [59]. Reason of this observation is "depolarization of the axon membrane resulting in inactivation of the sodium channel" [64]. When the amount of input current is increased, voltage over the leakage channels increases so in the hyperpolarization phase of first AP that is initiated, membrane voltage cannot decrease below resting membrane potential so inactivation gates of Na^+ channels cannot open fully. Since inactivation gates remain partially open, during the generation of the next AP Na^+ ion current through Na^+ channels decrease which results in partial depolarization of the membrane. As a result, amplitudes of the APs that follow the first one decrease. This phenomenon is known as *depolarization block*. The states of Na^+ inactivation gates during inputs of 200 and 300 pA currents for 29 ms is shown in Figure 8.7. When the input is 300 pA, the h value, which represents the probability of the inactivation gate to be in open state, is lower in comparison to its value when the input is 200 pA.

Any excitable cell model should predict the outcome of any change in physiological properties like the intracellular and extracellular ion concentrations and block of ion channels by blocking agents. Due to the changes in concentrations of extracellular and intracellular ions, response of the neuron changes dramatically. Also if the ionic channels are blocked by channel antagonists, neuron does not function properly. Tetrodotoxin is a substance that has a high affinity to bind to

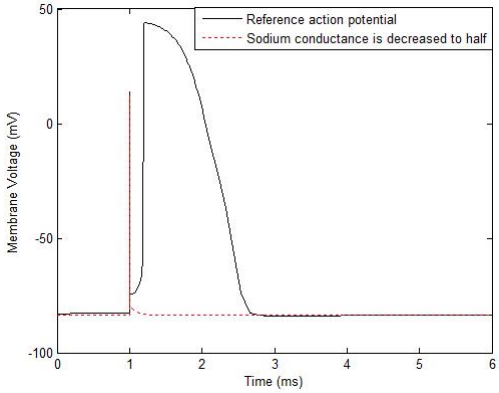

Figure 8.8 Response of the model when conductance of sodium channels becomes zero.

the opening pores of sodium channels block action potential generation. To eat a puffer fish, which posses this substance, may be fatal, since when action potential generation is blocked, information flow in nervous system does not occur and contraction and relaxation of muscles stop, which in turn stops vital physiological processes like breathing. If the conductance of sodium channels is decreased by half then there will be no action potential generation and this can be seen in the response of the developed model in this study as in Figure 8.8. If the concentration of extracellular sodium ion increases the reversal potential of sodium ion increases. If the sodium reversal potential increases by two fold, the model generates a train of action potentials with a higher frequency as shown in Figure 8.9. It should also be noted that, as the reversal potential of sodium ion increases, the resulting amplitude of action potentials also increases. This is because of the fact that as the reversal potential of sodium ion increases, the electrochemical driving force on sodium ions increases and neuron depolarizes to a greater extent and amplitude of the action potential increases. This is the main reason for the discrepancy between the amplitudes of APs generated in the current model and the ones that are experimentally recorded [8].

Another important aspect of the model is that it can summate the stimuli temporally. A current pulse, which has a pulse duration of 0.0005 ms and an amplitude of 2400 pA, will not elicit an AP, since it is lower than threshold.

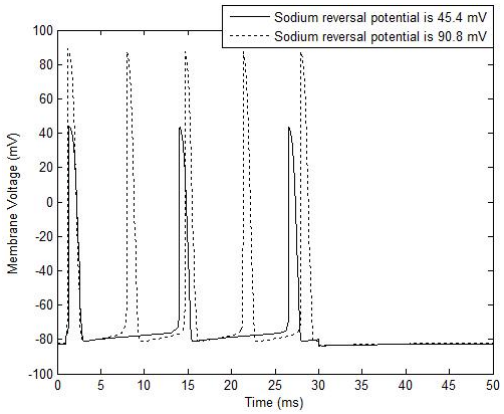

Figure 8.9 Response of the model when reversal potential of sodium ion is doubled.

If another current stimulus with same amplitude is applied after 0.00025 ms, model generates an action potential. This is due to the fact that, because of the membrane capacitance, membrane voltage attenuates in a certain time. If a second stimulus arrives before the voltage that is generated by the first stimulus attenuates, response of the second stimulus adds on the initial response and if this new voltage passes threshold, an action potential is elicited. The stimulus for this case is given in Figure 8.10(a) and the response of the model is shown in Figure 8.10(b).

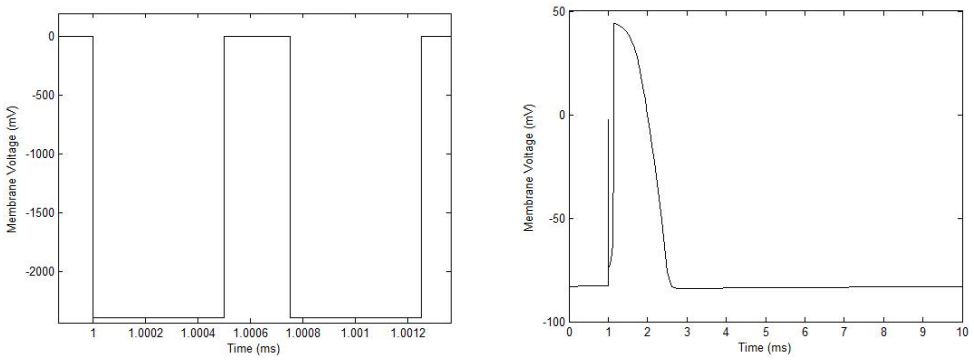

(a) Two consecutive inputs.

(b) Generated AP in response to two consecutive inputs.

Figure 8.10 Temporal summation.

Temporal summation is an important feature since it changes the response of the neuron. If the responses of the first stimulus and the second stimulus cannot be added, than to elicit an action potential, amplitudes of the incoming action potentials from other neurons must be very big and this is not energetically favorable since for bigger amplitudes, ion fluxes over cell membrane must be bigger and reallocation of the ions to their resting conditions will consume much more energy. If there was no temporal summation, then a neuron may never fire an action potential which will cause interruption of transmission of the signals.

8.2 Propagation Along Fibers

Gate control system includes one unmyelinated and one myelinated fibers. Conduction velocities, stimulus intensity-frequency characteristics and the ways of conduction differ for both fiber types.

First of all, AP spreads with passive conduction along unmyelinated fibers. When AP is initiated at one point of the fiber, ions in this depolarized part flow to adjacent parts so that adjacent parts are also depolarized and if the voltage exceeds threshold, he adjacent parts produce AP. By this way AP travels all along the fiber. While AP propagation, wherever the electrode is placed, an AP can be

recorded. However, in myelinated fibers the only points from where an AP can be recorded are the nodal parts because APs are generated only in these active parts. In this respect, a saltatory conduction is observed in myelinated fibers. AP propagation along myelinated fiber is given in Figure 8.11.

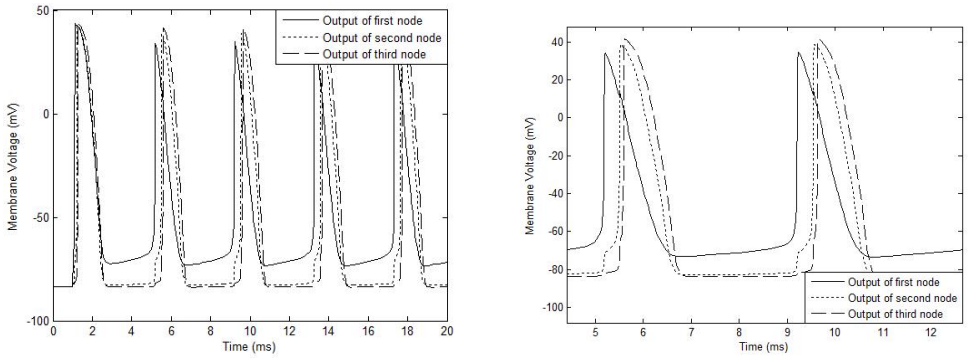

(a) Saltatory propagation. (b) Close up of saltatory propagation.

Figure 8.11 AP propagation along myelinated fiber.

To find the propagation velocity along the myelinated fiber, time difference between the peaks of APs that are generated by adjacent nodes should be calculated. Two adjacent nodes are separated by a paranodal part which is 0.5 cm in length. Calculation of propagation velocity along myelinated fiber is given in Figure 8.12 which is a close-up of Figure 8.11(b). A velocity of 64.35 $\frac{m}{s}$ is calculated and this velocity is in the range of physiological velocities for large diameter fibers [11]. As given in Chapter 6, the paranodal length, has an effect on the calculated velocity. During the modeling studies paranodal length is selected as 1.21 λ. However, in order to see the effect of paranodal length on the results other values for paranodal length are investigated. The results are given in Table 8.1. As it can be seen from Table 8.1, there is no significant difference between the velocities so the longest possible length can be used so that with myelination less nodes can be used which is energetically more efficient. In Figure 8.12 it is seen that third action potential is greater than the second one in amplitude. The

Table 8.1: Propagation velocity for different paranodal lengths

Paranodal length (μm)	Propagation velocity (m/s)
5000 (5 compartments)	64.35
5000 (10 compartments)	63.77
2500 (5 compartments)	61.0
2500 (10 compartments)	60.5
1250 (5 compartments)	60.8
1250 (10 compartments)	60.4

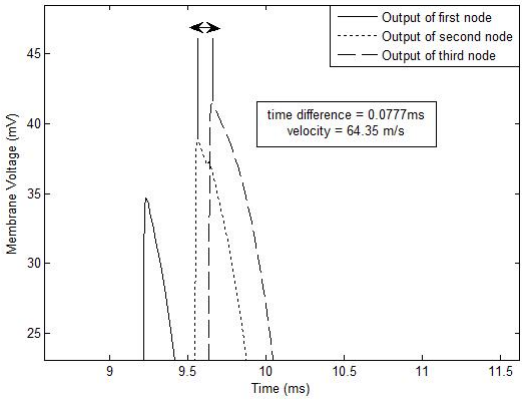

Figure 8.12 Calculation of conduction velocity along myelinated fiber.

reason is that, as the third node is the last compartment of the fiber, there is not a flow of ions to the adjacent compartment. Ions leave the compartment only through ion channels on the membrane. As a result, more ions accumulate in the last compartment and this causes AP amplitude to increase. When, a paranodal compartment is connected to this third node, since there would be another route for the ions to flow, accumulation of ions in this compartment decreased and in turn the difference between the amplitudes of APs of the second and third nodes disappears. In comparison to saltatory conduction in myelinated fibers, AP initiation can be observed at every point of unmyelinated fiber. Model of this fiber is composed of 100 nodal parts each of which has a length of 100 μm. This length is the longest length for nodal parts so that propagation along the fiber model can be observed. In fact, if the length of each part is kept smaller, the

model would simulate real fibers better, however, the computational burden will increase at the same time. Initiation and propagation of APs along unmyelinated fiber is given in Figure 8.13 upon stimulation of 29 ms long current pulse. For clarity, responses of four nodes are shown in Figure 8.13(a) and the responses of two nodes are given in Figure 8.13(b).

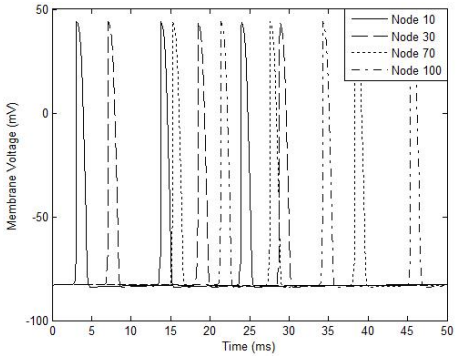

(a) AP initiation and propagation at four nodes.

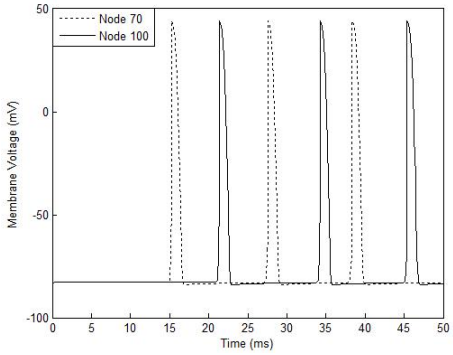

(b) AP initiation and propagation at two nodes.

Figure 8.13 AP propagation along unmyelinated fiber.

To find the propagation velocity along the unmyelinated fiber, time difference between the peaks of second APs of node 70 and node 100 is calculated as in Figure 8.14. Velocity along the unmyelinated fiber is found as 0.43 $\frac{m}{s}$ which is in agreement with the physiological values that are given for small diameter fibers as 0.25-1.25 $\frac{m}{s}$ [11]. In the developed model velocity along myelinated fiber is much more higher than the velocity along unmyelinated fiber. Also while myelinated fiber posses only three nodes, unmyelinated fiber has 100 nodal parts so myelinated fiber conducts much more faster with consumption of very little energy in comparison to unmyelinated fiber. Energy is consumed while regaining the ion concentrations on both sides of cell membrane after initiation of AP so as the number of nodal parts in the fiber decrease, consumed energy decreases. In this respect, myelinated fiber is energetically more favorable than unmyelinated

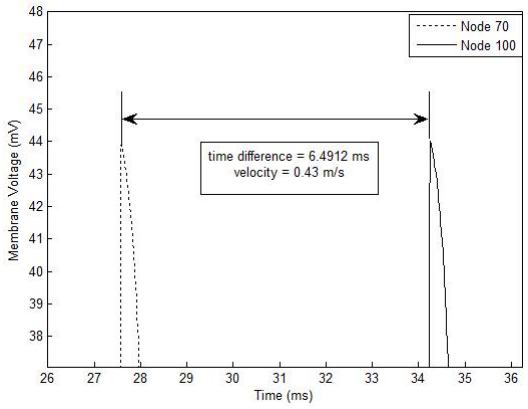

Figure 8.14 Close-up of Figure 8.13(b).

fiber.

When the intensity of stimulus is changed, frequency of the responses of the fibers change. There is a lower limit and and upper limit for the current intensity. Lower limit is determined by the threshold of excitation of the fiber. If the intensity of the stimulus cannot exceed the threshold, fiber would not initiate and AP and would not propagate it. The upper limit is determined by the phenomenon called as depolarization block. When the intensity of the stimulus is increased beyond a certain value, the excited node starts to fire APs with small amplitudes after the initiation of the first AP. When the amplitudes of the APs decrease, voltage difference, which is the driving force, between the adjacent nodes decrease and the adjacent node cannot be excited so signal cannot be propagated along the fiber. In fact, besides the psychological reasons, feeling no pain after getting severe wounds in war, may be due to this incapability of the fibers. The input current-frequency relations of myelinated and unmyelinated fibers are given in Figure 8.15.

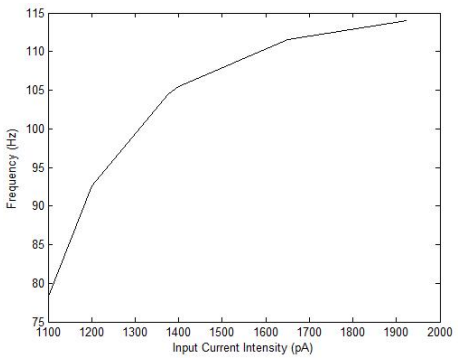

(a) Current-Frequency relation for unmyelinated fiber.

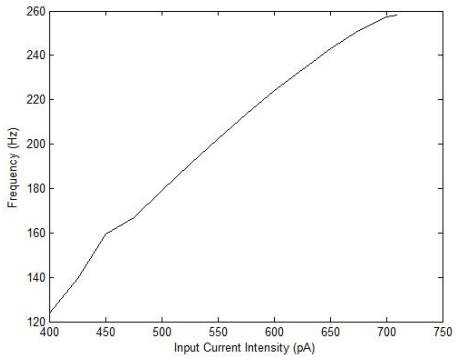

(b) Current-Frequency relation for myelinated fiber.

Figure 8.15 Current-Frequency relations for unmyelinated and myelinated fibers.

It is seen that for the initiation and conduction of APs along unmyelinated fiber, stimulus intensity must be in a higher range in comparison to intensity range of the myelinated fiber. Since unmyelinated fiber carries the nociceptive signals, for the initiation of nociceptive signal, a high intensity stimulus must be applied. When a spot on the skin is touched, initially only tactile signals are perceived. If the intensity of the stimulus is increases by pressure, then the nociceptive fibers also start to conduct APs so pain can be perceived.

8.3 Neurotransmitter Concentration In the Synaptic Cleft

With every incoming AP to the pre-synaptic neuron's terminal, neurotransmitters in the vesicles are released into the synaptic cleft. When the frequency of incoming APs is high, before the previously released neurotransmitters diffuse away from the synaptic cleft, new vesicles release neurotransmitters. By summation, concentration of neurotransmitters increase. However, increasing the frequency of APs does not increase the concentration of transmitters unlimitedly. The concentration is saturated and this is called tetanization. The first order model for time dependency of neurotransmitter concentration can predict the summation and saturation of neurotransmitters. In Figure 8.16 the change in neurotrans-

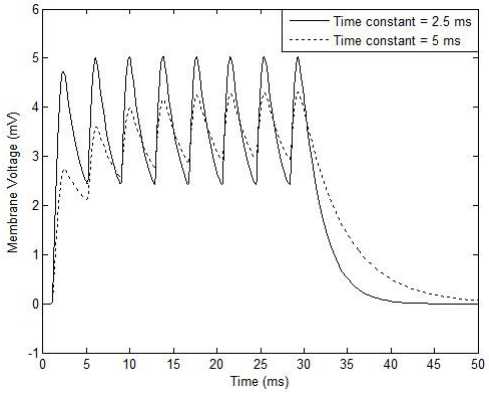

Figure 8.16 Concentration of neurotransmitter with different time constants.

mitter concentration in response to incoming APs with a frequency of 246 Hz is shown for two different time constants whereas the steady state gain is 5 for both cases. The summation property can be seen more clearly when the time constant is 5 ms. In both cases, concentration saturates at a certain value and oscillates around it since the release of neurotransmitters is dependent of AP waveform.

8.4 Response of Lamina I and II Neurons

Gate control structure is composed of four member components; myelinated fiber which conducts tactile signals, unmyelinated fiber which conducts nociceptive signals, islet neuron which is the interneuron and fusiform cell which is the projection neuron. While determining the contact points between these neurons and fibers, components that are connected with synapses are simulated separately and as the contact point, the furthest point where excitation or inhibition can be observed is chosen. In other words when determining the contact point of unmyelinated fiber and projection neuron, only unmyelinated fiber is excited and the response of the fusiform cell is examined. Contact point is chosen as the point where the fiber can excite the neuron without the need of increasing the synaptic conductance above physiological values. When connections are tested, unmyelinated fiber is found to be connected to the sixth part of fusiform cell whereas myelinated fiber is connected to the the second part on the same neuron. Excitation of islet cell

by myelinated fiber is achieved when connected to the second part of the cell and inhibition by unmyelinated fiber is accomplished when connection is at sixth part of the cell. For the connection between islet cell and fusiform cell, it is considered that inhibitory connections between neurons generally take place near to the soma of the cell [1] so that islet cell is connected to the fifth part of fusiform cell. All of the simulations are performed for this configuration.

Islet cell is modeled to be spontaneously active which means that without any need of excitation, islet cell continuously fires APs. This is because of the fact that any activity that would cause fusiform cell to integrate the sub-threshold voltages and fire APs should be inhibited so that pain sensation is prevented when nociceptive fibers are not conducting any signal. When myelinated fiber propagates APs, it would excite islet cell and for the time period that myelinated fiber is active, the frequency of the response of islet cell will increase. This can be seen clearly in Figure 8.17. In Figure 8.17(b), myelinated fiber generates APs between 100 and 200 ms and at that time period frequency of the response of islet cell increases from 72 Hz to 132 Hz. This increase in frequency will result in secretion of more GABA neurotransmitters so the effect of inhibition on fusiform cell increases.

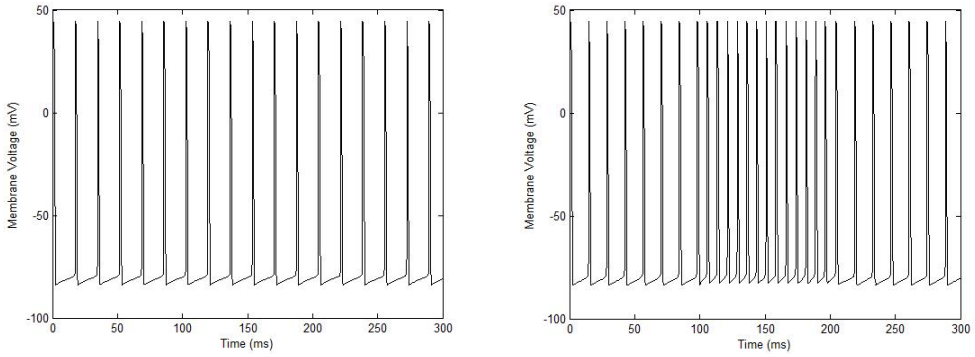

(a) Spontaneous firing of islet cell.

(b) Firing of islet cell when excited by myelinated fiber.

Figure 8.17 AP generation of islet cell with and without the effect of myelinated fiber.

When only the connection of the unmyelinated fiber and islet cell is simulated, it is seen that at the time period unmyelinated fiber is active, islet cell becomes silent. This is given in Figure 8.18. Between 100 ms and 200 ms, unmyelinated fiber conducts APs for 100 ms and islet cell is inhibited during the time period it receives those APs as it is shown in Figure 8.18(b). This inhibition is caused by the inhibitory post-synaptic potential (IPSP) that is created by the inhibitory connection between unmyelinated fiber and the islet cell. If the voltage of sixth part of islet cell is investigated, IPSPs can be observed as the membrane voltage of the part drops below the resting membrane potential with incoming signals from the unmyelinated fiber.

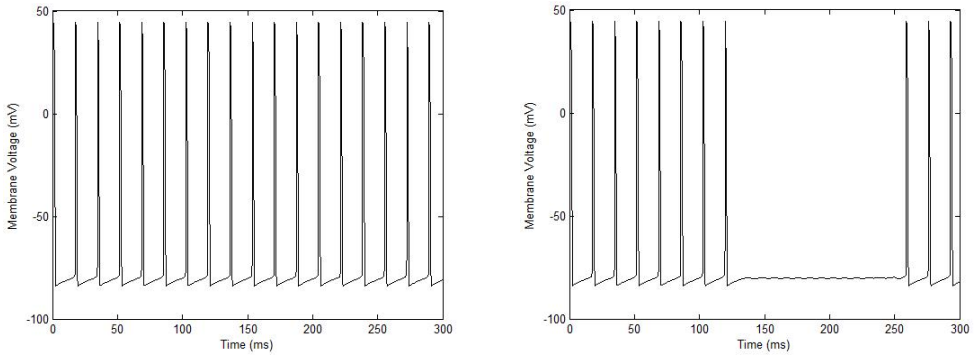

(a) Spontaneous firing of islet cell.

(b) Firing of islet cell when inhibited by unmyelinated fiber.

Figure 8.18 AP generation of islet cell with and without the effect of unmyelinated fiber.

The membrane voltage at the sixth part of islet cell is shown for the 100 ms period that the unmyelinated fiber is active in Figure 8.19. At the inhibitory synapse, as the GABA gated ion channels open, the flow of Cl^- ions into the cell decreases the membrane voltage and this is called IPSP. It should be noted that before inhibition starts, the last AP is generated at around 120 ms although current input to the unmyelinated fiber is starts to be applied at 100 ms. This

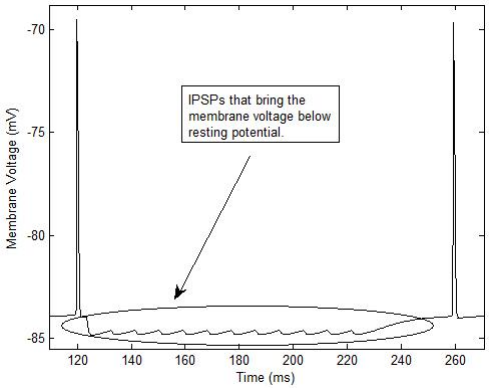

Figure 8.19 IPSPs at the sixth part of islet cell.

time lag arises because of the conduction velocity of the unmyelinated fiber. When both of the myelinated and unmyelinated fibers are active, during that time period islet cell generates APs. This is an expected result with respect to the gate control theory [15], because for the the tactile signals to suppress nociceptive signals islet cell should be activated in order to inhibit projection neuron. During myelinated and unmyelinated fibers are active, the frequency of response of islet cell is found to be 129 Hz and this value is very close to the obtained frequency when only myelinated fiber is active. When the synaptic conductance of the synapse between unmyelinated fiber and islet cell is increased from 100 nS to 150 nS, frequency of the response remains the same. However, when the contact point of unmyelinated fiber is shifted from sixth part to fifth part of islet cell, response frequency decreases to 117 Hz. This shows that as the contact point gets closer to the soma, effect of the inhibition increases.

In the gate control structure, if the myelinated fiber is dissected so that no tactile signal arrives at islet cell or fusiform cell, nociceptive signal cannot be suppressed. Unmyelinated fiber will inhibit islet cell and excite fusiform cell so that fusiform cell will fire APs that may be perceived as pain. To see the effect of inhibition that unmyelinated fiber exerts on islet cell, responses of the fusiform cell for two configurations are examined. In the first configuration, synapse between the unmyelinated fiber and the islet cell is blocked so that there are only two synaptic activity: one is the inhibitory effect of islet cell on fusiform cell and the

other is the excitatory effect of unmyelinated fiber on fusiform cell. In the other configuration, synapse between unmyelinated fiber and islet cell is active. The responses of fusiform cell are given in Figure 8.20.

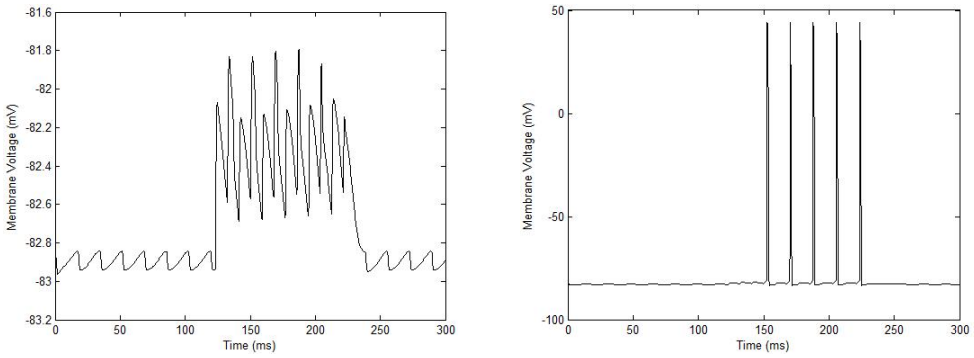

(a) Synapse between islet cell and unmyelinated fiber is blocked.

(b) Synapse between islet cell and unmyelinated fiber is active.

Figure 8.20 Responses of gate control structure when myelinated fiber is dissected.

When the connection between islet cell and unmyelinated fiber is blocked, islet cell manages to inhibit fusiform cell although there is an excitatory input to fusiform cell from the fiber. Response of fusiform cell is shown in Figure 8.20(a). Membrane voltage increases about 1 mV but since it does not exceed threshold, no APs are generated. However, when the connection between the fiber and the interneuron is active, fiber manages to inhibit the interneuron and excite the fusiform so that fusiform cell generates APs. These generated APs may be perceived as pain.

If the unmyelinated fiber is dissected, no nociceptive signal transmission will occur. In this case, myelinated fiber will excite both the fusiform cell and the islet cell. Since the response of fusiform cell will determine the level of pain, islet cell should inhibit the fusiform cell. Otherwise, tactile signals will create pain sensation. When the connection between the islet cell and the fusiform cell and

the connection between islet cell and the myelinated fiber are broken myelinated fiber will excite the fusiform cell and the response of it will be perceived as pain although incoming signal along the myelinated fiber is non-nociceptive. While keeping the connection between the interneuron and the myelinated fiber broken, if the connection between the interneuron and the projection neuron is reestablished, number of the APs that projection neuron generates decreases because of the inhibitory effect of the islet cell. Also if the myelinated fiber and interneuron is reconnected, after generating one spike, projection neuron becomes silent. This is because of the fact that frequency of the response of islet cell increases as it is excited by the myelinated fiber. Responses of fusiform cell, in other words responses of gate control structure, for these different configurations are shown in Figure 8.21. Myelinated fiber is active for 100 ms between 100 ms and 200 ms.

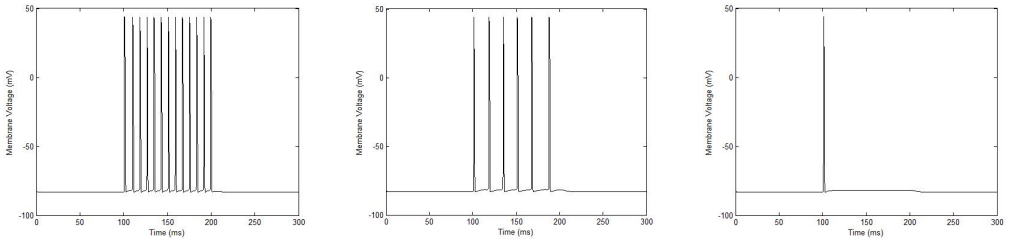

(a) Only myelinated fiber and fusiform cell are connected.

(b) Myelinated fiber and islet cell are not connected.

(c) Myelinated fiber, islet cell and fusiform cell are connected.

Figure 8.21 Responses of gate control structure when unmyelinated fiber is dissected.

In stressful situations like war, severe wounds that would normally cause great pain is not felt [11]. This psychological phenomenon is explained with the actions that brain take to inhibit such signals. But the mode of inhibition by brain is not understood fully. However, besides the effect of brain, physiological properties of the fibers that convey nociceptive signals may be responsible for this observation.

For the developed model, if an input stimulus is applied that is out of range of the current intensity-frequency relationship, unmyelinated fiber is blocked, which is called depolarization block. Since the unmyelinated fiber cannot convey nociceptive signals, no pain is perceived. Close-up signal waveform of the depolarization block that occurs when 8000 pA current is applied to unmyelinated fiber is shown in Figure 8.22(a)and the response of the fusiform cell to this input is shown in Figure 8.22(b).

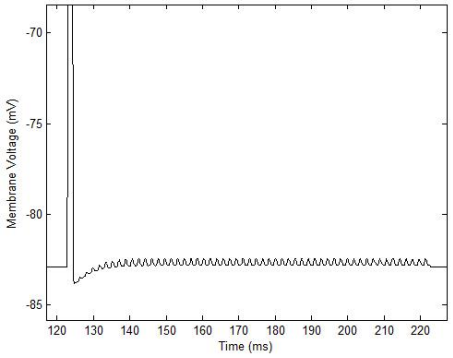

(a) Response of unmyelinated fiber to high intensity current input.

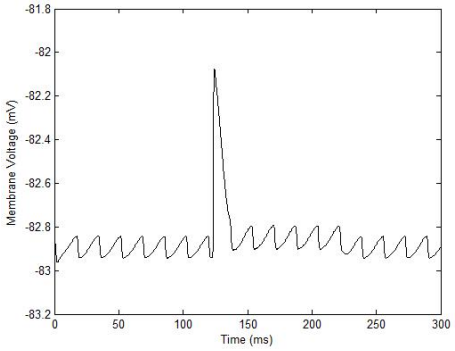

(b) Response of fusiform cell to unmyelinated fiber that is stimulated with high intensity input.

Figure 8.22 Responses of unmyelinated fiber and fusiform cell under high intensity input.

In Figure 8.22(a) it is seen that, after initiation of one AP at the start of the high intensity input, membrane voltage of the unmyelinated fiber remains subthreshold. It is obvious that when the input to the unmyelinated fiber exceeds the range of current-frequency relationship, fiber cannot excite fusiform cell so no pain signal is transmitted to upper centers of the nervous system.

While quantifying nociceptive signals with mathematical models, test of the accuracy of these models are very hard, if not impossible. Pain sensation is decoded with the nociceptive signals that convey to the higher centers of central

nervous system and these signals are encoded and perceived as pain or not in the brain. The most important handicap is the subjectiveness in the perception of pain. In other words, the outcome of the same stimulus that activates nociceptive fibers is different from person to person so to construct an input-output relationship experimentally and test the mathematical models with these experimental results will lead to wrong results. If this subjectiveness is to be eliminated and test the mathematical models accurately, recordings from the components of the gate control system must be done. However, this would be a highly invasive procedure since the system is situated in the spinal cord and very long electrodes must be inserted into the subject's body. Also, recording from the correct neuron is not guaranteed since the spinal cord is very crowded with heterogeneous types of neurons. With these insufficiencies in recording nociceptive signals and measuring the perceived pain that these signals cause, the mathematical model that is developed in this study is tested with the reported observations regarding the perception of pain from the literature. As the recording technologies develop and non-invasive techniques are found, models can be tested more accurately. Finally, for a more complete model, specific connectivity patterns between the fibers and neurons should be found. Also the synaptic conductances of inhibitory and excitatory synapses should be measured exactly. In the further studies, the effect of brain can be included when more information on the dynamics of the input that is exerted by the brain is gained.

CHAPTER 9

CONCLUSIONS

In this thesis work, a mathematical model of the gate control structure is developed. Model contains the electrophysiological and morphological characteristics of the component fibers and neurons. The model of an excitable cell is constructed in the Simulink simulation environment and the response of this model cell is investigated under different physiological conditions and different external stimulus pattern. Consequently, output of the gate control system is investigated for different configurations and the following conclusions are made:

- Absolute refractory period of the single cell model is found as 3.7 ms and this value introduces an upper limit for the frequency of generated APs as 270 Hz.
- Model can transduce the input current intensity to firing frequency as expected: as the current intensity increases, frequency of generated APs increases.
- Model can predict depolarization block that is due to the slow dynamics of sodium inactivation gates.
- Model neuron can add inputs as real neurons do: although model does not produce an AP for sub-threshold inputs, when two consecutive sub-threshold inputs are applied, AP is initiated.
- Tetrodotoxin is a substance that blocks sodium ion channels and its effect is predicted by the model; no action potential is produced after the blockage of sodium channels as in real neurons.

- If the extracellular Na^+ ion concentration is increased, the model generates train of APs with a higher frequency and the amplitudes of APs increase.
- Propagation velocities along myelinated and unmyelinated fibers are found in accordance with the literature. The velocity along myelinated fiber is almost 150 times of the velocity along unmyelinated fiber.
- Input current intensity-frequency relationships of myelinated and unmyelinated fibers are found. Myelinated fiber has lower threshold in comparison to unmyelinated fiber. Myelinated fiber starts to conduct when input is around 400 pA whereas unmyelinated fiber starts to conduct when input is around 1100 pA.
- Synaptic transmission is modeled with a two tank system and it is found that the developed model can add neurotransmitter concentration with every incoming action potential and shows the tetanization phenomenon that is seen in real synapses.
- Interneuron fires spontaneously and when it is under the effect of only myelinated fiber, during the fiber is active, frequency of the response of the interneuron increases. When it is only under the effect of unmyelinated fiber, interneuron becomes silent as long as the fiber is active. When both of the fibers are connected to the interneuron and they are active for the same time period, effect of myelinated fiber dominates and the firing frequency of the interneuron increases.
- When the contact point of unmyelinated fiber comes closer to the soma of the interneuron, its firing frequency decreases which shows that the effect of inhibition increases as the contact point is near soma.
- When only the myelinated fiber is dissected, projection neuron generates APs which means nociceptive signals project to upper centers. On the other hand, when only unmyelinated fiber is dissected, projection neuron becomes silent.

REFERENCES

[1] E. Kandel, J. Schwartz, and T. Jessell, *Principles of Neural Science*. Appleton & Lange, 2000.

[2] B. Graham, A. Brichta, and R. Callister, "Moving from an averaged to specific view of spinal cord pain processing circuits," *Journal of Neurophysiology*, vol. 98, pp. 1057–1063, 2007.

[3] S. Prescott and Y. Koninck, "Four cell types with distinctive membrane properties and morphologies in lamina I of the spinal dorsal horn of the adult rat," *The Journal of Physiology*, vol. 539, no. 3, pp. 817–836, 2002.

[4] I. Melnick, "Morphophysiologic properties of islet cells in substantia gelatinosa of the rat spinal cord," *Neuroscience Letters*, vol. 446, no. 2-3, pp. 65–69, 2008.

[5] A. Guyton and J. Hall, *Textbook of Medical Physiology, Edition 11*. 2006.

[6] B. Hille, *Ionic Channels of Excitable Membranes*. 1984.

[7] N. Purali, *Hücre Elektrofizyolojisi ve Görüntülemenin Temelleri*. Veri Medikal Yayincilik, 2008.

[8] J. Schwarz, G. Reid, and H. Bostock, "Action potentials and membrane currents in the human node of Ranvier," *Pflügers Archiv European Journal of Physiology*, vol. 430, no. 2, pp. 283–292, 1995.

[9] F. Doyle, L. Jovanovic, D. Seborg, R. Parker, B. Bequette, A. Jeffrey, X. Xia, I. Craig, and T. McAvoy, "A tutorial on biomedical process control," *Journal of Process Control*, vol. 17, no. 7, pp. 571–572, 2007.

[10] M. Stojanovic, "Stimulation methods for neuropathic pain control," *Current Pain and Headache Reports*, vol. 5, no. 2, pp. 130–137, 2001.

[11] N. Britton and S. Skevington, "A mathematical model of the gate control theory of pain.," *Journal of theoretical biology*, vol. 137, no. 1, pp. 91–105, 1989.

[12] M. Haeri, D. Asemani, and S. Gharibzadeh, "Modeling of pain using artificial neural networks," *Journal of Theoretical Biology*, vol. 220, no. 3, pp. 277–284, 2003.

[13] M. Von Frey, "Beitrage zur physiologie des schmerzsinns," *Akad Wiss Leipzig Math.-Naturwiss Kl Ber*, vol. 46, pp. 185–196, 1894.

[14] P. Nathan, "The gate-control theory of pain. A critical review.," *Brain*, vol. 99, no. 1, pp. 123–158, 1976.

[15] R. Melzack and P. Wall, "Pain mechanisms: a new theory," *Science*, vol. 150, no. 3699, pp. 971–978, 1965.

[16] Y. Lu and E. Perl, "Modular organization of excitatory circuits between neurons of the spinal superficial dorsal horn (laminae I and II)," *The Journal of Neuroscience*, vol. 25, no. 15, pp. 3900–3907, 2005.

[17] P. Wall, "The gate control theory of pain mechanisms," *Brain*, vol. 101, no. 1, pp. 1–18, 1978.

[18] H. Minamitani and N. Hagita, "Neural Network Model of Pain Mechanisms: Computer Simulation of the Central Neural Activities Essential for the Pain and Touch Sensations," *IEEE TRANS. SYS., MAN, AND CYBER.*, vol. 11, no. 7, pp. 481–493, 1981.

[19] R. Melzack, "From the gate to the neuromatrix," *Pain*, vol. 82, pp. S121–S126, 1999.

[20] F. Xu, T. Lu, and K. Seffen, "Skin thermal pain modeling-A holistic method," *Journal of Thermal Biology*, vol. 33, pp. 223–237, 2008.

[21] M. Chaudhari and P. Mackenzie, "Implantable technology for pain management," *Anaesthesia & Intensive Care Medicine*, vol. 9:2, pp. 69–74, 2007.

[22] A. Herz, T. Gollisch, C. Machens, and D. Jaeger, "Modeling single-neuron dynamics and computations: a balance of detail and abstraction," 2006.

[23] E. Izhikevich, "Simple model of spiking neurons," *IEEE Transactions on Neural Networks*, vol. 14, no. 6, pp. 1569–1572, 2003.

[24] A. Hodgkin and A. Huxley, "A quantitative description of membrane current and its application to conduction and excitation in nerve," *J. Physiol.(Lond.)*, vol. 117, pp. 500–544, 1952.

[25] W. Rall, "Branching dendritic trees and motoneuron membrane resistivity," *Exp Neurol*, vol. 1, no. 5, pp. 491–527, 1959.

[26] W. Rall, "Theory of biophysical properties of dendrites," *Ann NY Acad Sci*, vol. 96, pp. 1071–1092, 1962.

[27] R. Fitzhugh, "Computation of impulse initiation and saltatory conduction in a myelinated nerve fiber," *Biophysical Journal*, vol. 2, no. 1, pp. 11–21, 1962.

[28] L. Goldman and J. Albus, "Computation of impulse conduction in myelinated fibers; theoretical basis of the velocity-diameter relation," *Biophysical Journal*, vol. 8, no. 5, pp. 596–607, 1968.

[29] N. Sabah, "Aspects of nerve conduction," *IEEE ENGINEERING IN MEDICINE AND BIOLOGY MAGAZINE*, vol. 19, no. 6, pp. 111–118, 2000.

[30] C. Koch and I. Segev, *Methods in neuronal modeling: from ions to networks*. The MIT Press, 1998.

[31] D. Bergles, J. Diamond, and C. Jahr, "Clearance of glutamate inside the synapse and beyond," *Current Opinion in Neurobiology*, vol. 9, no. 3, pp. 293–298, 1999.

[32] A. Destexhe, Z. Mainen, and T. Sejnowski, "Fast kinetic models for simulating AMPA, NMDA, GABA (A) and GABA (B) receptors," *The Neurobiology of Computation*, pp. 9–14.

[33] A. Destexhe, Z. Mainen, and T. Sejnowski, "Synthesis of models for excitable membranes, synaptic transmission and neuromodulation using a common kinetic formalism," *Journal of Computational Neuroscience*, vol. 1, no. 3, pp. 195–230, 1994.

[34] F. Cervero and A. Iggo, "The substantia gelatinosa of the spinal cord: a critical review," *Brain*, vol. 103, no. 4, pp. 717–772, 1980.

[35] T. Yasaka, G. Kato, H. Furue, M. Rashid, M. Sonohata, A. Tamae, Y. Murata, S. Masuko, and M. Yoshimura, "Cell-type-specific excitatory and inhibitory circuits involving primary afferents in the substantia gelatinosa of the rat spinal dorsal horn in vitro," *The Journal of Physiology*, vol. 581, no. 2, pp. 603–618, 2007.

[36] D. Maxwell, M. Belle, O. Cheunsuang, A. Stewart, and R. Morris, "Morphology of inhibitory and excitatory interneurons in superficial laminae of the rat dorsal horn," *The Journal of Physiology*, vol. 584, no. 2, pp. 521–533, 2007.

[37] C. Daniele and A. MacDermott, "Low-threshold primary afferent drive onto GABAergic interneurons in the superficial dorsal horn of the mouse," *Journal of Neuroscience*, vol. 29, no. 3, pp. 686–695, 2009.

[38] T. Grudt and E. Perl, "Correlations between neuronal morphology and electrophysiological features in the rodent superficial dorsal horn," *The Journal of Physiology*, vol. 540, no. 1, pp. 189–207, 2002.

[39] L. Almarestani, S. Waters, J. Krause, G. Bennett, and A. Ribeiro-da Silva, "Morphological characterization of spinal cord dorsal horn lamina I neurons projecting to the parabrachial nucleus in the rat," *The Journal of Comparative Neurology*, vol. 504, pp. 287–297, 2007.

[40] Z. Han, E. Zhang, and A. Craig, "Nociceptive and thermoreceptive lamina I neurons are anatomically distinct," *Nature Neuroscience*, vol. 1, no. 3, pp. 218–225, 1998.

[41] E. Zhang and A. Craig, "Morphology and distribution of spinothalamic lamina I neurons in the monkey," *Journal of Neuroscience*, vol. 17, no. 9, pp. 3274–3284, 1997.

[42] A. Todd and J. McKenzie, "GABA-immunoreactive neurons in the dorsal horn of the rat spinal cord.," *Neuroscience*, vol. 31, no. 3, pp. 799–806, 1989.

[43] Y. Lu and E. Perl, "A specific inhibitory pathway between substantia gelatinosa neurons receiving direct C-fiber input," *Journal of Neuroscience*, vol. 23, no. 25, pp. 8752–8758, 2003.

[44] G. Kato, Y. Kawasaki, R. Ji, and A. Strassman, "Differential wiring of local excitatory and inhibitory synaptic inputs to islet cells in rat spinal lamina II demonstrated by laser scanning photostimulation," *The Journal of Physiology*, vol. 580, no. 3, pp. 815–833, 2007.

[45] C. Geankoplis, *Transport Processes and Unit Operations.* 1993.

[46] R. Silbey and R. Alberty, *Physical chemistry–3rd ed.* John Willey & Sons.

[47] S. Waxman and J. Ritchie, "Organization of ion channels in the myelinated nerve fiber," *Science*, vol. 228, no. 4707, pp. 1502–1507, 1985.

[48] A. Destexhe, *Computational Modeling of Genetic and Biochemical Networks.* 2000.

[49] M. Boada and C. Woodbury, "Myelinated skin sensory neurons project extensively throughout adult mouse substantia gelatinosa," *Journal of Neuroscience*, vol. 28, no. 9, pp. 2006–2014, 2008.

[50] R. Dingledine, K. Borges, D. Bowie, and S. Traynelis, "The glutamate receptor ion channels," *Pharmacological Reviews*, vol. 51, no. 1, pp. 7–61, 1999.

[51] D. Colquhoun, P. Jonas, and B. Sakmann, "Action of brief pulses of glutamate on AMPA/kainate receptors in patches from different neurones of rat hippocampal slices," *The Journal of Physiology*, vol. 458, no. 1, pp. 261–287, 1992.

[52] R. Coggeshall and S. Carlton, "Receptor localization in the mammalian dorsal horn and primary afferent neurons," *Brain Research Reviews*, vol. 24, no. 1, pp. 28–66, 1997.

[53] R. Macdonald and R. Olsen, "$GABA_A$ receptor channels," *Annual Review of Neuroscience*, vol. 17, pp. 569–602, 1994.

[54] B. Frankenhaeuser and A. Huxley, "The action potential in the myelinated nerve fibre of Xenopus laevis as computed on the basis of voltage-clamp data," *The Journal of Physiology*, vol. 171, pp. 302–315, 1964.

[55] W. Wesselink, J. Holsheimer, and H. Boom, "A model of the electrical behaviour of myelinated sensory nerve fibres based on human data," *Medical and Biological Engineering and Computing*, vol. 37, no. 1, pp. 228–235, 1999.

[56] A. Scholz, G. Reid, W. Vogel, and H. Bostock, "Ion channels in human axons," *Journal of neurophysiology*, vol. 70, no. 3, pp. 1274–1279, 1993.

[57] J. Ritchie and R. Rogart, "Density of sodium channels in mammalian myelinated nerve fibers and nature of the axonal membrane under the myelin sheath," *Proceedings of the National Academy of Sciences*, vol. 74, no. 1, pp. 211–215, 1977.

[58] J. Smit, T. Hanekom, and J. Hanekom, "Modelled temperature-dependent excitability behaviour of a generalised human peripheral sensory nerve fibre," *Biological Cybernetics*, vol. 101, no. 2, pp. 115–130, 2009.

[59] J. Frijns, J. Mooij, and J. Ten Kate, "A quantitative approach to modeling mammalian myelinated nervefibers for electrical prosthesis design," *IEEE Transactions on Biomedical Engineering*, vol. 41, no. 6, pp. 556–566, 1994.

[60] J. Clements, "Transmitter timecourse in the synaptic cleft: its role in central synaptic function," *Trends in Neurosciences*, vol. 19, no. 5, pp. 163–171, 1996.

[61] A. Destexhe, Z. Mainen, and T. Sejnowski, "An efficient method for computing synaptic conductances based on a kinetic model of receptor binding," *Neural Computation*, vol. 6, no. 1, pp. 14–18, 1994.

[62] N. Purali, "Firing properties of the soma and axon of the abdominal stretch receptor neurons in the crayfish (Astacus leptodactylus)," *General physiology and Biophysics*, vol. 21, no. 2, pp. 205–226, 2002.

[63] N. Purali, "Structure and function relationship in the abdominal stretch receptor organs of the crayfish," *Journal of Comparative Neurology*, vol. 488, no. 4, pp. 369–383, 2005.

[64] C. Tai, J. Roppolo, and W. de Groat, "Analysis of nerve conduction block induced by direct current," *Journal of Computational Neuroscience*, vol. 27, no. 2, pp. 201–210, 2009.

APPENDIX A

SIMULINK MODELS OF ION CHANNELS

Block diagrams of sodium and potassium conductance models are given in Figure A.1 and Figure A.2, respectively. Block diagram in Figure A.3 is the same for sodium activation (m) and inactivation (h) gating particles except the dynamics of m and h are doubled.

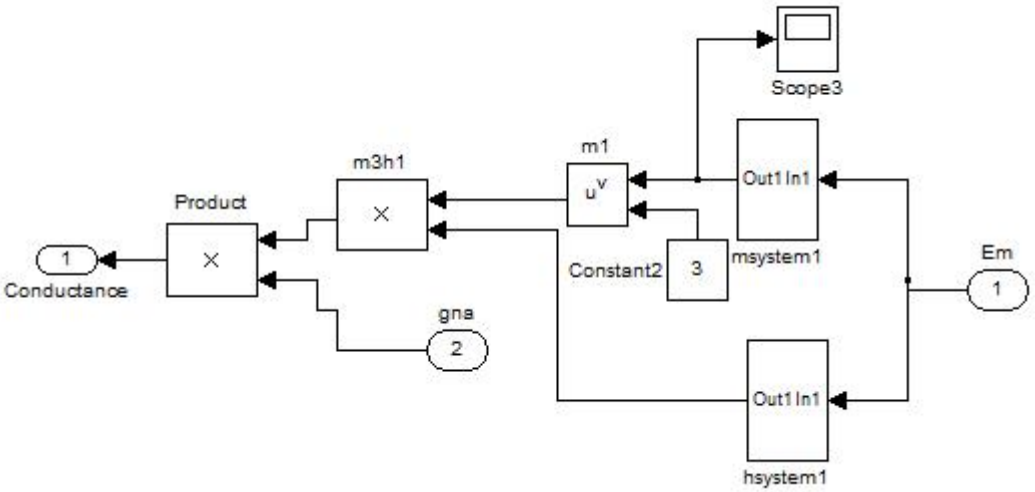

Figure A.1 Sodium conductance model.

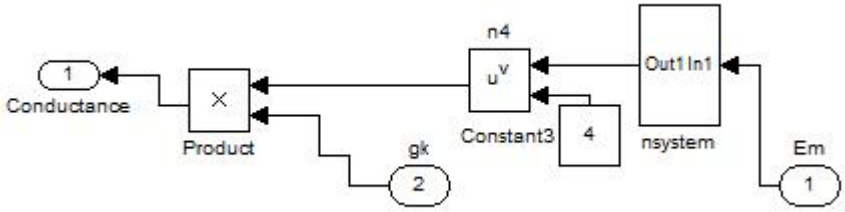

Figure A.2 Potassium conductance model.

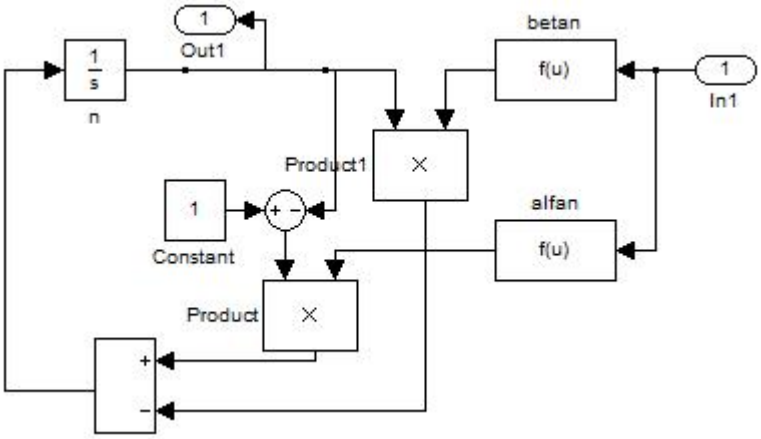

Figure A.3 Potassium channel gating variable model.

APPENDIX B

SIMULINK MODELS OF FIBERS AND NEURONS

In Figure B.1 figure starts with the model of a node and followed by the model of a paranode which is followed by another node. The block diagram of unmyelinated fiber is composed of a hundred nodal blocks but since the picture of the model is too big, it is not included. Block diagrams of interneuron and projection neuron are given in Figure B.2 and Figure B.3, respectively. Finally the block diagram of the complete model is presented.

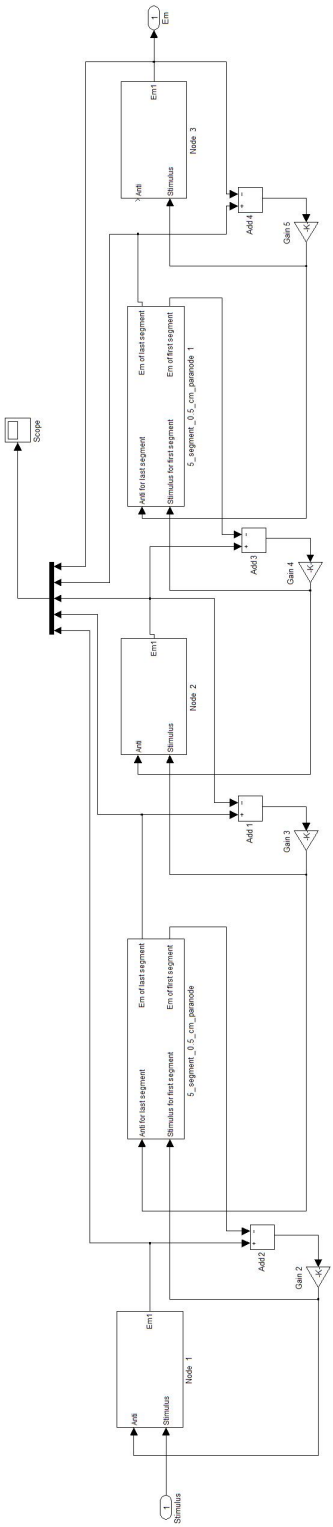

Figure B.1 Simulink model of the compartmental myelinated fiber.

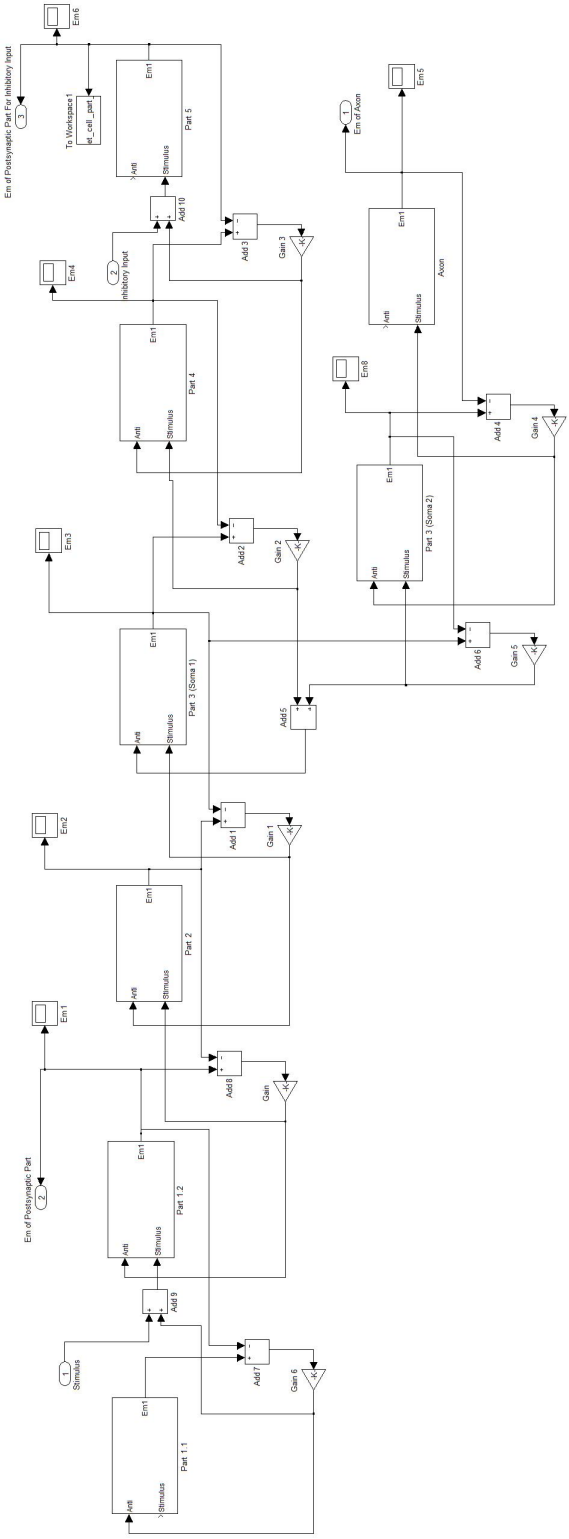

Figure B.2 Block diagram of interneuron.

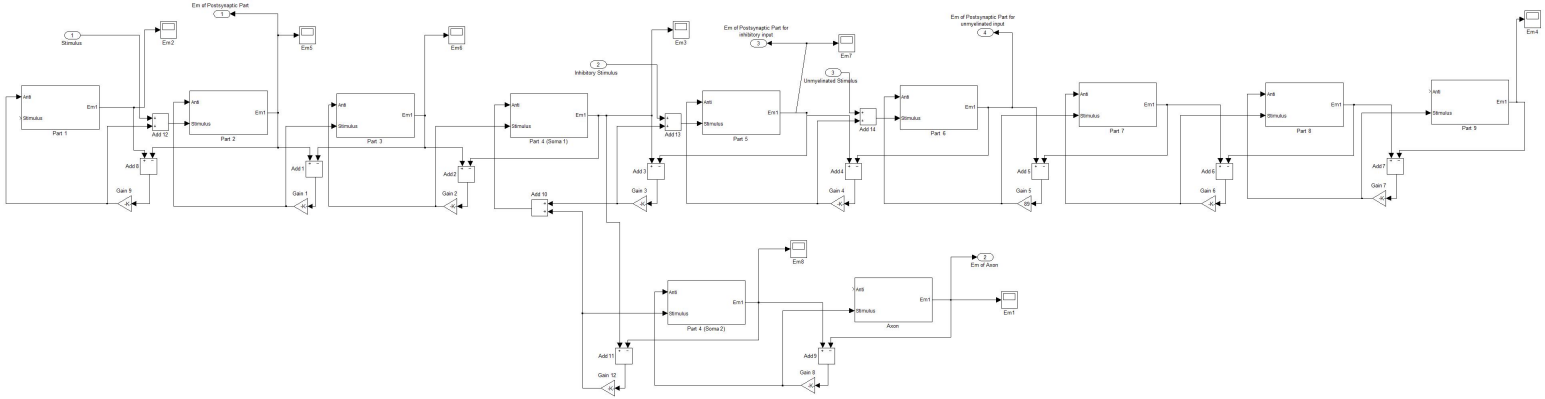

Figure B.3 Block diagram of projection neuron.

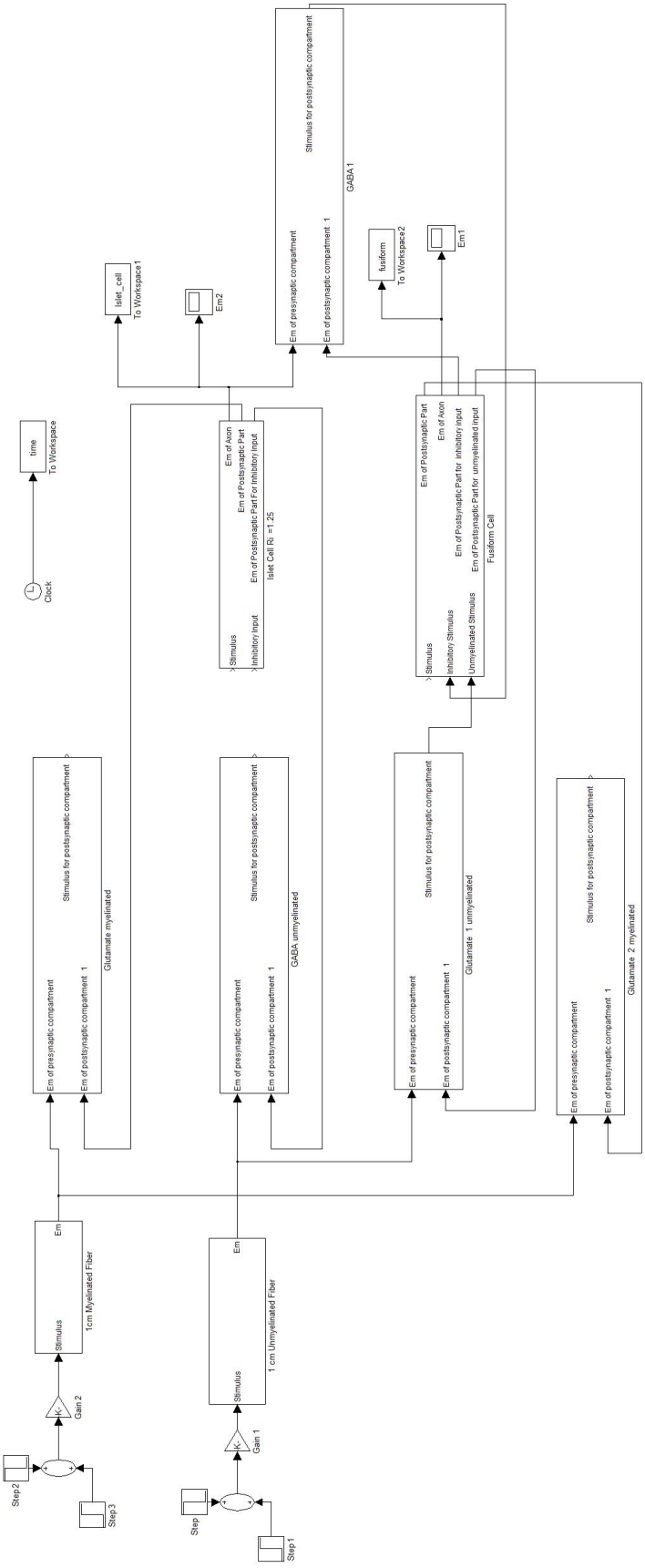

Figure B.4 Complete model.